2004-39

Final Report

SMALL STRAIN AND RESILIENT MODULUS TESTING OF GRANULAR SOILS

Research

Technical Report Documentation Page

1. Report No. 2004-39	2.	3. Recipients Accession No.
4. Title and Subtitle SMALL STRAIN AND RESILIENT MODULUS TESTING OF GRANULAR SOILS		5. Report Date August 2004 6.
7. Author(s) Peter Davich, Joseph Labuz, Bojan Guzina & Andrew Drescher		8. Performing Organization Report No.
9. Performing Organization Name and Address Department of Civil Engineering University of Minnesota 500 Pillsbury Drive S.E. Minneapolis, Minnesota 55455-0220		10. Project/Task/Work Unit No. 11. Contract (C) or Grant (G) No. (c) 81655 (w) 32
12. Sponsoring Organization Name and Address Minnesota Department of Transportation Research Services Section 395 John Ireland Boulevard Mail Stop 330 St. Paul, Minnesota 55155		13. Type of Report and Period Covered Final Report 14. Sponsoring Agency Code
15. Supplementary Notes www.lrrb.org/PDF/200439.pdf		

16. Abstract (Limit: 200 words)

Resilient modulus, shear strength, dielectric permittivity, and shear and compressional wave speed values were determined for 36 soil specimens created from the six soil samples. These values show that the soils had larger stiffnesses at low moisture contents. It was also noted during testing that some non-uniformity was present within the axial displacement measurements; larger levels of non-uniformity were associated with low moisture contents, possibly due to more heterogeneous moisture distributions within these specimens. Lastly, the data collected during this study was used to recommend a relationship between granular materials' small strain modulus and their resilient modulus. This relationship was given in the form of a hyperbolic model that accurately represents the strain-dependent modulus reduction of the base and subgrade materials. This model will enable field instruments that test at small strains to estimate the resilient modulus of soil layers placed during construction.

17. Document Analysis/Descriptors		18. Availability Statement	
Bender element testing Resilient modulus testing	Select granular soil	No restrictions. Document available from: National Technical Information Services, Springfield, Virginia 22161	
19. Security Class (this report) Unclassified	20. Security Class (this page) Unclassified	21. No. of Pages 117	22. Price

Small Strain and Resilient Modulus Testing of Granular Soils

Final Report

Prepared by:

Peter Davich
Joseph F. Labuz
Bojan Guzina
Andrew Drescher

Department of Civil Engineering
University of Minnesota

August 2004

Published by:

Minnesota Department of Transportation
Research Services Section
395 John Ireland Boulevard, Mail Stop 330
St. Paul, Minnesota 55155

Table of Contents

Chapter 1 – Introduction 1

1.1 Resilient Modulus 2

1.2 Small Strain Testing 3

1.3 Organization 4

Chapter 2 – Literature Review 5

2.1 Resilient Modulus Testing 5

2.1.1 Long Term Pavement Performance Protocol P46 6

2.1.2 Equipment Modifications 8

2.2 Bender Element Testing 9

2.2.1 Density Effects 10

2.2.2 Wave Speed Effects 11

2.2.3 Research Recommendations 12

Chapter 3 – Test Procedure 13

3.1 Test Equipment 13

3.1.1 Triaxial Cell 13

3.1.2 Load Cell and LVDTs 16

3.1.3 Bender Element System 17

3.1.4 Load Frame 19

3.2 Soil Samples 19

3.3 Specimen Preparation 21

3.3.1 Compaction 23

3.3.2 Percometer Measurements 25

3.3.3 Bender Element Protection 26

3.4 Specimen Testing 27

3.4.1 Resilient Modulus Test 28

3.4.2 Shear Strength Test 31

Chapter 4 – Discussion of Results..... 33

4.1 Testing Schedule.....33
4.2 Resilient Modulus Data Interpretation.....34
4.2.1 Sample Calculation..... 36
4.2.2 Deformation Homogeneity..... 36
4.3 Bender Element Data Interpretation..... 41
4.3.1 Cross Correlation..... 44
4.3.2 Sample Calculation..... 47
4.4 Test Data..... 48
4.4.1 Resilient Modulus Data.....48
4.4.2 Bender Element Data..... 53
4.4.3 Percometer Data.....59
4.4.4 Shear Strength Data..... 63
4.5 Degradation Curves..... 66

Chapter 5 – Summary and Conclusions.....70

References.....72

Appendix A..... A-1
Appendix B..... B-1
Appendix C..... C-1
Appendix D..... D-1
Appendix E..... E-1

List of Figures

1.1. Modulus Variation With Strain Level....3
2.1. LTPP P46 Load History....6
2.2. Bender Element Wave Generation....9
3.1. Triaxial Cell Diagram....14
3.2. Triaxial Cell Containing Specimen....15
3.3. Bender Element Incorporation Within Platen....16
3.4. Load Cell....16
3.5. LVDT Collars with Spacers....17
3.6. Bender Element Cantilever Strip....18
3.7. Load Frame....19
3.8. Labeled Soil Samples....20
3.9. Oversized Aggregate....21
3.10. Tempering Container....22
3.11. Compaction Data for Sample A....23
3.12. Stages of Specimen Preparation....24
3.13. Percometer Measurement....25
3.14. Bender Element Protection System....26
3.15. Stages of Element Protection....27
3.16. Specimen Loaded within Triaxial Cell....28
3.17. Fluid Pressure Transducer....29
3.18. M_R Test Displacement History....30
3.19. P-Wave Source and Receiver Time Histories....31
3.20. Specimen Failure....32
4.1. Displacement Histories....38
4.2. α-Value Variation....40
4.3. Deviator Stress and Deformation Homogeneity....41
4.4. Identification of Wave Arrivals....42
4.5. P-Wave Cross Correlation Results....45

4.6. S-Wave Cross Correlation Results....46
4.7. Resilient Modulus Data....51
4.8. M_R Versus Mean Stress for Sample A....53
4.9. M_R and E_{MAX} Curves....54
4.10. Bender Element Data....55
4.11. Data used in Dielectric-Moisture Relationship....61
4.12. Ultimate Shear Strength....66
4.13. Hyperbolic Predictions of Cyclic Triaxial Results....68
A.1. Gradations for Samples....A-2
A.2. Soil-Water Characteristic Curve for Sample A....A-3
A.3. Soil-Water Characteristic Curve for Sample D....A-3
A.4. Soil-Water Characteristic Curve for Sample F....A-4
A.5. Soil-Water Characteristic Curve for Sample H....A-4
A.6. Soil-Water Characteristic Curve for Sample J....A-5
A.7. Soil-Water Characteristic Curve for Sample N....A-5
D.1. Young's Modulus Data from Sample A....D-2
D.2. Young's Modulus Data from Sample D....D-3
D.3. Young's Modulus Data from Sample F....D-4
D.4. Young's Modulus Data from Sample H....D-5
D.5. Young's Modulus Data from Sample J....D-6
D.6. Young's Modulus Data from Sample N....D-7
D.7. Resilient Modulus Versus Confining Pressure Data....D-8
D.8. Resilient Modulus and Mean Stress Data from Sample A....D-11
D.9. Resilient Modulus and Mean Stress Data from Sample D....D-12
D.10. Resilient Modulus and Mean Stress Data from Sample F....D-13
D.11. Resilient Modulus and Mean Stress Data from Sample H....D-14
D.12. Resilient Modulus and Mean Stress Data from Sample J....D-15
D.13. Resilient Modulus and Mean Stress Data from Sample N....D-16
E.1. Resilient Modulus Values from both Protocols....E-5
E.2. NCHRP 1-28A and Bender Element Moduli....E-6

List of Tables

2.1. LTPP P46 Loading Sequences....7
3.1. Soil Sample Data....20
4.1. Test Matrix....34
4.2. M_R Test α Values....39
4.3. Wave Speeds at Variable Pulse Frequencies....43
4.4. Target and Measured Specimen Preparation Parameters....48
4.5. Resilient Modulus and E_{MAX}....57
4.6. Elastic Parameters Estimated from Bender Element Testing....58
4.7. Dielectric Permittivity and Conductivity....60
4.8. Dielectric Moisture Content Estimates....62
4.9. Deviator Stress Values at Shear Failure....63
4.10. Cohesion and Friction Angle of Samples....65
A.1. Soil Gradation Data....A-1
B.1. Phase Angles for Test System....B-1
B.2. Load and Displacement Measurements for University's Load Frame....B-3
B.3. Load Measurements for Mn/DOT's Load Frame....B-4

Executive Summary

Resilient modulus testing measures the mechanical response of a pavement base or subgrade soil to a cyclic load simulating traffic. The resilient modulus values measured during the test are commonly used as design parameters for pavement structures. In addition, a new generation of small-strain tests have recently been developed to aid the quality assurance during pavement construction. The purpose of this study is to compare the small strain modulus and resilient modulus of pavement foundation materials in the context of resilient modulus testing.

Thirty-six resilient modulus tests were performed on samples of six soils that are commonly used within pavement structures in Minnesota. These tests were performed at three different values of moisture content for each soil; one repetition of each test was carried out to investigate the repeatability of the data. To provide the data necessary to link the small-strain modulus to the resilient modulus, a sequence of bender element tests was performed on the soil specimens during each resilient modulus test.

Resilient modulus, ultimate shear strength, dielectric permittivity, and shear and compressional wave speed values were determined for 36 soil specimens created from the six soil samples. These values show that the soils had larger stiffnesses at low moisture contents. It was also noted during testing that some non-uniformity was present within the axial displacement measurements during testing; larger levels of non-uniformity were associated with low moisture contents, possibly due to more heterogeneous moisture distributions within these specimens. Lastly, the data collected during this study was used to recommend a relationship between granular materials' small strain modulus and their resilient modulus. This relationship was given in the form of a hyperbolic model that accurately represents the strain-dependent modulus reduction of the base and subgrade materials. This model will enable field instruments that test at small strains to estimate the resilient modulus of soil layers placed during construction.

Chapter 1
Introduction

Asphalt and concrete pavements rest on one or more layers of engineered soil. The overall stiffness of the pavement structure is greatly affected by the composition of these foundation layers, which are most often composed of soils containing primarily gravel and sand. Owing to the critical effect that the foundation layers have on the overall stiffness of the pavement structure, it is important to understand how these soils behave under traffic loading.

One of the most commonly used parameters that describe the foundation soil stiffness is the resilient modulus (M_R), which is a measure of the degree to which a soil can recover from stress levels commonly placed upon roadbed soils by traffic. Many pavement engineering firms and agencies, including the Minnesota Department of Transportation (Mn/DOT), currently use M_R values as a measure of the base and subgrade stiffnesses in their pavement design procedures.

Unfortunately, many pavements fail before the end of their predicted design life. There are a variety of causes for this, but one of the most common is poor construction. As a result, the importance of quality control procedures is being emphasized more than ever. One of the difficulties in determining the quality of base layer compaction is that it is impossible to directly measure a soil's M_R at a construction site. The resilient modulus test can only be performed in a laboratory, and taking core samples from the compacted soil is both time-consuming and harmful to the pavement under construction. As a result, it is difficult to determine if the base layers at a construction site have the M_R values that are required by the pavement design. Therefore, a fundamental relationship between the resilient modulus values and quantities that can be measured in the field (e.g. small-strain modulus) would be an indispensible tool to elevate the quality of pavements.

Partially in response to this need, Mn/DOT recently initiated a series of studies designed to test the stiffness properties of base layers in the field. Several of these projects, such as the portable deflectometer study carried out by Hoffmann et al.[1], deal with instruments designed to measure the small strain modulus of in-situ soils undergoing small mechanical vibration. Many of these projects were successful in developing or creating test protocols for instrumentation that

can measure small strain modulus values using non-destructive wave sources. The objective of this study is to link the small strain modulus values of pavement foundation layers obtained from small strain testing to their M_R counterparts obtained in the laboratory. An accurate correlation between these parameters would enable better monitoring of base properties during construction and, ultimately, reduce the number of premature pavement failures.

1.1 Resilient Modulus

Many highway departments use the resilient modulus as one of the primary parameters in their pavement design procedures. One test protocol for measuring M_R is Long Term Pavement Protocol (LTPP) P46, which was developed by the Strategic Highway Research Program (SHRP) [2]. A revised version of this protocol, the National Cooperative Highway Research Program (NCHRP) 1-28 A, was released in 2002 [3]. It is different from LTPP P46 in many ways; one of the most significant is that it involves larger stresses on specimens. These stresses are large enough to cause the failure of some soils. In addition, NCHRP 1-28A has yet to be widely implemented and the majority of existing M_R data was generated using LTPP P46. For these reasons, it was decided that LTPP P46 would be used for the purposes of this research. For completeness, however, one M_R test using the NCHRP 1-28A protocol was performed during the course of this study to compare the moduli values resulting from the two testing procedures.

The LTPP P46 test protocol revolves around the cyclic triaxial testing of a soil specimen. Each test cycle consists of a loading portion as well as time for material recovery. The load path consists of an axial, haversine load pulse 0.1 s in duration. This is followed by 0.9 s of material recovery for a total cycle time of 1 s. This cycle is intended to simulate the passing of one axle over a pavement followed by a period of rest before the next axle. It is repeated 100 times while the applied load and deformation of the specimen are measured. This loading sequence is repeated 15 times at different values of confining pressure and deviator stress. The resilient modulus values are calculated by dividing the cyclic axial stress by the recoverable axial strain. The LTPP P46 protocol will be explained in further detail in section 2.1.1 of this report.

1.2 Small Strain Testing

The amount of strain developed when a material undergoes a loading depends upon the level of stress applied. For typical soils, the moduli observed at high strain levels will be smaller than those observed at low strain levels. Therefore, material comparison using modulus values is difficult; strictly controlled tests like LTPP P46 are needed to provide a standard range of stresses and strains [2].

However, there is another option. Atkinson and Sallfors [4] and Lai and Rix [5], among others, claim that the stress-strain curve is linear at strain levels below 0.001% for uncemented coarse-grained soils. In addition, the slope of the linear portion of the curve is the same as the initial slope of an unloading and reloading curve after nonlinear deformation has taken place (Figure 1.1). The modulus value over the linear portion of the curve in the stress-strain diagram is known as a material's maximum modulus, commonly denoted E_{MAX}, maximum Young's modulus, or G_{MAX}, maximum shear modulus. These maximum moduli allow for the direct comparison of stiffnesses because they are constant at small strain.

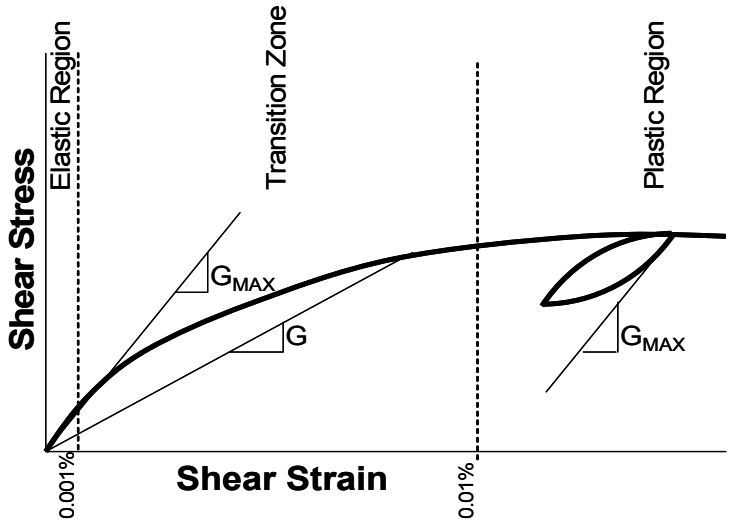

Figure 1.1: Modulus Variation With Strain Level

A laboratory method for testing these small strain moduli is the bender element. There are several different variations of bender elements currently being used, but the concept behind each apparatus is the same. Two small elements are inserted into opposite faces of a soil specimen. One of these elements is electrically excited and it produces small-strain shear and compressional waves that travel through the specimen. The element on the opposite side of the specimen receives the wave and the time history is recorded. After identifying the arrival times of the shear and compressional waves, it is possible to calculate Poisson's ratio and shear modulus of the soil being tested. The bender element system used in this study will be further detailed in section 3.1.2; the equations used in featured calculations are listed in section 4.3.

1.3 Organization

This report presents the results of the resilient modulus and small-strain bender element testing of several soils. Chapter 2 reviews the literature pertaining to the design and usage of a triaxial cell and bender element system. Chapter 3 contains a detailed description of the experimental setup and a summary of test procedures. Chapter 4 focuses on the discussion of test results. Chapter 5 summarizes and concludes the findings of this research.

Chapter 2
Literature Review

In recent years several protocols have been developed to measure the resilient modulus and small strain modulus values of soils. These quantities have been used in conjunction with pavement design and quality control processes. As a result, pavement engineering firms and agencies have devoted many resources toward the investigation of these quantities. Many of these studies recommend improvements to the testing apparatus and data interpretation algorithms. Their findings will be discussed as they relate to this research.

2.1 Resilient Modulus Testing

The concept of the resilient modulus was developed by the Strategic Highway Research Program in 1987. In subsequent years, several test protocols were suggested and discarded as implementation problems arose. Then, in 1996, the Federal Highway Administration (FHWA) set forth a standard protocol for M_R testing known as Long Term Pavement Performance Protocol P46 [2]. At this point, many pavement engineers were sufficiently convinced of the usefulness of the M_R parameter to acquire their own M_R test systems. A large amount of M_R data was produced and used in the late 1990s as the parameter became more heavily involved in pavement design processes.

In 2002 a new protocol, the National Cooperative Highway Research Program (NCHRP) 1-28A, was released to improve upon the old protocol [3]. There were several differences between the procedures. For example, NCHRP 1-28A has a larger number of test sequence variations for different soil classifications and the load pulse that simulates a traffic loading is lengthened from 0.1 s to 0.2 s. However, the primary difference for granular soils (which will be used in this study) is the number of loading sequences carried out; LTPP P46 requires cyclic testing at 15 different combinations of confining pressure and deviator stress while NCHRP 1-28A requires 30. In addition, NCHRP 1-28A requires deviator stress values much larger than those used by LTPP P46.

The decision was made to use LTPP P46 for this study. However, one M_R test was performed using NCHRP 1-28A to compare the modulus values. The results of this test, as well as itemized procedures from both protocols, are included in Appendix E.

2.1.1 Long Term Pavement Performance Protocol P46

LTPP P46 requires that the resilient modulus values of a soil specimen be determined by performing dynamic triaxial testing on a cylindrical soil specimen [2]. A haversine load pulse 0.1 s in duration simulates the passing of an axle over a pavement. This load pulse is followed by a 0.9 s period in which only a seating load equal to 10% of the peak stress is applied to the specimen while the soil recovers from the loading. An example segment of a load history from a M_R test is shown in Figure 2.1.

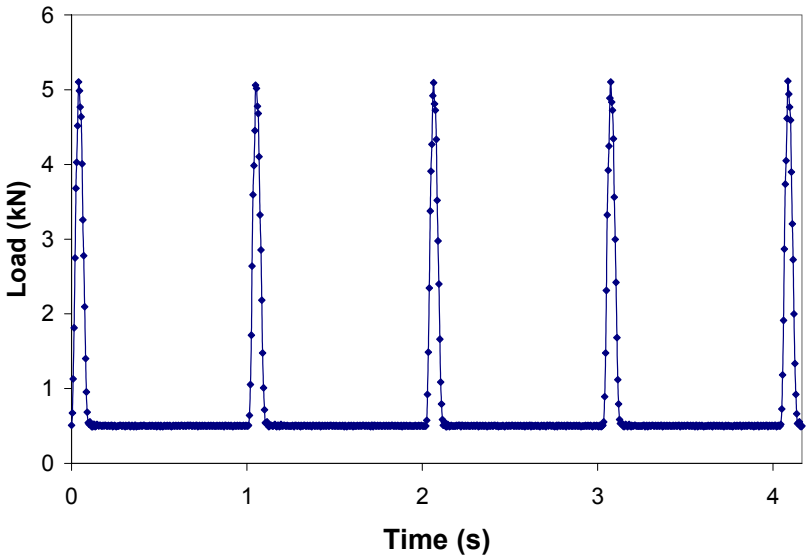

Figure 2.1: LTPP P46 Load History

This one second cycle is repeated 500 times at a particular confining pressure and deviator stress to condition the specimen before M_R data collection. The cycle is then repeated 100 more times in each of 15 data collection loading sequences. (Table 2.1) Resilient modulus values are calculated for the last five cycles in each loading sequence using a procedure contained in section 4.2.

Table 2.1: LTPP P46 Loading Sequences

Sequence Number	Confining Pressure	Max. Axial Stress	Cyclic Stress	Contact Stress	Load Applications
	kPa	kPa	kPa	kPa	
Conditioning	103.4	103.4	93.1	10.3	500
1	20.7	20.7	18.6	2.1	100
2	20.7	41.4	37.3	4.1	100
3	20.7	62.1	55.9	6.2	100
4	34.5	34.5	31.0	3.5	100
5	34.5	68.9	62.0	6.9	100
6	34.5	103.4	93.1	10.3	100
7	68.9	68.9	62.0	6.9	100
8	68.9	137.9	124.1	1.6	100
9	68.9	206.8	186.1	20.7	100
10	103.4	68.9	62.0	6.9	100
11	103.4	103.4	93.1	10.3	100
12	103.4	206.8	186.1	20.7	100
13	137.9	103.4	93.1	10.3	100
14	137.9	137.9	124.1	13.8	100
15	137.9	275.8	248.2	27.6	100

LTPP P46 requires specimens of different sizes depending on the gradation of the soil [2]. According to the protocol, a soil with less than 70% passing the No. 10 sieve and less than 20% passing the No. 200 sieve should be formed into specimens 152 mm (6 in.) in diameter. The soils provided by Mn/DOT fall into this classification. Therefore, specimens 152 mm (6 in) in diameter were used for this study.

LTPP P46 requires that the sample have its moisture content adjusted at least one night prior to testing [2]. This allows time for the moisture content to equilibrate overnight in a sealed container; the sample's moisture content is assumed to be uniform after this period. LTPP P46 requires that the specimen be compacted using a vibratory compactor such as an electric rotary

or demolition hammer. In addition, the specimen must be compacted in six 51 mm (2 in.) lifts to create a specimen 305 mm (12 in.) in height.

The lifts are compacted by the compactive effort of the rotary hammer acting on a compaction plate set on the surface of the sample within the mold; the purpose of the compaction plate is to spread the force evenly over the surface of the specimen. LTPP P46 requires that compaction plates be at least 13 mm (0.5 in.) in thickness and 146 mm (5.75 in.) in diameter to prevent soil from escaping around its edges. Following the compaction of each lift, LTPP P46 requires that the density of the specimen be calculated. Lastly, the specimen is moved to the load frame to undergo the loading sequences detailed in Table 2.1.

2.1.2 Equipment Modifications

LTPP P46 sets forth several requirements for M_R specimen preparation. However, the protocol leaves room for technicians to improve upon the standard triaxial apparatus if a superior option is available. As a result, many M_R testing laboratories have made adjustments to the triaxial cell and load frame that they believe to be beneficial. In particular, many researchers have proposed improvements to the specimen deformation measurement procedure. LTPP P46 requires no more than two linear variable differential transformers (LVDTs) measuring the displacement of the load shaft relative to the top cap on the exterior of the cell. However, Tatsuoka et al. [6] recommend measuring displacement values locally. They found that LVDT measurements on the exterior of the cell often overestimated the displacement within the specimen due to bedding errors near the platens. Furthermore, they found that this measurement error was noticeable during both cyclic and static testing for a wide range of strains. These findings, as well as similar reports from other researchers, prompted the development of systems designed to measure the specimens' deformations locally by fixing three LVDTs to the surface of the specimen.

Cuccivillo and Coop [7] note that the verticality of the LVDTs may be difficult to guarantee using this arrangement; the orientation of the LVDTs may be affected by specimen barreling, tilting, and plastic deformations. However, Cuccivillo and Coop point out that the error produced by tilted LVDTs is relatively small; a relatively large 8° angle between an LVDT and a specimen would reduce the LVDT's axial displacement reading by only 1%. In most

specimens, any LVDT tilting that occurs will have a far smaller angle and, therefore, its affect on the axial displacement reading will often be negligible.

LTPP P46 does not require that the load cell be placed in any particular location relative to the specimen and chamber as long as the axial force is measured directly. However, it is considered good practice to place the load cell inside of the pressure vessel. An interior placement ensures that any affects from the friction produced along the load shaft will not appear in the load data. Also, when placing the load cell internally there are fewer interfaces between the load cell and specimen within which similar problems may develop.

It is often recommended that the aggregate present in a soil specimen be no larger than 10% of the specimen's diameter. Triaxial testing is based on the assumption that the specimen is relatively uniform; aggregate larger than 10% of the specimen's diameter is too large for this assumption to be valid. Therefore, it is recommended that all aggregate over this threshold be removed from samples prior to specimen preparation.

2.2 Bender Element Testing

Bender elements are short, piezoelectric cantilever strips that contact a specimen. Motion is triggered in the piezoelectric material by sending an electrical pulse to one of the elements; this ultimately produces compressional (P) or shear (S) waves in the soil depending upon the orientation of the piezoelectric material (Figure 2.2).

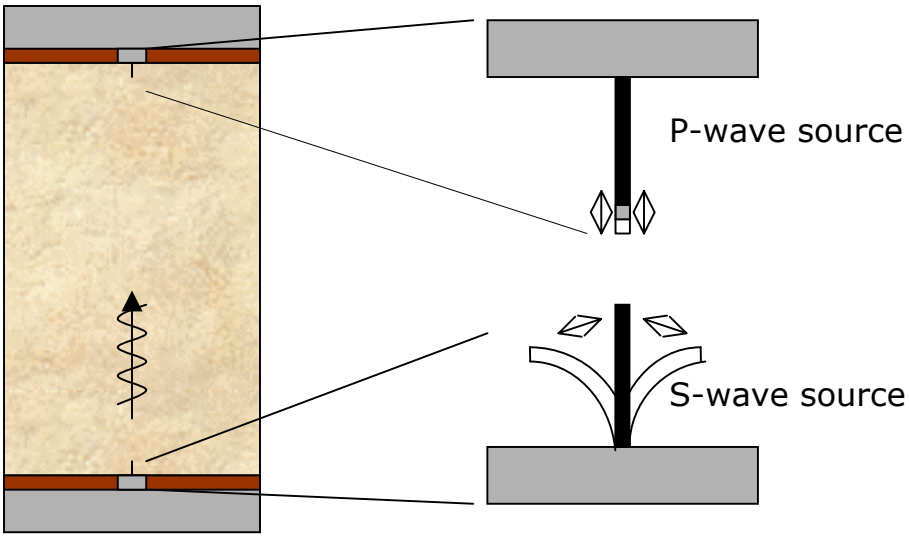

Figure 2.2: Bender Element Wave Generation

The wave produced by the element propagates through the specimen and induces a voltage in a second bender element located on an opposing surface. A number of quantities, including small strain modulus values, can be calculated by recording the time histories of these waves. This calculation procedure is contained in section 4.3.

2.2.1 Density Effects

The small strain shear modulus is calculated using:

$$G = \rho c_s^{\,2} \tag{2.1}$$

where G is the shear modulus, ρ is the density, and c_s is the shear wave speed. Therefore, the density of the soil is an important quantity and it should be carefully monitored throughout M_R testing to ascertain that the correct value of ρ is used for the time at which the bender element test is performed.

The density variation produced by cyclic loading and changes in confinement influence the value of G. The density of a specimen is difficult to measure after being sealed in a chamber. Therefore, only the initial value of density is readily available for use in equation (2.1). The assumption must be made that the change in density over the course of the test is negligible. Jovicic and Coop [8] studied the effects of confining pressure on the density of three different sandy soils by steadily increasing confinement to 138 kPa (20 psi), which is the maximum value of confining pressure in LTPP P46, while periodically taking measurements. Jovicic and Coop observed increases in density of up to 2% over this range. However, Jovicic and Coop were quick to note that the average density increase was closer to 1% and that this amount of error is often negligible in soil testing.

A second cause of density increases in triaxial testing is the applied loading. The only method by which changes in specimen density due to loading can be measured is by calculating the density of a specimen before and after testing. This often proves difficult because accumulated plastic deformations typically cause specimen barreling, which makes it difficult to model the volume of the specimen. Limited measurements performed for this study indicated that the density increase was no more than 2% due to the applied loading.

2.2.2 Wave Speed Effects

A second variable that affects the calculation of G is the shear wave speed, which is squared in equation (2.1). As a result, G is more sensitive to variation in the wave speed of a specimen than it is to variation in its density. Small variations in the shear wave speed that are not the result of variation in a material's modulus have the potential to introduce significant error into the calculation of G. Therefore, it is important to identify potential sources of this error.

One variable that affects the shear wave speed in a soil is the strain level induced by the shear wave. The stress-strain curve is assumed to be linear at small strain values; G is at its maximum value in this region (G_{MAX}). However, if the shear strain passes the elastic limit, G begins to deviate from G_{MAX}. Atkinson and Sallfors [4] suggest that the strain level dividing the elastic and elastoplastic regions of the stress-strain plot, known as the elastic limit, is 0.001% for sandy soils. Figure 1.1 shows examples of modulus behavior within differing regions of the stress-strain plot. Lai and Rix [5] agree that 0.001% is an accurate estimate of the elastic limit for sands. However, they note that the elastic limit for fine-grained materials is an order of magnitude or larger. Fortunately, bender elements produce shear strains significantly below the 0.001% elastic limit suggested by the literature. As a result, the assumption that bender elements measure G within the linear portion of the stress-strain curve (G_{MAX}) should be reasonable regardless of a soil's composition.

Another variable that may affect the calculation of G is the strain rate of the test. Iwasaki et al. [9] and Bolton and Wilson [10] demonstrated that there was a strong correspondence between sand specimens' dynamic and continuous static loading stiffnesses by comparing the results from resonant and torsional shear tests. They concluded that the value of G is not rate dependent for sands. However, Jovicic and Coop [8] point out that there are no displacement transducers capable of accurately measuring the strains produced by bender elements. They state that G_{MAX} may be sensitive to the shear strain rate for these strain levels.

2.2.3 Research Recommendations

A number of other issues merit consideration while performing bender element tests during a cyclic triaxial test. To begin with, the effects of the load pulses, dither, and electrical noise of the load frame on the bender element system are largely unknown. Therefore, Jovicic and Coop [11] recommend performing bender element measurements during periods in which the specimen is not being loaded axially. They also recommend powering down all nearby equipment to prevent it from affecting the data; this includes the load frame and other instrumentation.

In separate studies, Jovicic and Coop [12] and Schmertmann [13] found that periods of rest between bender element tests may induce volumetric creep due to the confining pressure and aging processes within the specimen. The apparent aging of the specimen results in a small increase in G_{MAX} with no measurable volumetric change. Jovicic and Coop found that sand specimens are particularly vulnerable to these time-dependent processes; one specimen underwent a 10% increase in G_{MAX} after being allowed to rest for one hour between tests. Furthermore, they noted that this effect was proportionally worse for specimens being tested at lower stress levels and for specimens undergoing their first loading. LTPP P46 does not require any significant pauses between testing sequences [2]. However, small amounts of volumetric creep may occur simply due to the length of the M_R test, which lasts more than one hour.

Chapter 3
Test Procedure

LTPP P46 has specific requirements regarding the instrumentation used to test the resilient modulus values of a soil [2]. In addition, this study requires that several modifications be made to the standard resilient modulus test system. The load cell and LVDT instrumentation must be capable of accurately measuring the load and displacement values produced during the protocol's loading sequences. The load frame must be large enough to accommodate the cell, be capable of producing the forces required in the protocol, and have a known phase angle. The triaxial cell must be capable of accommodating cylindrical specimens 152 mm (6 in.) in diameter with functioning bender elements mounted inside its platens. In addition, this cell must be able to allow the load cell and LVDTs to work while in contact with the specimen. The components of this test system, the composition of the soil samples, and the test procedure followed during this study will be discussed. A step-by-step list of the test procedure is included in Appendix E.

3.1 Test Equipment

A large variety of equipment was necessary to perform the testing desired for this study. A bender element system was purchased and incorporated into triaxial platens. A triaxial cell meeting the requirements of both LTPP P46 and the bender element instrumentation was designed and manufactured. Load cell and LVDT instrumentation were purchased and incorporated into the cell. The design and use of this equipment is contained in this section.

3.1.1 Triaxial Cell

The first objective of this study was to create a triaxial cell that meets the requirements of LTPP P46, the bender element system, and the internal instrumentation. LTPP P46 requires that the triaxial cell be large enough to contain a cylindrical specimen 305 mm (12 in.) in height and 152 mm (6 in.) in diameter that can withstand internal pressures of at least 170 kPa (25 psi). The bender element system requires upper platens at least 30 mm (1.2 in.) in thickness as well as two

pressure feedthroughs for its cords. The load cell requires 60 mm (2.4 in.) of open space above the specimen, and the LVDT apparatus requires at least 13 mm (0.5 in.) of open space around the specimen's diameter.

A triaxial cell meeting these specifications was purchased from Research Engineering (Grass Valley, CA); Figure 3.1 is a diagram of this cell.

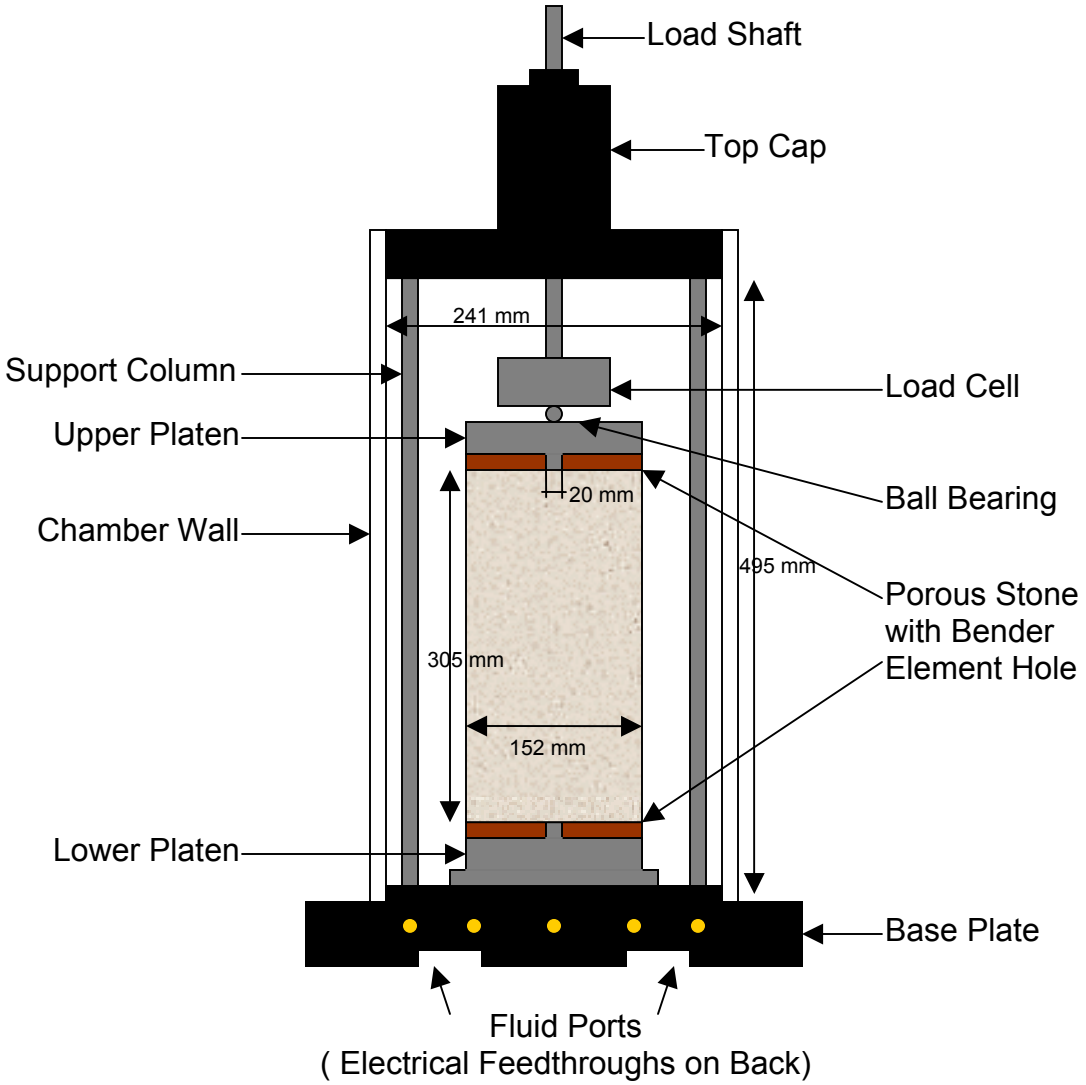

Figure 3.1: Triaxial Cell Diagram

The interior of the cell is 495 mm (19.5 in.) in height, 241 mm (9.5 in.) diameter, and bounded by a plexiglass chamber 13 mm (0.5 in.) in thickness. A brass port in the front of the base plate serves as the connection for the air supply. Four more of these ports are mounted on either side of the air supply connection; these lead to tubing which connects to ports on the platens. They are used to control the air and water pressure within a specimen. Seven electrical feedthroughs pass from the back of the base plate to the interior of the cell. The chamber is sealed by O-rings mounted on vertical surfaces of portions of the top cap and base plate around which the chamber fits. Three steel columns located on the cell's interior maintain proper spacing between the base plate and top cap. Figure 3.2 is a photograph of the cell in use during a test.

Figure 3.2: Triaxial Cell Containing Specimen

The platens used in the triaxial cell were specially designed to house the bender elements. Each platen is 152 mm (6 in.) in diameter and contains two ports for air and water supply tubes. In addition, each platen was designed with a 20 mm (0.79 in.) cylindrical hole in the center for the bender element transducers. The S-wave emitter is housed in the lower platen, and the P-wave emitter is housed in the upper platen. The cords from each element are run from the interior of the platen to the triaxial cell's electrical feedthroughs. It was necessary to cut 20 mm circles in the center of each platen's porous stones to allow the bender elements access to the specimen. The platens and one of the bender element transducers are shown in Figure 3.3.

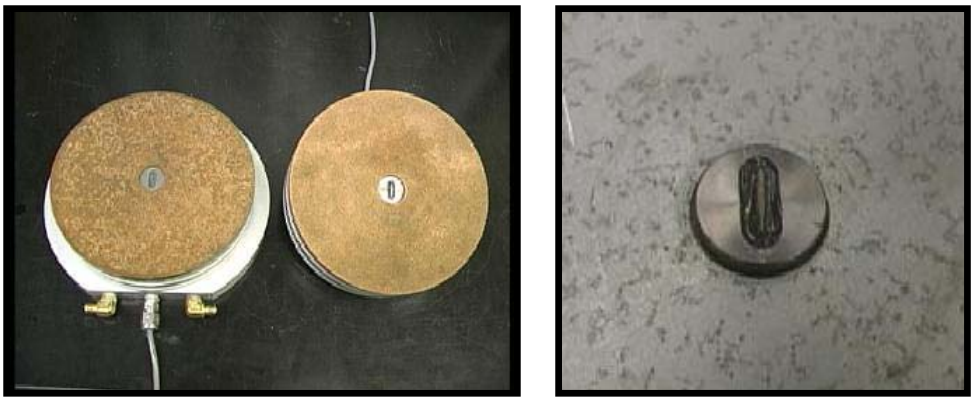

Figure 3.3: Bender Element Incorporation Within Platen

3.1.2 Load Cell and LVDTs

The triaxial cell contains three types of instrumentation: a load cell, three LVDTs, and a bender element system, which will be discussed in section 3.1.3. The load cell (Figure 3.4) has a flat, "pancake" style and a 22.2 kN (5 kip) capacity. This load cell is used to measure the axial force applied to the specimen. It is screwed onto the load shaft above the specimen and presses directly against the ball bearing on the upper platen. This placement allows for the axial load to be measured with a minimum of interfaces between the load cell and specimen. The calibration for this load cell is included in Appendix B.

Figure 3.4: Load Cell

The three LVDTs used to measure the specimen's deformation in this system have 12.7 mm (0.5 in.) strokes and spring-loaded tips (Figure 3.5). These LVDTs are positioned at equal distances around an aluminum collar, which clings to the specimen's membrane. A second

collar clings to the specimen 152 mm (6 in.) below the first, which has columns mounted below the positions of the LVDTs as contacts for the spring-loaded tips of the instruments. This arrangement allows the two collars to move independently of each other. Therefore, the displacement of the axially-mounted LVDTs should mirror the deformation of the specimen over the 152 mm (6 in.) gage length. Spacers hold the collars 152 mm apart while the apparatus is placed on the specimen to make certain that the correct distance is maintained between the collars.

Figure 3.5: LVDT Collars with Spacers

3.1.3 Bender Element System

The bender elements used to measure the wave speeds in this study were manufactured by GDS Instrumentation (London, England). These elements are short cantilevers composed of small strips of piezoelectric metals separated by a non-conductive buffer. This cantilever can be made to bend in particular ways by applying a voltage to the piezoelectric materials. One of the two elements used in this research has its two piezoelectric strips polarized in the same direction. Therefore, the cantilever arcs when a voltage is applied; this produces a shear wave (S-wave) in the surrounding soil. The second element's piezoelectric strips are polarized in opposite directions. Therefore, the cantilever undergoes a change in length when a voltage is applied; this produces a compression wave (P-wave) in the material. This process is sketched in Figure 2.2.

The bender elements manufactured by GDS Instrumentation are designed to be used as inserts for the platens bounding a triaxial specimen. A wave produced by one of these elements travels through the soil specimen and causes the opposing element's cantilever to deflect; the history of the voltage that this induces is a record of the received waveform. Therefore, the element that emits S-waves also receives P-waves. Likewise, the element that emits P-waves receives S-waves. A photograph of an element mounted within one of the porous stones is included as Figure 3.6.

Figure 3.6: Bender Element Cantilever Strip

The bender elements are controlled by the Bender Element System (GDS-BES) program. It is possible to change the frequency, amplitude, and time history of the electrical pulse applied to the elements using this program. The testing performed in this study makes use of a 5,000 Hz haversine pulse for P-waves and 2,000 Hz pulse for S-waves. It was demonstrated in section 2.2.2 that the frequency of the pulse does not significantly affect the wave speed over this range. Therefore, the 5,000 and 2,000 Hz values were used because they tend to induce the cleanest initial deflections within the received traces. The waves were emitted using the largest amplitude available within the system, 14 V, so that the signal can be distinguished from environmental noise.

3.1.4 Load Frame

The servo-hydraulic load frame (MTS Systems, Eden Prairie, MN) has a maximum capacity of 22.2 kN (5 kips) and a maximum stroke of 102 mm (4 in.). This frame's actuator is mounted in a crossbeam capable of being raised and lowered to accommodate cells of different sizes, which rest on a steel plate at the base of the frame. The system is operated using a digital controller named MTS TestStar.

The delay between the load and displacement histories caused by this frame was calculated to be 0.014 ms using the procedure recommended by LTPP P46. This results in a phase angle of 0.25°. The complete phase angle data for each LVDT are contained in Appendix B.1. A photograph of the load frame is included as Figure 3.7.

Figure 3.7: Load Frame

3.2 Soil Samples

Mn/DOT provided six soil samples for use in this study (Figure 3.8). These samples were selected to represent the range of granular materials that would be classified as "selected granular or granular" subbase in pavement structures throughout Minnesota.

Figure 3.8: Labeled Soil Samples

These samples were collected as part of a larger study being performed by Mn/DOT. Therefore, each was assigned an identification letter; the soils obtained for this study are A, D, F, H, J, and N (Table 3.1).

Table 3.1: Soil Sample Data

Identification Letter	Description	Fines Content	Maximum Density	Optimum Moisture Content
	(AASHTO, ASTM)	%	kg/m^3	%
A	Well-graded sand with gravel (A-1-a, SW)	3.6	2158	7.9
D	Well-graded sand (A-1-b, SW)	4.3	1839	10.0
F	Fine sand with 10% fines (A-3, SP-SM or SP-SC)	10.3	1900	9.3
H	Fine sand with 21% fines (A-2, SM or SC)	21.4	1725	12.6
J	Fine sand (A-3, SP)	2	1791	9.5
N	Well-graded sand with 7% fines (A-1-b, SW-SM or SW-SC)	7.4	2014	8.8

Mn/DOT performed gradations and standard Proctor compaction data for these samples; the data are included in Appendix A. These charts and tables indicate that the properties of the soils vary significantly; both coarse and fine-grained materials are included.

A common guideline for triaxial testing requires that all aggregate larger than 10% of the diameter of the specimen be removed from the sample in order to ensure specimen homogeneity. The diameter of the specimens is 152 mm. Therefore, the specimens should not contain aggregate larger than 15.2 mm (0.6 in.) in diameter. In addition, the waves produced by

the bender elements must follow direct paths for accurate wave speed measurements; large aggregate may obstruct the path and interfere with the measurement. Due to these considerations, all aggregate larger than 13 mm (0.5 in.) in diameter was removed from these samples. However, only sample A contained enough large aggregate for it to compose a significant percentage of its mass. Figure 3.9 shows a portion of the large aggregate removed from sample A.

Figure 3.9: Oversized Aggregate

3.3 Specimen Preparation

The preparation of a soil specimen for a resilient modulus test is a lengthy procedure that begins at least one day prior to testing. LTPP P46 requires that the sample being used to prepare the specimen have its moisture content adjusted at least one day prior to the test to allow it time to temper [2]. In this study, the moisture adjustment began approximately 24 hours prior to testing with the placement of 25 kg of the sample to be used in a large, airtight container (Figure 3.10).

Figure 3.10: Tempering Container

The amount of water necessary to bring the sample to the target moisture content was calculated using:

$$W_{aw} = W\left(\frac{\omega - \omega_1}{100}\right) \tag{3.1}$$

where W_{aw} is the weight of water to add, W is the weight of the sample, ω is the desired moisture content, and ω_1 is the current moisture content. This water was added to the sample by sprinkling small amounts over its entire surface while mixing thoroughly. After adding the water, three moisture content samples were taken from several different locations within the container and placed in an oven overnight at 52° C (125° F). The container was then sealed and the soil's moisture content was left to equilibrate.

The following day the moisture contents samples were removed from the oven and the sample's moisture content was calculated. If the moisture content of the sample was within 0.5% of the desired moisture content, then the sample was prepared for compaction. If the measured moisture content was outside of the acceptable range, however, it was necessary to make a second adjustment. Additional water or dry soil was added until the correct moisture content was achieved.

3.3.1 Compaction

LTPP P46 requires that specimens be compacted in six lifts using vibratory compaction [2]. This compaction took place on a countertop near the load frame. The rubber membrane used to surround the specimen was slid over the bottom platen and porous stone and sealed with two O-rings. The vacuum mold was placed on top of the platen and sealed with two ring clamps. The upper clamp was placed over the portion of the membrane emerging from the vacuum mold to hold it in place. A 30 kPa (4.2 psi) vacuum was applied.

Before compacting the soil, it was necessary to protect the lower platen's bender element from large aggregate by covering it with a small amount of fine sand (Ottawa 50-70). The rationale behind this protection is discussed in section 3.3.3. After adding the buffer sand the entire mold was weighed.

The target density values of each lift were calculated using the compaction data provided by Mn/DOT. The peak of the compaction curve is the standard Proctor maximum density for the soil; the target densities for this testing are these peaks for each soil. An example compaction curve from sample A is contained in Figure 3.11; the data from the other samples are provided in Appendix A.

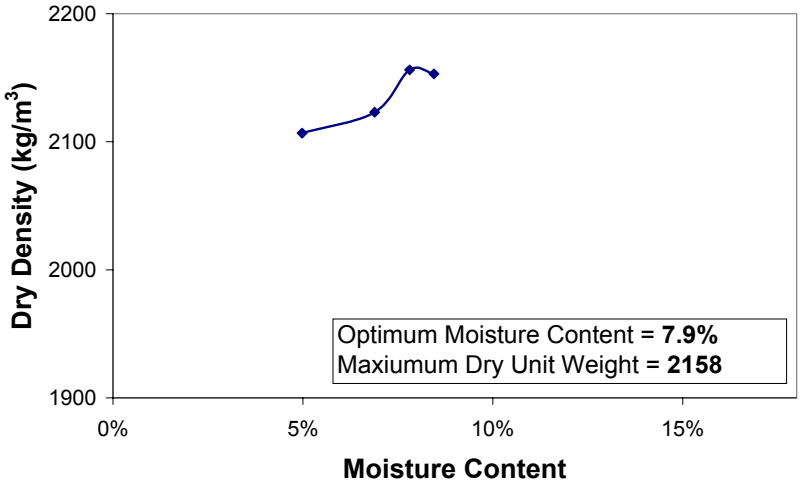

Figure 3.11: Compaction Data for Sample A

The amount of soil necessary to create a 51 mm (2 in.) lift with the target density was placed inside the vacuum mold. The soil was covered by a plastic spacer, measuring 149 mm (5.875 in.) in diameter and 3 mm (0.125 in.) in thickness, and the compaction plate, measuring 149 mm (5 7/8 in.) in diameter and 25 mm (1 in.) in thickness. The purpose of the spacer was to prevent the soil from sticking to the compaction plate. The bit of the vibratory hammer was then lowered into the mold and pressed into a depression on the compaction plate's surface with approximately 100 N (22 lbf) of force. The hammer was then run at 3,000 beats per minute until the desired density was achieved. Compaction lasted between 5 and 60 seconds depending on the sample.

If calculated density of any of the lifts was significantly larger than the target density, the lift was loosened and compacted a second time. Following the compaction of the sixth lift, the surface of the specimen was smoothed so that the platens would be parallel during testing. Several steps from the compaction process are shown in Figure 3.12.

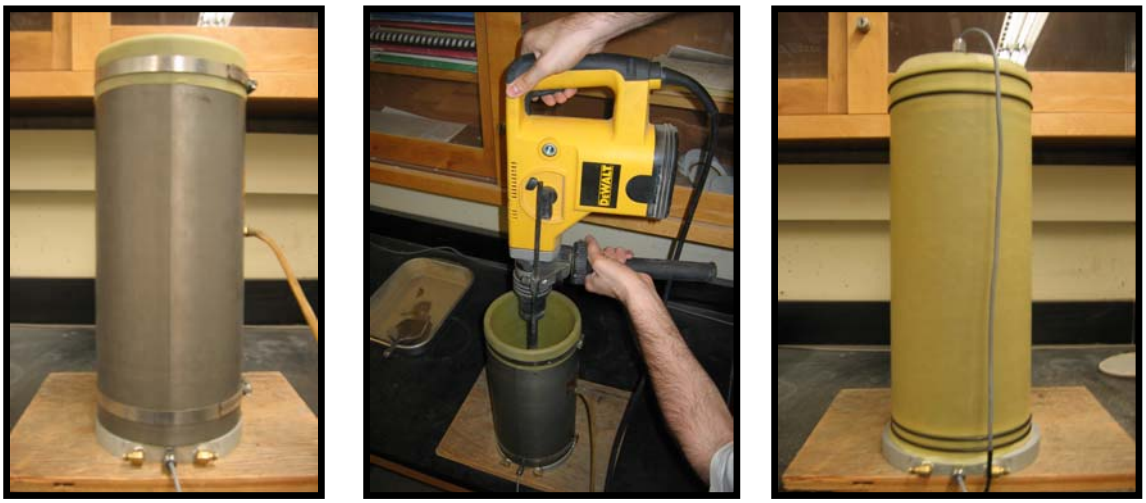

Figure 3.12: Stages of Specimen Preparation

The porous stone was placed on top of the specimen after creating the bender element protection layers as described in section 3.3.3. The hole in the center of the stone was partially filled with the fine sand used to protect the element. The amount of sand in this hole was

adjusted until the transducer and platen sat on top of it evenly and it could be seen that the transducer was pressing into the soil. O-rings were used to seal the membrane and the vacuum supply was shut off. All of the specimens prepared contained enough cohesion to hold the specimens together without confinement.

A second membrane was pulled over the first after removing the split vacuum mold. The pounding of the rotary hammer caused small tears in some of the specimens' membranes. Therefore, it was necessary to make certain that the specimen remained sealed using this additional membrane. Lastly, O-rings were placed over the surface of the outer membrane to seal it.

3.3.2 Percometer Measurements

The Percometer (Figure 3.13) is a portable instrument manufactured by Adek (Saku, Estonia) that measures a soil's dielectric permittivity and conductivity. It consists of a small, battery powered microprocessor connected to an electrode by a cord approximately 2 m (6 ft) in length. The microprocessor directs the electrode to produce a sequence of electrical signals when pressed against a material's surface. The microprocessor then calculates dielectric permittivity and conductivity values from the received data and displays them on-screen. These quantities can be used to estimate the test material's volumetric moisture content. However, the equation for doing so varies with the soil type.

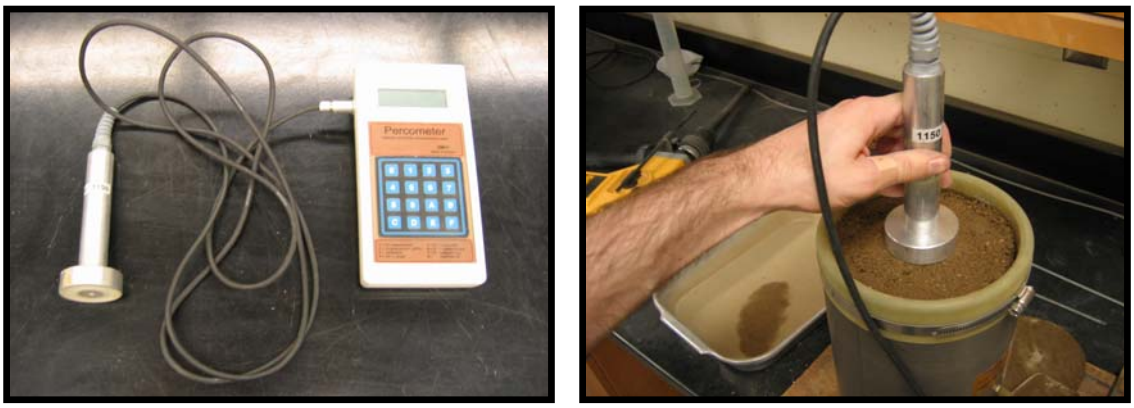

Figure 3.13: Percometer Measurement

In this study, the Percometer was used on the surface of the specimen following compaction. Three measurements were taken across a diameter of the compacted specimen in order to account for any edge effects from the aluminum split mold.

3.3.3 Bender Element Protection

It was necessary to provide the bender elements with protection against the larger aggregate present within some of the soil samples (Figure 3.14). Aggregate had the potential to migrate upward during the M_R cycles until coming into contact with the upper element. Over the course of the test, some of the aggregate may have been pressed into the cantilever hundreds of times. At two points during this research, the upper element was damaged by this phenomenon. This caused delays in testing as well as the loss of some data.

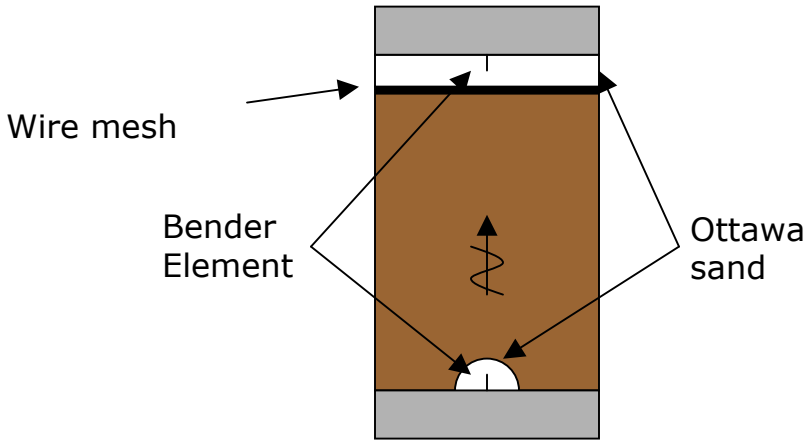

Figure 3.14: Bender Element Protection System

This damage to the bender elements made it necessary to implement a system for protecting the transducers. It was found that the best method for doing this consisted of surrounding each bender element with a layer of fine sand. This layer was sufficient protection for the lower element. However, it was necessary to place a thin wire mesh over the surface of the specimen to protect the upper element from migrating aggregate. The mesh was placed after the Percometer measurements and covered by approximately 5 mm (0.2 in.) of moistened fine (Ottawa 50-70) sand. The sand was compacted using a short burst from the rotary hammer. Figure 3.15 contains photographs of this process.

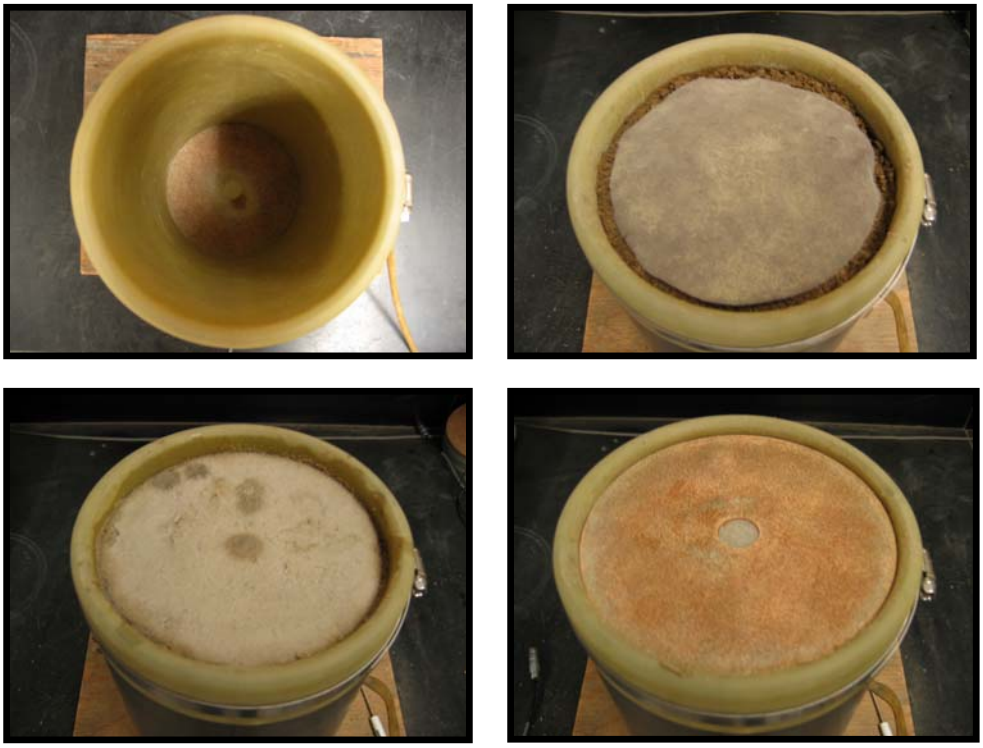

Figure 3.15: Stages of Element Protection

3.4 Specimen Testing

The testing of a soil specimen began by placing it inside of the triaxial cell. The specimen was carefully lifted from the compaction surface by hand and lowered into the triaxial cell; a short stub rising from the base of the cell fit into a hole in the lower platen to center the specimen. The LVDT apparatus was slid into the cell and placed over the middle of the specimen; each of the collars was made to grip the specimen by bridging the open section of the apparatus with an O-ring. The three spacers separating the collars were removed so that they could move in relation to each other as the specimen deformed. With the LVDT apparatus in place, the cords from the LVDTs, bender elements, and load cell were attached to the electrical feedthroughs and the fluid tubing was attached to the exterior of the cell. The plexiglass chamber was slid into place over

the specimen and supports. Figure 3.16 shows a photograph of the specimen following the placement of this chamber.

Figure 3.16: Specimen Loaded within Triaxial Cell

The entire triaxial cell was then lifted and slid into the load frame. The cords from the signal conditioners were attached to the electrical feedthroughs. The triaxial cell's load shaft, with the top cap and load cell attached, was screwed onto the load frame's shaft. The load cell's cord was attached and the ball bearing was placed on the top of the upper platen. The top cap was then lowered into position and held in place using three bolts. Two circular plates on the top cap were rotated over the top of the chamber to prevent it from sliding upward during the test.

3.4.1 Resilient Modulus Test

The resilient modulus test protocol in this study followed the confining pressure and deviator stress sequence required by LTPP P46 (Table 2.1). The only modification made to the protocol for the purposes of this research was the complete removal of the axial load before and after changes in the cell's confining pressure; these short rest periods were used to perform the bender element tests.

The first step in the test protocol was the pressurization of the cell for the conditioning loading sequence. The confining pressure was manually adjusted by turning a knob on the

pressure transducer shown in Figure 3.17 and watching a pressure gage as the system came to equilibrium; this process often took several minutes. Once the pressure within the chamber came to equilibrium, the load shaft was lowered until the load cell came into contact with the ball bearing and a small contact pressure was applied to the specimen.

Figure 3.17: Fluid Pressure Transducer

A data collection program named "M_R Data Acquisition" was opened on the personal computer connected to the instruments' signal conditioners. This program was created using LabVIEW (National Instruments, Austin, TX). The program recorded data from the load cell, the stroke LVDT, and the three LVDTs attached to the specimen at a rate of 200 points per second.

A system control routine named "M_R Test - Final External" was opened within TestWare. This routine contained the load paths for each loading sequence in the M_R test. After completing all of the above steps, M_R Data Acquisition was launched followed immediately by M_R Test – Final External to begin the first loading sequence.

Each loading sequence in this test consisted of haversine load pulses 0.1 s in duration followed by 0.9 s of soil recovery time. A small contact load was held on the specimen during the recovery period equal to 10% of the maximum axial stress. An example of the displacement produced by these cycles is contained in Figure 3.18.

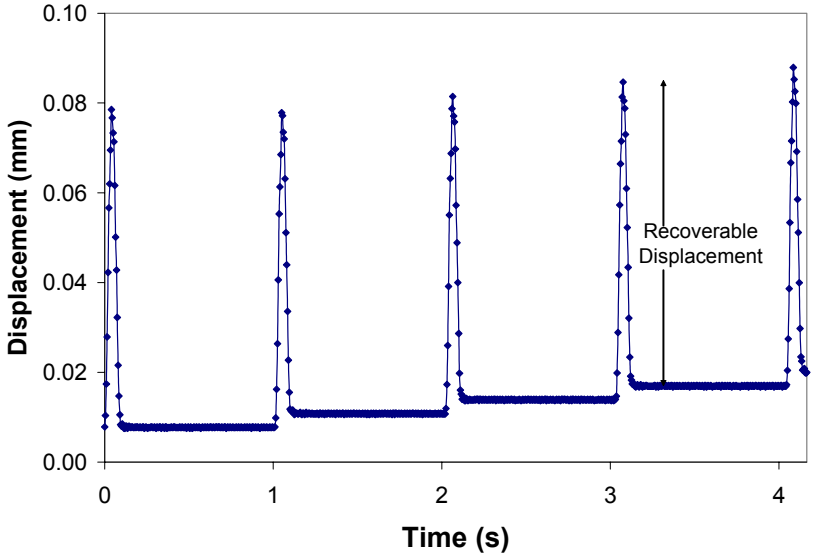

Figure 3.18: M_R Test Displacement History

These cycles were repeated 500 times during the conditioning loading sequence and 100 times during each of the subsequent data loading sequences. Each of these loading sequences took place at the deviator stress and confinement levels in Table 2.1 and was initiated in the same manner as the conditioning sequence. M_R Data Acquisition saved the data from each loading sequence in a file named, for example, "N8 3-3 1-15," where N was the sample used to make the specimen, 3-3 was the confining pressure and deviator stress values in psi, and 1-15 was the date of the test. These files were converted into resilient modulus values using the process described in section 4.2.

Bender element testing was carried out immediately preceding and following each change in confinement on Table 2.1. After the completion of the final loading sequence at a particular level of confinement, the load shaft was removed from the surface of the specimen and all unnecessary electrical equipment was shut down. The GDS-BES program was then used to produce a 2,000 Hz S-wave pulse at the largest amplitude possible, 14 V. The time history induced in the opposing element by the resulting wave was recorded for 5 ms. This process was repeated fifty times to produce fifty time histories. These histories were automatically stacked to

reduce noise in the data and a composite trace was displayed on-screen. A function within GDS-BES allowed the point at which the S-wave arrived at the receiving element to be manually selected from the on-screen trace. The program automatically calculated S-wave speed values for each wave based on the identified arrival; these values were recorded in a spreadsheet and later converted to E_{MAX} values using the process described in section 4.3. Fifty 5,000 Hz P-wave pulses were generated and analyzed in the same manner following the completion of the S-wave testing. The source and receiver time histories from a typical P-wave bender element test are shown in Figure 3.19.

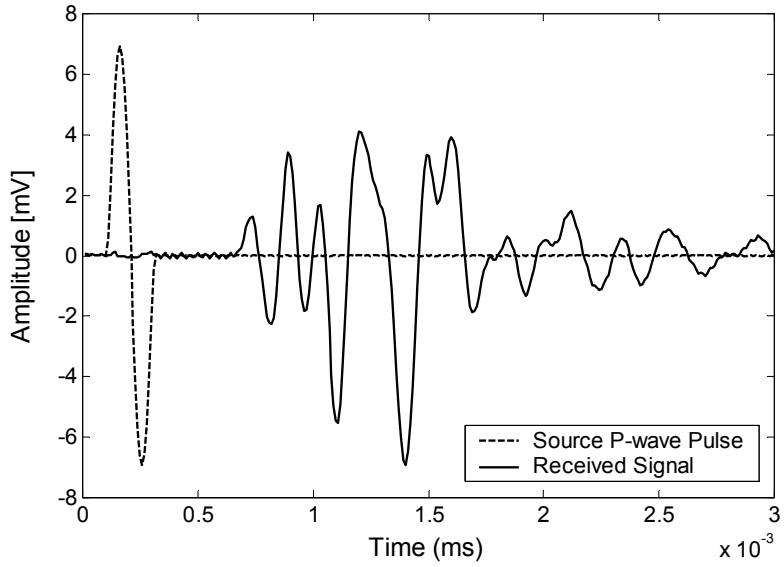

Figure 3.19: P-Wave Source and Receiver Time Histories

3.4.2 Shear Strength Test

The final load path programmed into M_R Test – Final External was a shear strength test. A small contact load was applied to the specimen following the completion of the LTPP P46 load sequences. M_R Data Acquisition and M_R Test – Final External were launched following the same procedure used for the LTPP P46 loading sequences. The specimen was loaded at a constant rate of 0.76 mm/s (0.03 in./s); this rate was used by Mn/DOT during the shear strength tests. The loading continued until the specimen failed and the observed axial load began to fall.

At this point the actuator was halted and load was slowly removed from the specimen. The results from a typical shear strength test are shown in Figure 3.20.

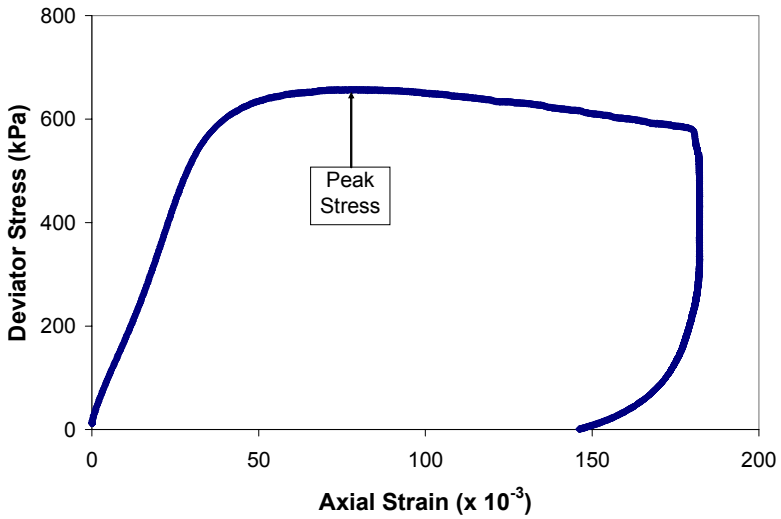

Figure 3.20: Specimen Failure

After completing the test protocol on a particular specimen, the process was repeated on an identical specimen to test the repeatability of the data. Therefore, the original specimens and their repeats were able to have their shear strength measured at two different levels of confinement. The shear strength of the first specimen was measured at a confining pressure of 27.5 kPa (4 psi). The shear strength of the second specimen was measured at 55.1 kPa (8 psi). These data were used to calculate the cohesion and friction angle of the soil using the process described in section 4.4.4.

Chapter 4
Discussion of Results

The six soil samples were tested at three moisture contents at one density using the procedures described in Chapter 3. The load and displacement data files from the loading sequences were input into a MATLAB program to calculate resilient modulus values. The wave speeds measured by the bender elements were used to calculate maximum Young's modulus values. The values generated by these procedures were checked for reasonability and repeatability. Lastly, the hyperbolic model was used to create degradation curves for these data.

4.1 Testing Schedule

Resilient modulus and maximum Young's modulus values were determined for six soil samples at three values of moisture content each. These 18 tests were each repeated one time. In total, the test procedure for this study was performed on 36 different soil specimens.

Mn/DOT provided standard Proctor compaction data for each soil sample so their optimum moisture content and maximum density values were known. Using these data, it was decided that the soil samples should be tested at a moisture content near the optimum moisture content, at a moisture content near the "dry" moisture content of these soils in the field, and at a value halfway between optimum and "dry". Soils rarely have moisture contents below approximately 3% in the field. Therefore, the majority of the "dry" moisture content values were selected near this value. Each of these samples was compacted to its maximum dry density. Table 4.1 contains the sample, moisture content, and dry density data for each test.

Table 4.1: Test Matrix

Sample	Description	% Fines	Standard Proctor		Test Number	Target Moisture Content
			Optimum Moisture Content	Maximum Dry Density		
	(AASHTO, ASTM)	%	%	kg/m^3		%
A	Coarse sand with large aggregate (A-1-a, SW)	3.6	7.9	2158	1,2	2.5
					3,4	5.0
					5,6	7.5
D	Well-graded sand (A-1-b, SW)	4.3	10.0	1839	7,8	3.0
					9,10	6.0
					11,12	9.0
F	Poorly graded fine sand with 10% silt (A-3, SP-SM or SP-SC)	10.3	9.3	1900	13,14	3.5
					15,16	6.0
					17,18	8.5
H	Poorly graded fine sand with 20% silt (A-2, SM or SC)	21.4	12.6	1725	19,20	3.0
					21,22	7.0
					23,24	11.0
J	Poorly graded fine sand (A-3, SP)	2	9.5	1791	25,26	3.5
					27,28	6.0
					29,30	8.5
N	Well-graded sand (A-1-b, SW-SM or SW-SC)	7.4	8.8	2014	31,32	3.0
					33,34	5.5
					35,36	8.0

4.2 Resilient Modulus Data Interpretation

The load and displacement data recorded by M_R Data Collection was stored in 15 separate data files following the test. Each of these data files consisted of the load, stroke, and three LVDT displacement values recorded during the test. A MATLAB (Mathworks, Natick, MA) program titled "M_R Calculator" was written to convert these data files into resilient modulus values. The program searched for local maxima in the load and three displacement data sets; these peak values correspond to the peak load and displacement pulses observed during the haversine load pulse. Therefore, 100 load and displacement values were identified in each column. The

program then calculated baseline load and displacement values during the material recovery periods of each cycle averaging the data over the final 0.75 seconds of each one second cycle, as instructed by LTPP P46.

M_R Calculator determined the recoverable axial displacement of each LVDT (d_1, d_2, and d_3) by subtracting the baseline displacement during the recovery period from the peak displacement. The recoverable axial strain, ($\Delta\varepsilon_a$), was calculated by averaging the three recoverable displacement values and dividing by the gage length (l_o):

$$\Delta\varepsilon_a = \frac{\frac{1}{3}(d_1 + d_2 + d_3)}{l_o} \tag{4.1}$$

The cyclic axial stress ($\Delta\sigma_a$) induced in the specimen was the peak load (P_{max}) less the load during the recovery period (P_o) divided by the cross-sectional area of the specimen:

$$\Delta\sigma_a = \frac{(P_{\max} - P_o)}{\pi * r^2} \tag{4.2}$$

An M_R value was calculated by dividing the cyclic axial stress by the recoverable axial strain:

$$M_R = \frac{\Delta\sigma_a}{\Delta\varepsilon_a} \tag{4.3}$$

This calculation was repeated for each of the final five cycles in the loading sequence. In addition, M_R Calculator also determined the mean stress, θ, for each loading sequence:

$$\theta = \frac{\sigma_1 + 2\sigma_3}{3} \tag{4.4}$$

where σ_1 - σ_3 is deviator stress of σ_3 (confining pressure). M_R Calculator exported these values to a data file after the calculations were performed for each of the 15 cycles. Sample

calculations for this process are contained in section 4.2.1. A copy of the M_R Calculator MATLAB program is contained in Appendix C.

4.2.1 Sample Calculation

The following calculations illustrate the process described in section 4.2 using real data. The following data comes from cycle 15 of test #24: the repeat of sample H at an 11% moisture content. The recoverable axial strain for one of the loading sequences was calculated using equation (4.1). The gage length was 0.1524 m (6 in.).

$$\varepsilon_a = \frac{\left(3.58*10^{-5}m + 3.86*10^{-5}m + 3.71*10^{-5}m\right)}{3*0.1524m} = 0.24*10^{-3}$$

The cyclic stress was then calculated using equation (4.2). The radius of the specimen was 0.0762 m (3 in.).

$$\sigma_a = \frac{\left(1900(N) - 217(N)\right)}{\pi*0.0762^2(m^2)} = 92.3kPa$$

The resilient modulus for this cycle was calculated using equation (4.3).

$$M_R = \frac{92.3kPa}{0.24*10^{-3}} = 378MPa$$

Lastly, the mean stress was calculated using equation (4.4).

$$\theta = \frac{242kPa + 137kPa + 137kPa}{3} = 173kPa$$

4.2.2 Deformation Homogeneity

One of the difficulties encountered during this testing was the occasional presence of large discrepancies between the three LVDT readings. The three displacement histories recorded during the M_R loading sequences were often within 10% of each other. However, there were also times in which the displacements differed by 100% or more. Several factors may have contributed to these discrepancies among the three LVDT readings: specimen ends may not have been parallel, specimens may have tilted or barreled during testing, or there may have been slippage between the LVDT holder and the membrane.

The LVDT readings were averaged during the calculation of M_R so it was difficult to say what effect, if any, poor LVDT agreement had upon the data. Therefore, it would be beneficial to identify a homogeneous deformation coefficient, α, to quantify the deformation homogeneity of the specimens:

$$\alpha = \frac{\sqrt{\delta_1^{\,2} + \delta_2^{\,2} + \delta_3^{\,2}}}{d} \tag{4.5}$$

where δ_i is the difference between the average LVDT displacement and the displacement from LVDT 'i':

$$\delta_i = d - d_i \tag{4.6}$$

and d is the average LVDT displacement:

$$d = \frac{d_1 + d_2 + d_3}{3} \tag{4.7}$$

An α-value of 0 indicates perfect LVDT agreement. Larger α-values indicate increasing discrepancies between the displacement values.

Examples of loading histories with small and large α-values are shown in Figure 4.1. The loading sequence with the α-value of 1.30 (Figure 4.1b) was from an M_R test in which the specimen began to bend during the load pulses. Every time that a load pulse was applied during

this sequence the sample and upper LVDT holder bent to the side; it can be seen that significant positive and negative displacements occurred immediately after the application of as the load.

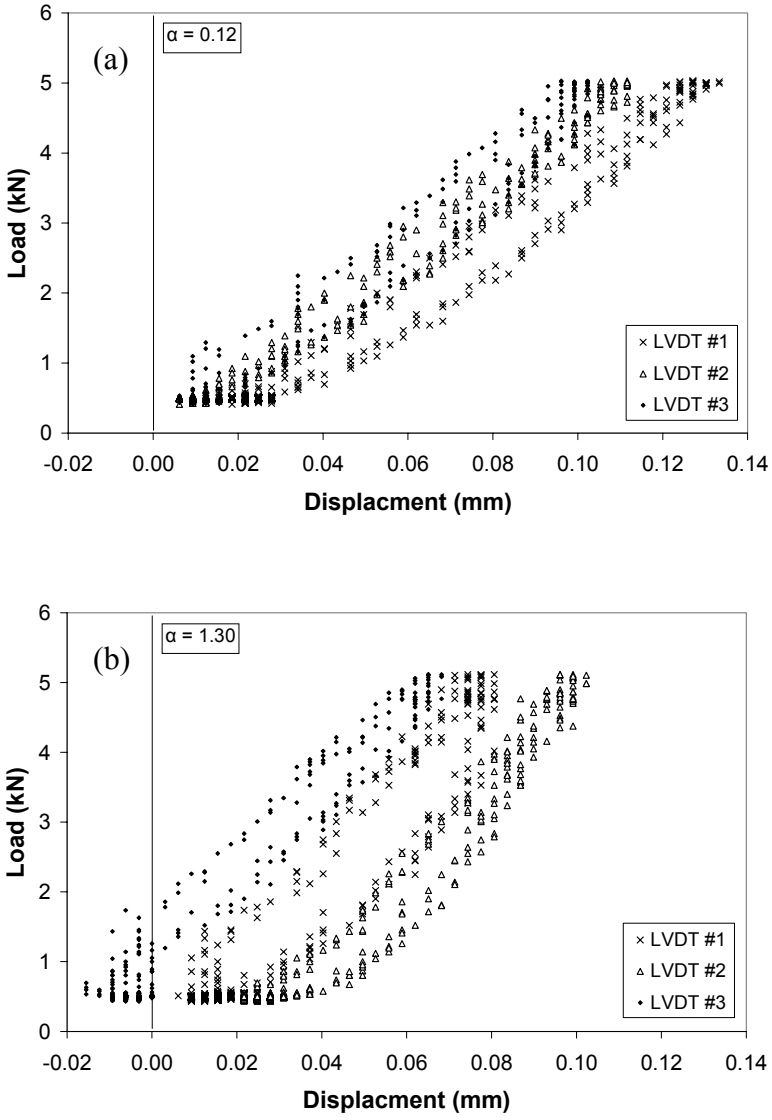

Figure 4.1: Displacement Histories

The α-values were calculated for each loading sequence of every M_R test performed using this process. When the 15 α-values from each M_R test were averaged the values ranged from 0.1 to 1.1. The tests with α-values near 0.1 had individual LVDT readings that differed from the

mean displacement by approximately 10%; the tests with α-values near 1.1 had individual LVDT readings that differed from the mean displacement by more than 100%. The average α-values for each M_R test in this study are included in Table 4.2.

Table 4.2: M_R Test α-Values

Test Number	Sample	Moisture Content	α	Test Number	Sample	Moisture Content	α
		%				%	
1	A	2.6	**0.71**	19	H	3.1	**1.06**
2	A	3.4	**0.8**	20	H	3.5	**1.02**
3	A	5.2	**0.6**	21	H	7.4	**0.54**
4	A	5.3	**0.71**	22	H	7.1	**0.63**
5	A	7.9	**0.28**	23	H	11	**0.37**
6	A	7.6	**0.52**	24	H	10.6	**0.2**
	Mean		**0.60**		**Mean**		**0.64**
	Coef of variation (%)		**28.14**		**Coef of variation (%)**		**49.56**
7	D	2.6	**0.61**	25	J	3.3	**0.46**
8	D	2.7	**0.73**	26	J	3.5	**0.45**
9	D	6.2	**0.41**	27	J	6.2	**0.27**
10	D	6.1	**0.28**	28	J	5.9	**0.54**
11	D	9	**0.26**	29	J	7.9	**0.35**
12	D	10.1	**1.08**	30	J	8.6	**0.11**
	Mean		**0.56**		**Mean**		**0.36**
	Coef of variation (%)		**51.02**		**Coef of variation (%)**		**39.11**
13	F	3.2	**1.11**	31	N	3.2	**0.28**
14	F	3.4	**0.35**	32	N	3.1	**0.91**
15	F	5.7	**0.75**	33	N	5.5	**0.32**
16	F	6.3	**0.91**	34	N	5.5	**0.83**
17	F	9	**0.58**	35	N	8.2	**0.63**
18	F	7.3	**0.36**	36	N	7.9	**0.38**
	Mean		**0.68**		**Mean**		**0.56**
	Coef of variation (%)		**41.09**		**Coef of variation (%)**		**44.40**

Overall, the LVDT readings appeared to be the most consistent for sample J and the least consistent for sample H. However, the difference in α-values between soils was small; the sample used to create the specimen did not appear to have a large effect on the deformation homogeneity of the specimen. The moisture content of the specimen, however, had a significant effect on the deformation homogeneity (Figure 4.2).

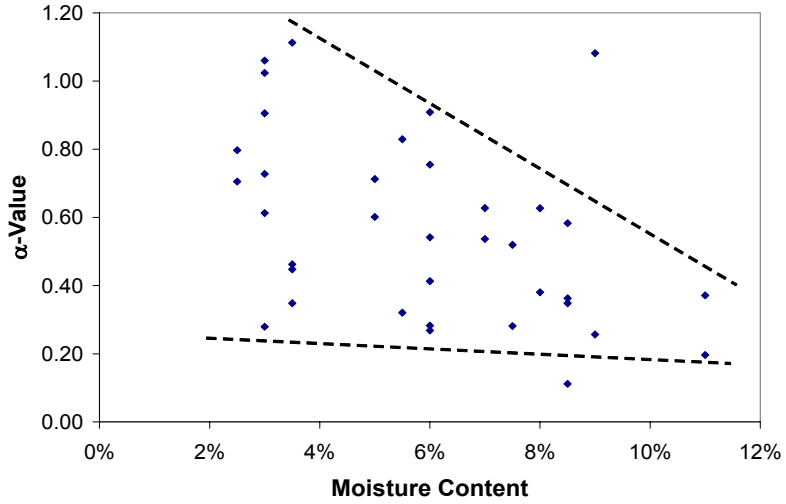

Figure 4.2: α-Value Variation

Figure 4.2 shows that specimens with larger moisture contents tended to deform in a more uniform manner. It is possible that the specimens with smaller moisture contents were not as homogenous due to regions of varying moisture content within the soil. This may have resulted in uneven deformations during the load cycles.

Another variable that significantly affected the deformation homogeneity was the sequence of deviator stresses used to test specimens at a particular confining pressure. At a given level of confinement, the load sequences that applied the smallest deviator stresses to the specimen (sequences 1, 4, 7, 10, and 13 in Table 2.1) consistently had the largest α-values. The effect of the deviator stress on α can be seen in Figure 4.3.

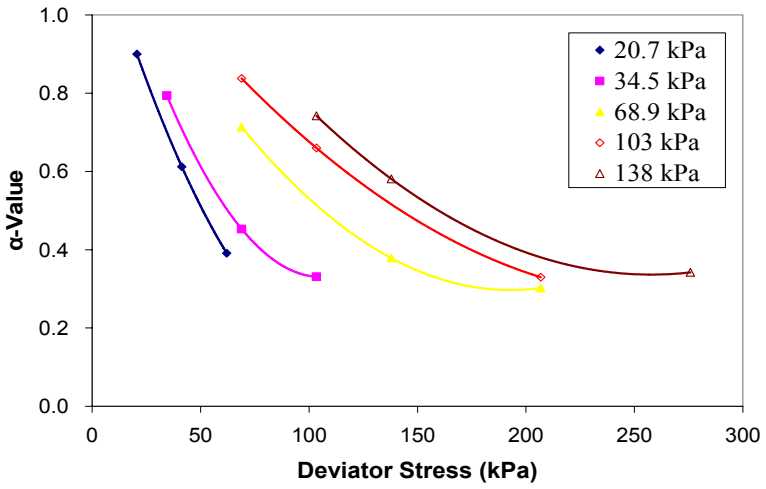

Figure 4.3: Deviator Stress and Deformation Homogeneity

The α-values for the loading sequences with the smallest deviator stresses at a particular level of confinement were significantly larger than the α-values for the largest deviator stresses. Displacement readings from tilted specimens were the most affected at small axial stress values because the loading may have caused the specimen to deform unevenly immediately upon application of the load. Figure 4.1b is an example of this. This non-uniformity was more difficult to detect at large deviator stresses because of the larger axial deformation induced in the specimen.

4.3 Bender Element Data Interpretation

The GDS-BES program records time histories for five milliseconds after the emission of a P-wave or S-wave. Fifty of these time histories are then stacked to reduce noise in the data. In some situations, the noise in the data was not adequately filtered after stacking 50 time histories; in these cases, additional stacking was performed until the trace appeared sufficiently clear.

The arrival of each wave was identified using one of several methods. In most cases, the points at which the waves arrived were clearly identifiable during tests. Figure 4.4 displays time histories from typical P-wave and S-wave tests.

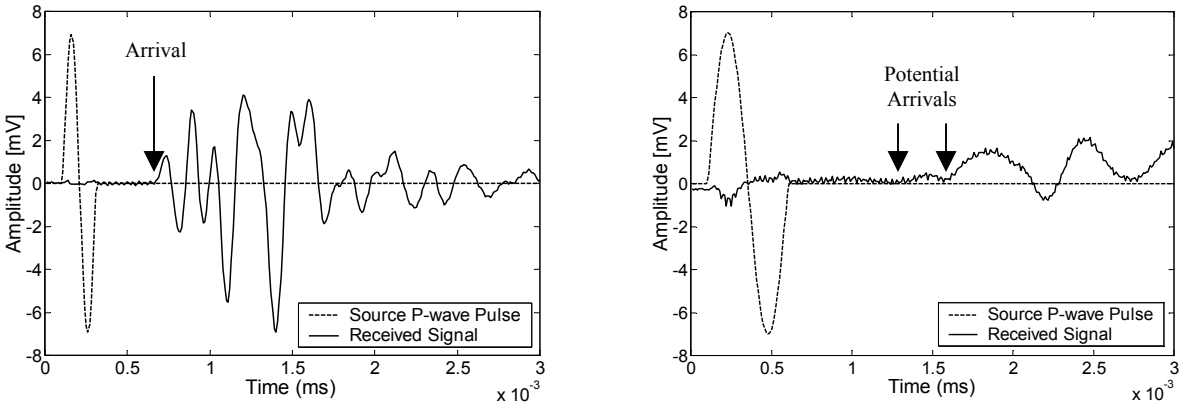

Fig. 4.4: Identification of Wave Arrivals

The initial rise from the baseline is sharp and easily identifiable for the P-wave test. On the other hand, there are two points that could be identified as the wave arrival in the time history from the S-wave test. There is a small rise visible in the data before the first large deflection; initially it would be unclear whether the beginning of this region represents a wave arrival.

In situations such as these, the first option is to continue stacking the data in the hopes that the irregularity will become more prominent or disappear in a manner that leaves only one possible wave arrival point. If uncertainty remains after hundreds of stacks, however, it may be necessary to perform the test again with pulses of different frequencies.

The P-wave and S-wave speed does not vary over the range of frequencies used by the bender elements: 2,000 to 10,000 Hz. A test was performed to demonstrate this. Bender elements were used to induce waves of several frequencies at a variety of confining pressures. The results of this test are summarized in Table 4.3; from 2,000 to 10,000 Hz the effect of frequency upon the calculation of G is negligible.

Table 4.3: Wave Speeds at Variable Pulse Frequencies

Confining Pressure	Pulse Frequency	Shear Wave Speed	Compression Wave Speed
kPa	(Hz)	(m/s)	(m/s)
248	2000	324	522
248	5000	324	518
248	10000	321	521
124	2000	278	446
124	5000	275	447
124	10000	278	445
62	2000	235	378
62	5000	234	376
62	10000	235	378
31	2000	193	314
31	5000	192	314
31	10000	192	315

This table makes it clear that pulses of different frequencies can be used to produce a different waveform within the received trace without affecting the speed of the waves. The advantage of this is that the point of wave arrival is often easier to identify in the new waveform. If not, this process can be repeated at different frequencies until the point at which the wave arrives is clearly identifiable. The results of procedure were verified using the cross-correlation method, which will be detailed in section 4.3.1.

Wave speed can be calculated after determining the travel time of the wave (t_{ai}):

$$c_s = \frac{l}{t_{as}}$$
$$c_p = \frac{l}{t_{ap}} \tag{4.8}$$

where l is the length of the specimen. After the wave speeds are known, Poisson's ratio can be calculated:

$$\upsilon = \frac{1}{2}\frac{\left(\frac{c_p}{c_s}\right)^2 - 2}{\left(\frac{c_p}{c_s}\right)^2 - 1} \tag{4.9}$$

The shear modulus is calculated directly from the shear wave speed and the soil density:

$$G = \rho c_s^{\,2} \tag{4.10}$$

The modulus in equation (4.10) is the maximum shear modulus because the bender elements test within the elastic portion of the stress-strain curve. Lastly, the maximum shear modulus is converted into the maximum Young's modulus so that it can be compared to the resilient modulus values:

$$E = 2G(1+\upsilon) \tag{4.11}$$

The moduli measured during the small strain bender element testing are the maximum moduli, E_{MAX} and G_{MAX}.

4.3.1 Cross Correlation

Cross correlation is a method by which the time histories of an input and received wave can be compared to determine the point at which the wave arrives at the receiver. The theory behind this method is described by Santamarina and Fratta [14]. In a perfectly elastic, homogenous, and infinite material, the waveform recorded by a receiving element would have the same form as the wave emitted by its source, although their amplitudes will differ.

Santamarina and Fratta hypothesize that the beginnings of the sections over which the received signal resembles the input signal the most closely, are the points at which a wave arrival may have occurred. They suggest moving the input pulse along the received waveform point-by-point looking for positions at which the signals "match." A numerical value representing the quality of the match is generated by multiplying selected data points from both time histories together. The first point in the input pulse's time history is multiplied by the first point of the section of the received time history that is currently being tested. Following that the second points in each history are multiplied together and summed with the first. This continues until the entire length of the trace has been tested and each of the multiplied values has been summed.

The resulting sum is the "cross-correlation" value that represents the match of the traces at that particular point of the received signal's trace. This process is repeated at every point along a received pulse's length. A plot of the resulting cross-correlation values will have local maxima and minima at points where the signals correspond. The authors of the method suggest that the maxima and minima in these plots represent potential wave arrivals.

The cross correlation method was used to verify the first arrival identification method used in this study. Several bender element signals were selected for cross correlation analysis. When the cross correlation sums are plotted against the time histories, local minima and maxima occurred regularly along the length of the plot. The results from two P-wave cross correlations are displayed in Figure 4.5.

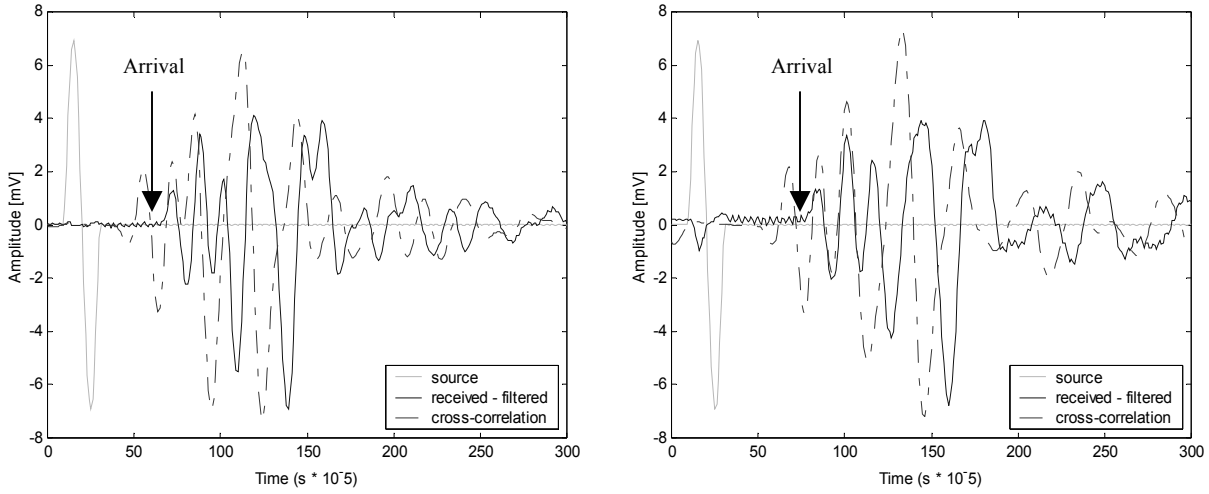

Figure 4.5: P-Wave Cross Correlation Results

In these graphs the first large negative minima is assumed to indicate the arrival of the P-wave pulse. This minima occurs at the same point as the beginning of the first significant deflection in the time history. Therefore, it is safe to assume that the manually identified arrival times, which are located at the first significant deflections in the time histories, are accurate. Almost all the P-wave time histories follow this pattern. Therefore, the cross correlation results indicate that the manual first arrival identification method is sufficient for P-wave tests.

S-wave data often contains more noise than P-wave data due to weaker signals. Therefore, it is often more difficult to identify the arrival of the pulse for the S-waves. In many

cases there is a shallow rise or depression before the first significant deflection in the time history; it is important to know whether these deviations are physically significant. Figure 4.6 displays two cross-correlation results from S-wave time histories. The cross correlation in the first plot conforms with expectations; the first significant cross correlation maxima appears over the center of the small depression where the first significant deflection in the trace begins. The cross correlation in the second plot, however, does not reach a minima or maxima over any logical point; the first significant positive maxima in the cross correlation data occurs over a point well after the first significant deflection in the S-wave time history. In this case the results are inconclusive. In situations such as this experience must be used to identify the wave arrival.

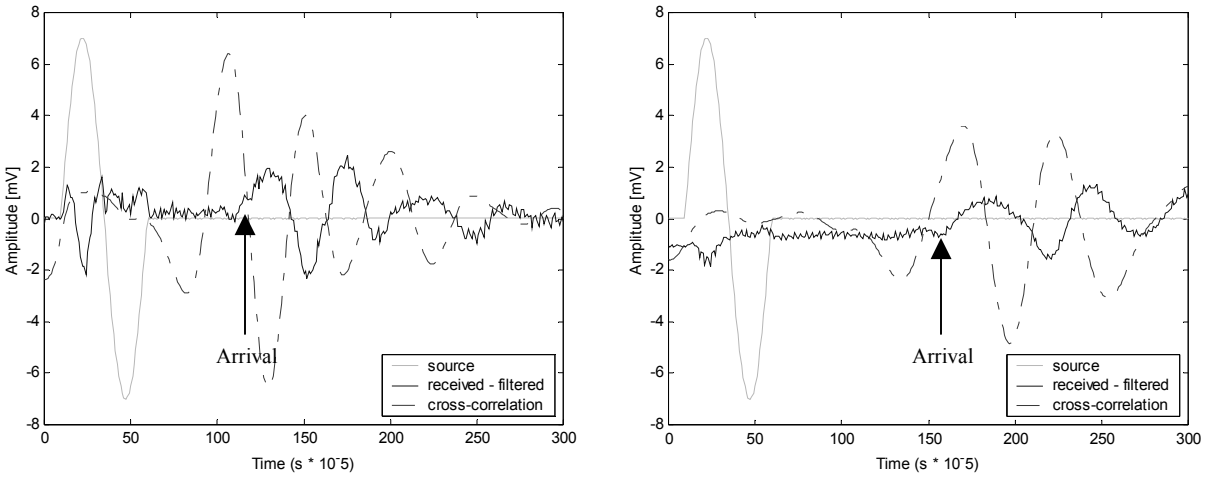

Figure 4.6: S-Wave Cross Correlation Results

There are several potential explanations for why cross correlations may provide poor results: poor homogeneity of the sample, electrical noise, and excessive wave reflections. Fortunately, plots such as the first in Figure 4.6 are the most prevalent; the cross-correlation method usually produces a peak over a possible arrival. Therefore, the results indicate that manually identifying the first significant deflection of the time history is an accurate way to determine wave arrival points.

4.3.2 Sample Calculation

The following calculations illustrate the process described in section 4.3 using real data. The following data comes from cycle 15 of test #24: the repeat of sample H at an 11% moisture content. The wave speeds for this specimen were calculated using equation (4.8):

$$c_s = \frac{.303(m)}{1.00*10^{-3}(s)} = 303\frac{m}{s}$$
$$c_p = \frac{.303(m)}{5.18*10^{-4}(s)} = 585\frac{m}{s}$$

Poisson's ratio was calculated using equation (4.9):

$$\upsilon = \frac{1}{2}\frac{\left(\frac{585}{303}\right)^2 - 2}{\left(\frac{585}{303}\right)^2 - 1} = 0.317$$

The shear modulus was calculated using equation (4.10):

$$G = G_{\max} = 1714\left(\frac{kg}{m^3}\right)*303\left(\frac{m}{s}\right)^2 = 157MPa$$

Young's modulus was calculated using equation (4.11):

$$E = E_{\max} = 2*157MPa*(1+0.317) = 414MPa$$

4.4 Test Data

The 36 test specimens described in section 4.1 were tested using the triaxial and bender element test protocol described in Chapter 3. Unfortunately, a short time before the testing was to begin, one of the bender element cantilevers was damaged due to the aggregate problem discussed in section 3.3.3 and a replacement element was not immediately available. Fortunately, bender element testing performed prior to the damage indicated that the measured wave speeds were highly repeatable. Therefore, the test matrix was begun without operational elements; 14 tests in the sequence were completed before a replacement element was installed.

4.4.1 Resilient Modulus Data

Thirty-six resilient modulus tests were performed on six soil samples that were each made into three specimens with varying moisture contents. In addition, each of these specimens was reproduced a second time to check the repeatability of the data. The target moisture content and dry density values from these 36 scheduled tests are compared to the values measured in the actual specimens in Table 4.4.

Table 4.4: Target and Measured Specimen Preparation Parameters

Test Number	Sample	Moisture Content		Difference	Dry Density		Percent Difference
		Target	Measured		Target	Measured	
		%	%		kg/m^3	kg/m^3	%
1	A	2.5	2.6	0.1	2158	2083	-3.5
2	A	2.5	3.4	0.9	2158	2117	-1.9
3	A	5.0	5.2	0.2	2158	2098	-2.8
4	A	5.0	5.3	0.3	2158	2168	0.5
5	A	7.5	7.9	0.4	2158	2194	1.7
6	A	7.5	7.6	0.1	2158	2225	3.1
					Mean	2147.5	
					Coef. of Variance	2.4	
7	D	3.0	2.6	-0.4	1839	1954	6.3
8	D	3.0	2.7	-0.3	1839	1954	6.3
9	D	6.0	6.2	0.2	1839	1983	7.8
10	D	6.0	6.1	0.1	1839	1984	7.9

Table 4.4 Continued: Target and Measured Specimen Preparation Parameters

Test Number	Sample	Moisture Content		Difference	Dry Density		Percent Difference
		Target	Measured		Target	Measured	
		%	%		kg/m^3	kg/m^3	%
11	D	9.0	9.0	0.0	1839	1966	6.9
12	D	9.0	10.1	1.1	1839	1984	7.9
					Mean	1975.0	
					Coef. of Variance	0.5	
13	F	3.5	3.2	-0.3	1900	1820	-4.2
14	F	3.5	3.4	-0.1	1900	1828	-3.8
15	F	6.0	5.7	-0.3	1900	1840	-3.2
16	F	6.0	6.3	0.3	1900	1857	-2.3
17	F	8.5	9.0	0.5	1900	1884	-0.8
18	F	8.5	7.3	-1.2	1900	1853	-2.5
					Mean	1847.0	
					Coef. of Variance	1.1	
19	H	3.0	3.1	0.1	1725	1703	-1.3
20	H	3.0	3.5	0.5	1725	1732	0.4
21	H	7.0	7.4	0.4	1725	1760	2.0
22	H	7.0	7.1	0.1	1725	1760	2.0
23	H	11.0	11.0	0.0	1725	1786	3.5
24	H	11.0	10.6	-0.4	1725	1788	3.7
					Mean	1754.8	
					Coef. of Variance	1.7	
25	J	3.5	3.3	-0.2	1791	1865	4.1
26	J	3.5	3.5	0.0	1791	1849	3.2
27	J	6.0	6.2	0.2	1791	1837	2.6
28	J	6.0	5.9	-0.1	1791	1858	3.7
29	J	8.5	7.9	-0.6	1791	1852	3.4
30	J	8.5	8.6	0.1	1791	1854	3.5
					Mean	1852.5	
					Coef. of Variance	0.5	
31	N	3.0	3.2	0.2	2014	1929	-4.2
32	N	3.0	3.1	0.1	2014	1941	-3.6
33	N	5.5	5.5	0.0	2014	1980	-1.7
34	N	5.5	5.5	0.0	2014	2040	1.3
35	N	8.0	8.2	0.2	2014	2030	0.8
36	N	8.0	7.9	-0.1	2014	2064	2.5
					Mean	2028.5	
					Coef. of Variance	1.5	

Several things about these data are noteworthy. To begin with, the target dry density values proved to be difficult to achieve for many of the specimens. Samples such as D, H, and J often became compacted to a value larger than the maximum dry density indicated by Mn/DOT's compaction curves almost immediately after the rotary hammer was placed in operation. On the other end of the spectrum, sample F and some sample A and N specimens proved to be difficult to compact to the intended density regardless of the compactive effort used. As a result, the specimen unit densities vary to a degree. However, the majority are within 5% of the target value.

The measured moisture content of the specimens was usually within $\pm 0.5\%$ of the target moisture content as required by LTPP P46. Only three of the 36 tests fell outside of this range, and none of the three was more than 1.0% away from its target.

Figure 4.7 contains plots of the resilient modulus data generated from the 36 specimens in Table 4.4. A different plot was created for each sample, and the three trendlines on each of the plots were calculated using the data from the specimens prepared at each of the soil's three moisture contents. Similar plots that include the data from the bender elements were generated for each moisture content. These plots are included in Appendix D.1.

The resilient modulus values recorded during this series of testing tended to decrease as the moisture content of the specimens increased. Sample N (Figure 4.7f) was the only significant exception; the trendline calculated for the 8.0% moisture content plotted directly over the trendline for the 3.0% moisture content. However, in the case of N all three of the trendlines were located within a small range; further testing of sample N may prove this result to be a sample size error. The increase in M_R with decrease in moisture content may be related to the compactive effort used to reach the maximum dry density. In addition, the specimens created at smaller moisture contents were found to have significantly larger values of cohesion. Cohesion and the shear strength data are discussed in section 4.4.4.

Figure 4.7 also makes it clear that some of the data was difficult to repeat. The specimens created by compacting sample J at a 3.5% moisture content (Figure 4.7e), for example, produced M_R values that differ from each other by almost 50%. Fortunately, the majority of the specimens generated data that were within 20% of their repeat.

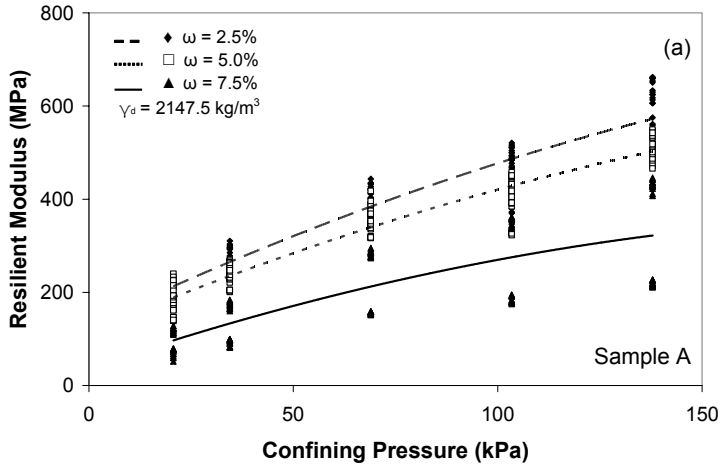

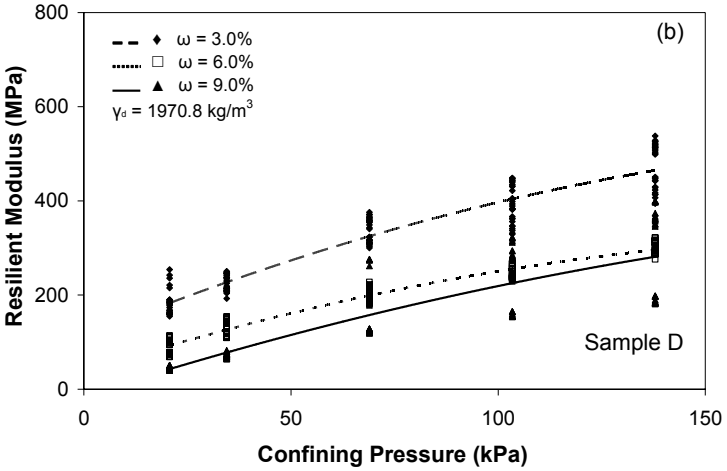

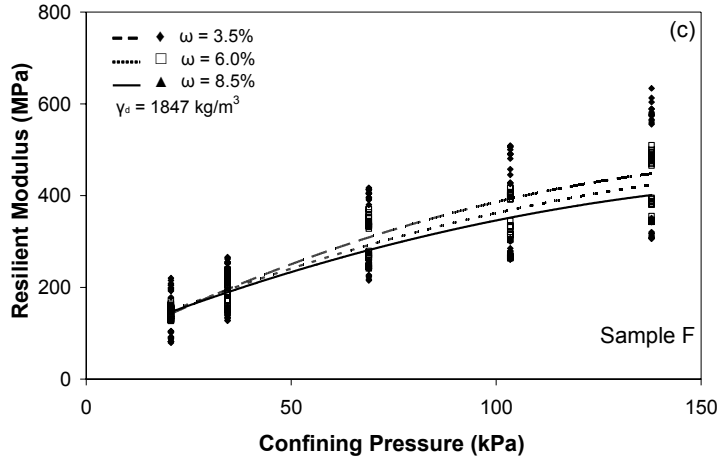

Figure 4.7: Resilient Modulus Data

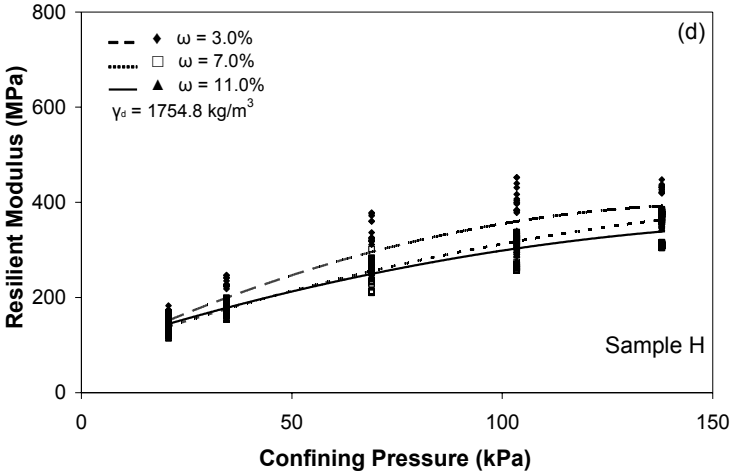

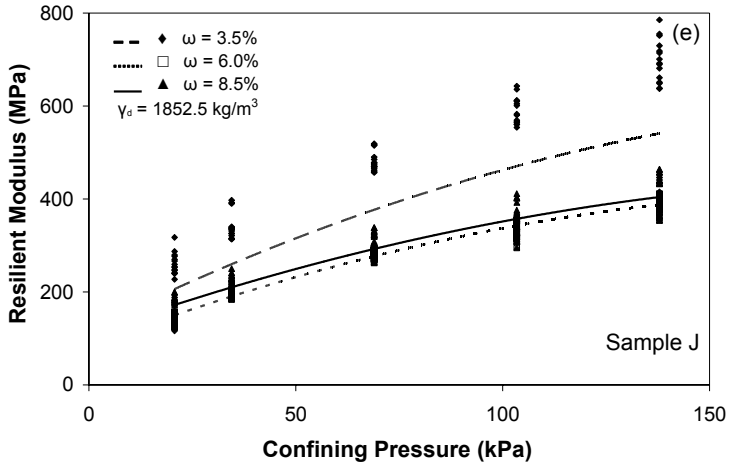

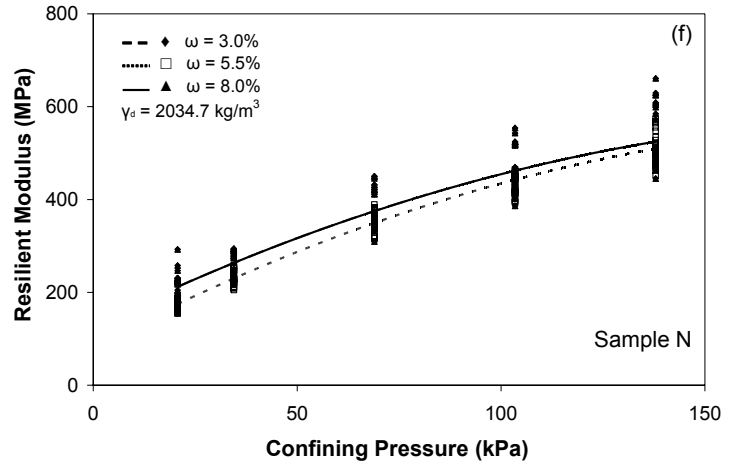

Figure 4.7 Continued: Resilient Modulus Data

The mean stress is equal to the average of the three principal stresses acting on a specimen. Therefore, mean stress values reflect changes in the deviator stress. Resilient modulus versus confining pressure and mean stress for each sample and moisture content are included in Appendix D.2 and D.3. One example plot for the mean stress effect is shown in Figure 4.8.

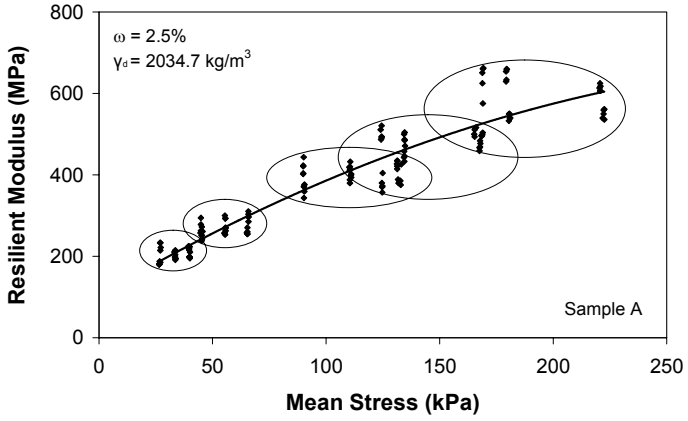

Figure 4.8: M_R Versus Mean Stress for Sample A

Figure 4.8 shows the data from the two repeats of sample A at a 2.5% moisture content. The circles surround the data from the five levels of confinement that could clearly be seen in Figure 4.7. The data points in these circles have approximately the same M_R values; the tests that were performed at the larger deviator stresses recorded approximately the same M_R values as the tests with lower deviator stresses at a particular confining pressure. Therefore, the stiffness of the specimens being tested varied significantly with the confining pressure but the deviator stress had little effect.

4.4.2 Bender Element Data

Bender element tests were performed immediately before and after each change in confining pressure during the resilient modulus test. This practice resulted in two sets of P-wave and S-wave speeds for each confining pressure. In every case, the wave speeds recorded immediately after the change in confining pressure were larger than the wave speeds recorded at the end of

the confining pressure's loading sequences, although each of the changes was smaller than 2% of the first wave speed measured. This decline in wave speed was most likely the result of permanent deformations, from change in length (<1%) and change in volume, taking place within the specimen during the loading sequences. For example, these deformations reduced the volume of the specimen and, because the wave speeds are inversely proportional to material density, the waves slowed in the higher density soil after loading sequences. Fortunately, the difference between the two wave speeds was small; most values differed by no more than 2%. The reported E_{MAX} values are the averaged results from both wave speed measurements. These values are compared with the M_R values produced during the three loading sequences that took place between the changes in confining pressure.

Direct comparisons between E_{MAX} and M_R for each soil at each moisture content are included in appendix D.1. Figure 4.9 contains an example of these plots. The majority of the plots appear similar to this curve; the bender element data follows a trend similar to the M_R data at larger values.

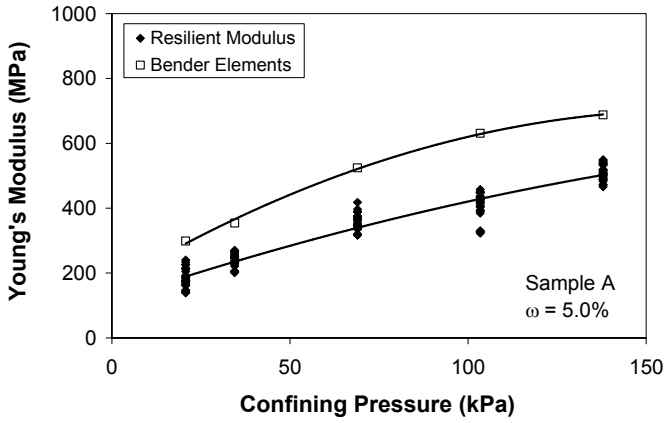

Figure 4.9: M_R and E_{MAX} Curves

Figure 4.10 contains the bender element data from each of the soils. These data are in good agreement with the M_R data; in most cases, the specimens with smaller moisture contents have larger E_{MAX} values. However, the specimens from sample F (Figure 4.10c) and sample J (Figure 4.10e) were exceptions. Sample F had unusually

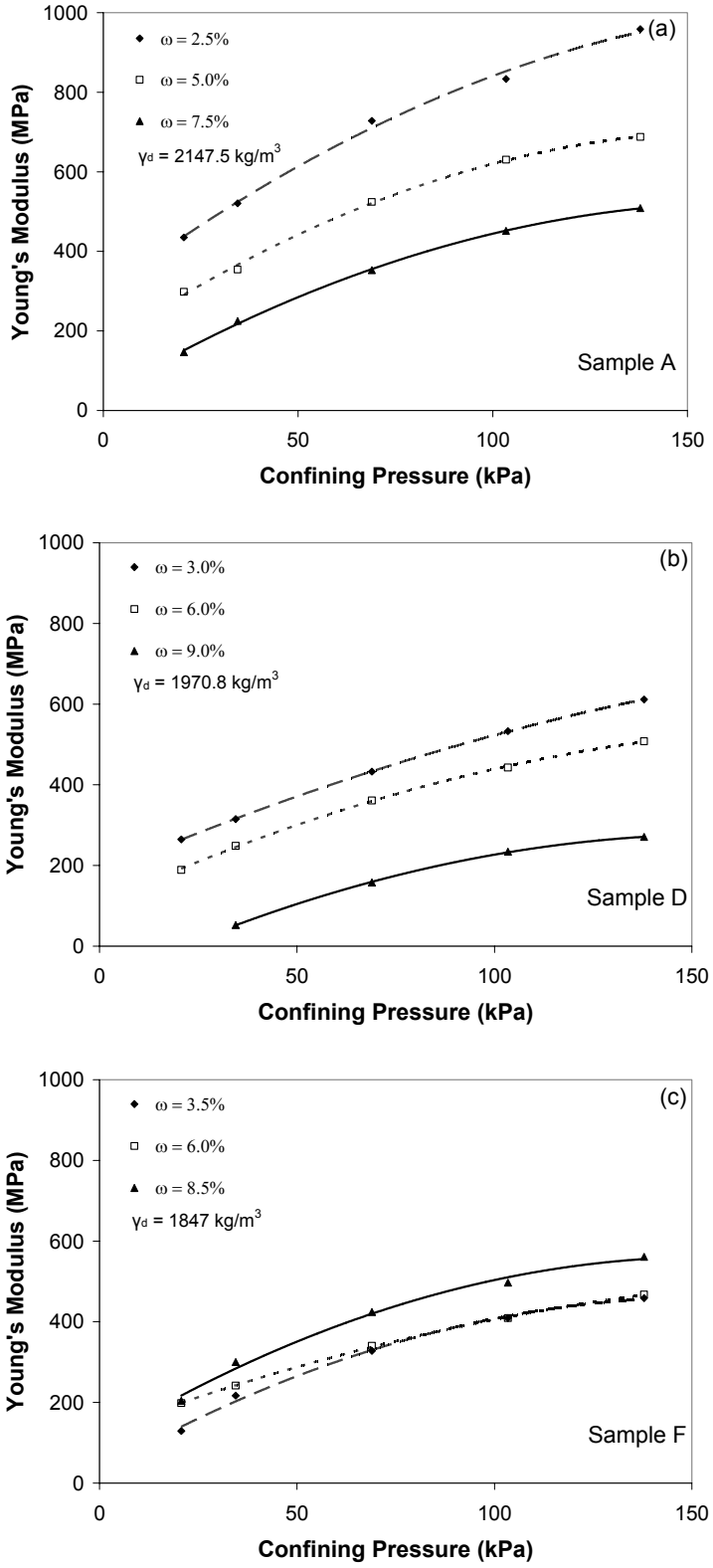

Figure 4.10: Bender Element Data

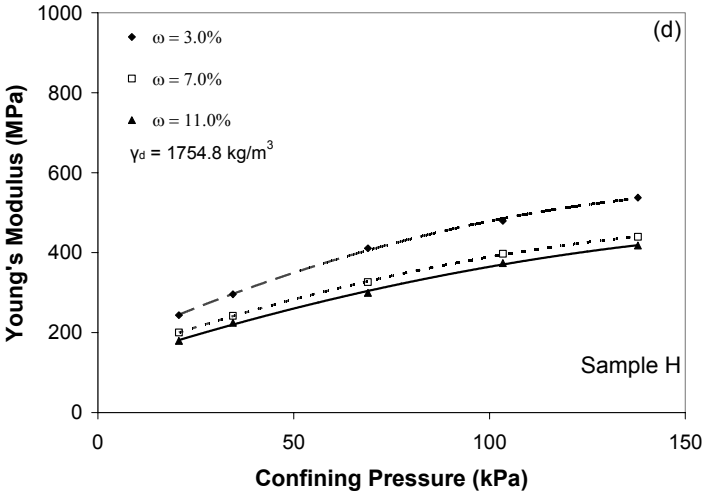

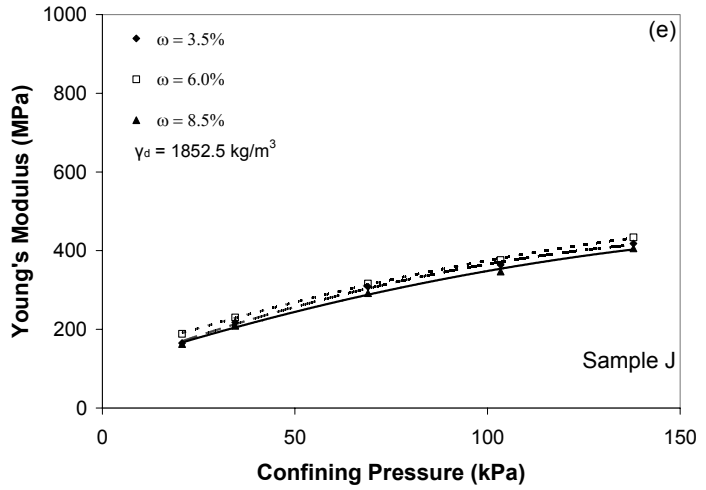

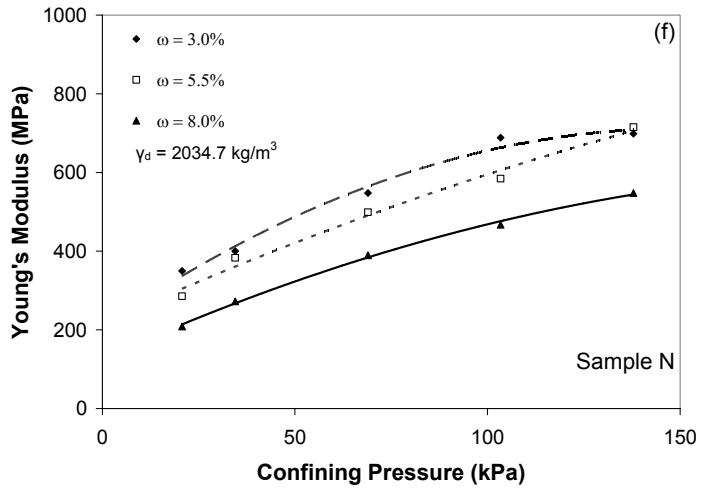

Figure 4:10 Continued: Bender Element Data

large stiffnesses at a moisture content of 6% and small confinement; sample J had stiffnesses that were similar in magnitude at every moisture content. Sample J more likely acted differently from the other samples because of its poor gradation and small fine content. The discrepancy recorded in sample F was most likely a sample size error.

E_{MAX} and M_R data from each level of confinement can be seen in Table 4.5.

Table 4.5: Resilient Modulus and E_{MAX}

Test Number	M_R					E				
	Confinement (kPa)					Confinement (kPa)				
	20.7	34.5	68.9	103	138	20.7	34.5	68.9	103	138
(Sample)	(MPa)					(MPa)				
1 (A)	217	285	421	499	632	-	-	-	-	-
2 (A)	193	256	380	430	530	435	521	728	833	958
3 (A)	163	222	336	384	504	-	-	-	-	-
4 (A)	203	255	376	432	516	299	354	524	631	688
5 (A)	72	92	156	184	219	-	-	-	-	-
6 (A)	119	173	284	350	431	147	225	353	452	509
7 (D)	201	240	359	424	516	-	-	-	-	-
8 (D)	162	210	312	360	421	265	315	433	533	612
9 (D)	74	116	194	243	298	-	-	-	-	-
10 (D)	104	142	217	250	300	189	249	361	443	508
11 (D)	48	73	124	159	189	-	-	-	-	-
12 (D)	45	72	193	295	372	181	52	158	234	271
13 (F)	189	245	403	477	582	-	-	-	-	-
14 (F)	92	143	240	281	323	129	217	328	409	459
15 (F)	134	171	262	306	373	169	204	297	362	424
16 (F)	155	221	346	403	485	228	280	384	456	511
17 (F)	133	173	277	328	386	157	282	411	480	548
18 (F)	158	203	305	355	424	251	318	438	514	575
19 (H)	137	183	266	318	372	-	-	-	-	-
20 (H)	135	170	260	299	362	244	296	411	480	538
21 (H)	130	174	257	306	358	174	217	302	356	399
22 (H)	167	230	338	407	429	226	267	351	438	481
23 (H)	98	142	222	263	309	145	183	273	330	372
24 (H)	153	194	277	327	373	214	266	326	418	464

Table 4.5 Continued: Resilient Modulus and E_{MAX}

Test Number	M_R					E				
	Confinement (kPa)					Confinement (kPa)				
	20.7	34.5	68.9	103	138	20.7	34.5	68.9	103	138
(Sample)	(MPa)					(MPa)				
25 (J)	260	341	481	591	697	-	-	-	-	-
26 (J)	137	194	284	329	394	165	217	308	364	418
27 (J)	150	198	284	332	391	-	-	-	-	-
28 (J)	138	194	282	333	392	188	230	316	376	434
29 (J)	184	229	320	371	440	-	-	-	-	-
30 (J)	149	200	281	320	377	162	209	292	347	406
31 (N)	197	236	345	419	475	-	-	-	-	-
32 (N)	230	285	409	504	574	350	400	547	689	699
33 (N)	166	222	342	428	493	-	-	-	-	-
34 (N)	177	242	373	437	533	285	383	499	584	715
35 (N)	88	135	225	273	336	-	-	-	-	-
36 (N)	140	186	276	332	400	208	273	390	467	548

The data missing from this table are from the tests in which the bender elements were damaged. Fortunately, at least one set of bender element data was created for each target moisture content of each sample. Table 4.6 shows the elastic parameters estimated from bender element testing.

Table 4.6: Elastic Parameters Estimated from Bender Element Testing

Test Number	E					G					ν				
	Confinement (kPa)					Confinement (kPa)					Confinement (kPa)				
	20.7	34.5	68.9	103	138	20.7	34.5	68.9	103	138	20.7	34.5	68.9	103	138
	(MPa)					(MPa)									
2 (A)	435	521	728	833	958	158	188	265	305	352	0.38	0.38	0.37	0.37	0.36
4 (A)	299	354	524	631	688	109	129	192	232	251	0.37	0.37	0.37	0.36	0.37
6 (A)	147	225	353	452	509	54	83	131	167	189	0.36	0.36	0.35	0.35	0.35
8 (D)	265	315	433	533	612	96	115	159	198	227	0.38	0.37	0.36	0.35	0.35
10 (D)	189	249	361	443	508	76	101	153	186	215	0.24	0.23	0.18	0.19	0.18

Table 4.6 Continued: Elastic Parameters Estimated from Bender Element Testing

Test Number	E					G					ν				
	Confinement (kPa)					Confinement (kPa)					Confinement (kPa)				
	20.7	34.5	68.9	103	138	20.7	34.5	68.9	103	138	20.7	34.5	68.9	103	138
	(MPa)					(MPa)									
14 (F)	129	217	328	409	459	46	80	121	153	171	0.4	0.36	0.35	0.34	0.34
15 (F)	169	204	297	362	424	62	76	111	136	160	0.35	0.35	0.34	0.33	0.33
16 (F)	228	280	384	456	511	85	104	143	171	193	0.35	0.35	0.34	0.33	0.32
17 (F)	157	282	411	480	548	63	116	170	198	224	0.26	0.22	0.21	0.22	0.22
18 (F)	251	318	438	514	575	91	117	163	190	214	0.38	0.36	0.34	0.35	0.34
20 (H)	244	296	411	480	538	92	111	157	182	206	0.33	0.33	0.31	0.32	0.31
21 (H)	174	217	302	356	399	64	81	113	133	150	0.35	0.34	0.34	0.34	0.33
22 (H)	226	267	351	438	481	84	100	131	166	183	0.35	0.34	0.34	0.32	0.32
23 (H)	145	183	273	330	372	54	69	103	126	142	0.34	0.32	0.32	0.31	0.31
24 (H)	214	266	326	418	464	79	99	121	158	176	0.36	0.35	0.35	0.32	0.32
26 (J)	165	217	308	364	418	62	83	119	142	163	0.34	0.31	0.29	0.28	0.28
28 (J)	188	230	316	376	434	69	86	120	143	164	0.36	0.34	0.32	0.32	0.32
30 (J)	162	209	292	347	406	61	79	112	133	156	0.33	0.32	0.31	0.3	0.3
32 (N)	350	400	547	689	699	126	144	198	252	253	0.38	0.39	0.38	0.37	0.38
34 (N)	285	383	499	584	715	105	141	184	215	267	0.36	0.36	0.35	0.36	0.34
36 (N)	208	273	390	467	548	77	102	147	177	209	0.35	0.34	0.33	0.32	0.31

4.4.3 Percometer Data

Three Percometer tests were performed across the diameter of the surface of each specimen. These tests measure the dielectric permittivity and conductivity values of the soil being tested, which can be used to estimate the volumetric moisture content of the soil being tested. The raw data from this testing is contained in Table 4.7.

Table 4.7: Dielectric Permittivity and Conductivity

Test Number	Sample	Moisture Content	Dielectric Permittivity			Conductivity		
			Left	Center	Right	Left	Center	Right
		(Percent)	J	J	J	uS/cm	uS/cm	uS/cm
1	A	2.5	5.91	7.27	7.07	0	0	0
2	A	2.5	7.5	7.06	6.88	0	0	0
3	A	5	8.34	10.1	7.56	9	0	8
4	A	5	6.74	10	9.67	5	9	5
5	A	7.5	11	9.77	9.16	11	7	8
6	A	7.5	7.9	7.91	9.61	12	11	18
7	D	3	4.77	5.63	5.63	0	0	0
8	D	3	5.95	5.98	4.83	0	1	0
9	D	6	6.56	7.33	7.17	9	6	8
10	D	6	-	-	-	-	-	-
11	D	9	12.6	10.9	11.9	33	28	25
12	D	9	12.9	11.5	11.6	45	36	40
13	F	3.5	6.69	6.45	6.69	1	3	2
14	F	3.5	6.82	6.24	6.55	2	2	3
15	F	6	8.18	8.32	7.55	6	7	8
16	F	6	8.6	8.63	8.42	12	15	8
17	F	8.5	10.9	10.8	10.6	12	22	34
18	F	8.5	8.59	7.39	9.32	3	4	13
19	H	3	6.07	5.65	5.62	0	1	0
20	H	3	5.42	5.62	5.65	0	2	2
21	H	7	8.07	5.76	8	9	5	10
22	H	7	8.88	7.1	8.53	13	5	3
23	H	11	9.27	8.25	11.5	6	8	6
24	H	11	12.5	12	11.2	7	12	11
25	J	3.5	5.29	5.28	5.11	2	3	1
26	J	3.5	5.14	5.63	4.98	2	3	3
27	J	6	7.22	8.14	7.54	7	4	5
28	J	6	7.71	8.1	7.63	5	6	7
29	J	8.5	8.52	8.48	9.52	5	6	3
30	J	8.5	8.87	9.58	9.15	7	5	9
31	N	3	6.5	6.56	5.86	0	1	0
32	N	3	5.26	5.97	4.74	1	1	0
33	N	5.5	7.82	7.95	9.41	3	3	3
34	N	5.5	6.35	9.21	8.16	10	12	17
35	N	8	11.1	10.2	9.47	26	16	18
36	N	8	9.25	9.23	9.43	26	22	24

A portion of the motivation behind the Percometer testing was to determine whether the dielectric and conductivity values were affected by the test location on each soil specimen's surface. It was postulated that these values may change as measurements are taken closer to the

edge of the specimen due to interference from the aluminum split mold or uneven soil properties. The data in Table 4.7 make it clear that the dielectric permittivity values remained constant across the diameter of the specimen. The conductivity values measured in the center of the specimen, on the other hand, were about 6% smaller then the values measured near the edges. It is possible that this effect was caused by electrical noise from the specimen's boundary, however, more testing would be necessary to validate this conclusion.

The dielectric value, k, recorded by the Percometer can be used to estimate the volumetric moisture content of the soil after a sufficient amount of data has been accumulated to establish a trend. The Percometer data collected over the course of this study indicated that the following function was an approximate way to estimate a soil's gravimetric moisture content directly from dielectric permittivity values without accounting for density variation.

$$\omega = 1.18k - 3.47 \tag{4.12}$$

This relationship (Figure 4.11) is most likely accurate only for the soil specimens used in this test; the addition of more soil samples to the test pool would most likely have a large effect on the values in this relationship. The dielectric and oven dry moisture data used to create this relationship are summarized in Table 4.8.

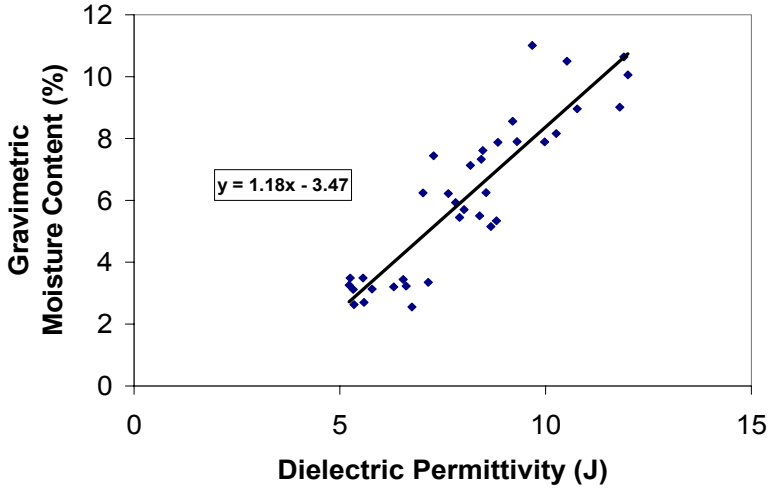

Figure 4.11: Data used in Dielectric-Moisture Relationship

Table 4.8: Dielectric Moisture Content Estimates

Test #	Sample	Percometer Results		Gravimetric Moisture Content			
		Dielectric	Conductivity	Target	Measured from Oven	Predicted from Dielectric	Difference
		J	uS/cm	%	%	%	%
1	A	6.75	0.00	2.5	2.55	4.46	1.91
2	A	7.15	0.00	2.5	3.35	4.72	1.37
3	A	8.67	5.67	5	5.15	5.72	0.57
4	A	8.80	6.33	5	5.34	5.81	0.47
5	A	9.98	8.67	7.5	7.89	6.58	-1.31
6	A	8.47	13.67	7.5	7.61	5.59	-2.02
7	D	5.34	0.00	3	2.63	3.53	0.90
8	D	5.59	0.33	3	2.70	3.69	0.99
9	D	7.02	7.67	6	6.24	4.63	-1.61
10	D	-	-	6	6.10	-	-
11	D	11.80	28.67	9	9.01	7.79	-1.22
12	D	12.00	40.33	9	10.06	7.92	-2.14
13	F	6.61	2.00	3.5	3.23	4.36	1.13
14	F	6.54	2.33	3.5	3.44	4.31	0.87
15	F	8.02	7.00	6	5.7	5.29	-0.41
16	F	8.55	11.67	6	6.25	5.64	-0.61
17	F	10.77	22.67	8.5	8.96	7.11	-1.85
18	F	8.43	6.67	8.5	7.33	5.57	-1.76
19	H	5.78	0.33	3	3.13	3.81	0.68
20	H	5.56	1.33	3	3.49	3.67	0.18
21	H	7.28	8.00	7	7.44	4.80	-2.64
22	H	8.17	7.00	7	7.13	5.39	-1.74
23	H	9.67	6.67	11	11.01	6.38	-4.63
24	H	11.90	10.00	11	10.64	7.85	-2.79
25	J	5.23	2.00	3.5	3.26	3.45	0.19
26	J	5.25	2.67	3.5	3.49	3.47	-0.03
27	J	7.63	5.33	6	6.22	5.04	-1.18
28	J	7.81	6.00	6	5.93	5.16	-0.77
29	J	8.84	4.67	8.5	7.88	5.83	-2.05
30	J	9.20	7.00	8.5	8.56	6.07	-2.49
31	N	6.31	0.33	3	3.20	4.16	0.96
32	N	5.32	0.67	3	3.12	3.51	0.39
33	N	8.39	3.00	5.5	5.50	5.54	0.04
34	N	7.91	13.00	5.5	5.45	5.22	-0.23
35	N	10.26	20.00	8	8.16	6.77	-1.39
36	N	9.30	24.00	8	7.90	6.14	-1.76

The moisture contents calculated from the dielectric values using equation (4.12) tended to be overestimated for specimens with smaller moisture contents and underestimated for specimens with larger moisture contents. The difference between the estimates and the true values was often 2%, although the difference was greater than 4% for some specimens. Based on these results the dielectric relationship should not be used for anything more than an estimate of the moisture content without a greater pool of data.

4.4.4 Shear Strength Data

Each specimen that was tested was reproduced and tested a second time at nearly the same density and moisture condition. This provided the opportunity to measure the shear strength at two different confining pressures. The first specimen prepared at a particular moisture content was tested at 27.6 kPa (4 psi) of confinement; the second specimen was tested at 55.2 kPa (8 psi). The shear strength testing was carried out at a constant stroke rate of 0.76 mm/s (0.03 in./s). As a result, specimens fail within a matter of seconds (Table 4.9).

Table 4.9: Deviator Stress Values at Shear Failure

Test #	Sample	Moisture Content	Density	σ_3	Deviatoric Stress
		%	kg/m^3	kPa	kPa
1	A	2.55	2083	27.6	423
2	A	3.35	2117	55.2	590
3	A	5.15	2098	27.6	418
4	A	5.34	2168	55.2	625
5	A	7.89	2194	27.6	193
6	A	7.61	2225	55.2	657
7	D	2.63	1954	27.6	345
8	D	2.70	1954	55.2	457
9	D	6.24	1983	27.6	253
10	D	6.10	1984	55.2	773
11	D	9.01	1966	27.6	-
12	D	10.06	1984	55.2	-
13	F	3.23	1820	27.6	137
14	F	3.44	1828	55.2	326
15	F	5.70	1840	27.6	180
16	F	6.25	1857	55.2	472

Table 4.9 Continued: Deviator Stress Values at Shear Failure

Test #	Sample	Moisture Content	Density	σ_3	Deviatoric Stress
		%	kg/m^3	kPa	kPa
17	F	8.96	1884	27.6	156
18	F	7.33	1853	55.2	462
19	H	3.13	1703	27.6	259
20	H	3.49	1732	55.2	411
21	H	7.44	1760	27.6	158
22	H	7.13	1760	55.2	414
23	H	11.01	1786	27.6	199
24	H	10.64	1788	55.2	353
25	J	3.26	1865	27.6	203
26	J	3.49	1849	55.2	298
27	J	6.22	1837	27.6	183
28	J	5.93	1858	55.2	299
29	J	7.88	1852	27.6	189
30	J	8.56	1854	55.2	305
31	N	3.20	1929	27.6	351
32	N	3.12	1941	55.2	457
33	N	5.50	1980	27.6	417
34	N	5.45	2040	55.2	575
35	N	8.16	2030	27.6	321
36	N	7.90	2064	55.2	545

The data from these tests can be used to calculate the friction angle and cohesion for each soil; these quantities are useful in a number of applications. In particular, the data can be used to calculate E/E_{MAX} curves using the hyperbolic model; this process is explained in section 4.5. The friction angle (ϕ) and cohesion (c) values can be calculated by plotting both shear strength tests, which were performed at 27.6 and 55.2 kPa, on the same principal stress plot, σ_1 versus σ_3:

$$\sigma_1 = 2c\sqrt{K_p} + K_p\sigma_3 \tag{4.13}$$

$$K_p = \frac{1+\sin\phi}{1-\sin\phi}$$

The slope of the trendline formed by the two points, K_p, is needed to calculate the friction angle of the specimen. Once the friction angle is known, the cohesion can be calculated from the y-

intercept of the principal stress plot. The cohesion and friction angle values calculated using this procedure are summarized in Table 4.10.

Table 4.10: Cohesion and Friction Angle of Samples

Sample	Average Moisture Content	Average Density	Cohesion	Friction Angle ø
	%	kg/m^3	kPa	Degrees
A	2.95	2100	48.0	48.8
A	5.25	2133	36.5	52.1
A	7.75	2210	0.0	57.7
D	2.67	1954	51.8	42
D	6.17	1984	0.0	60.1
D	9.54	1975	-	-
F	3.34	1824	0.0	47.8
F	5.98	1849	0.0	53.4
F	8.15	1869	0.0	52.8
H	3.31	1718	21.1	47.2
H	7.29	1760	0.0	51.4
H	10.83	1787	8.6	47.5
J	3.38	1857	25.6	39.3
J	6.08	1848	14.5	42.7
J	8.22	1853	16.0	42.6
N	3.16	1935	55.8	41
N	5.48	2010	50.0	47.8
N	8.03	2047	16.2	53.3

As expected, the specimens' shear strength decreased as their moisture content increased. However, because only two shear strength tests could be performed per moisture content, these values are based on the results from only two points and some trendlines were forced through zero.

4.5 Degradation Curves

Several methods have been proposed to model the relationship between a material's modulus and maximum modulus at a given strain level; one such method is a degradation curve, which plots E/E_{MAX} values at different strains. At strain levels below 0.001%, a sandy soil's Young's modulus is equal to E_{MAX}. Therefore, E/E_{MAX} is equal to one. However, at larger strain levels, the values begin to diverge. In addition, the E/E_{MAX} relationship will be different for tests conducted at different levels of confinement.

A variety of methods are used to estimate modulus degradation curves. One of them, the hyperbolic model, calculates a material's degradation curve using only the friction angle and cohesion of a soil. These values are relatively easy to acquire from a soil sample. Therefore, the hyperbolic model may be of interest to practioners looking to compare the results from small strain testing devices that operate at a known strain level to M_R values.

The first step in using the hyperbolic model is to calculate the ultimate shear strength, τ_{ult}, of a test specimen, which is the shear stress at which the specimen fails upon a particular plane. As an example, τ_{ult} would be equal to τ_{max} along the plane oriented at 45° to the major principal stress when φ=0°. These quantities are plotted in Figure 4.12.

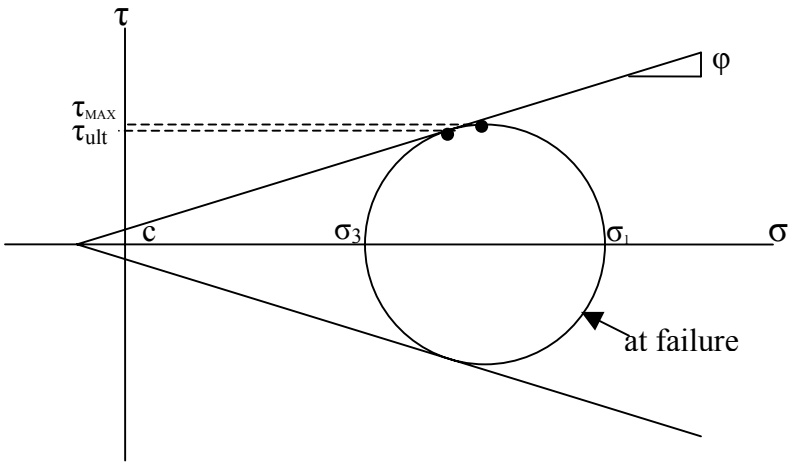

Figure 4.12: Ultimate Shear Strength

By measuring the friction angle and cohesion for a soil, τ_{ult} can be estimated using:

$$\tau_{ult} = \sqrt{\left(\left(\frac{1+k_0}{2}\right)\sigma_n' * \sin\phi' + c * \cos\phi'\right)^2 - \left(\left(\frac{1-k_o}{2}\right)\sigma_n'\right)^2} \tag{4.14}$$

where σ_n' is the effective normal stress, φ is the friction angle, c is the cohesion, and k_o is the coefficient of earth pressure at rest, which can be calculated using:

$$k_o = 1 - \sin\phi \tag{4.15}$$

The hyperbolic model also makes use of a shear strain variable called γ_R, which is defined as the ratio between τ_{ult} and G_{MAX}:

$$\gamma_R = \frac{\tau_{ult}}{G_{MAX}} \tag{4.16}$$

Finally, G/G_{MAX} can be calculated using γ and γ_R in the hyperbolic equation:

$$\frac{G}{G_{MAX}} = \frac{1}{1+\frac{\gamma}{\gamma_R}} \tag{4.17}$$

Several cyclic triaxial tests were performed at different confining pressures (24.1 kPa, 48.3 kPa, and 96.5 kPa) after completing the original test matrix for this study. The purpose of this testing was to create the data needed to determine the reliability of the hyperbolic model curves for the soils being tested. Sample N was used for this project because its gradation was a good average representation of all six samples. These tests involved loading a soil with ten sine-wave load paths 10 s in duration moving from a small contact load to the peak stress. This loading history was repeated with up to ten different maximum stress values for each level of confinement. Bender elements were used to measure wave speeds at the beginning of the test. A

shear strength test was conducted after completing the cyclic tests at each confining pressure to gather the data needed to calculate the friction angle and cohesion of the sample.

Values of Young's modulus were calculated for each cycle by dividing the peak stress applied by the peak displacement for one of the latter cycles in the 10-cycle series. The latter cycles were used because the initial cycles in the series often contained significant amounts of plastic deformations. These Young's moduli were divided by the E_{MAX} values calculated from the wave speed data. The hyperbolic model was then used to calculate the degradation curves for the soil being tested; these quantities are plotted in Figure 4.13.

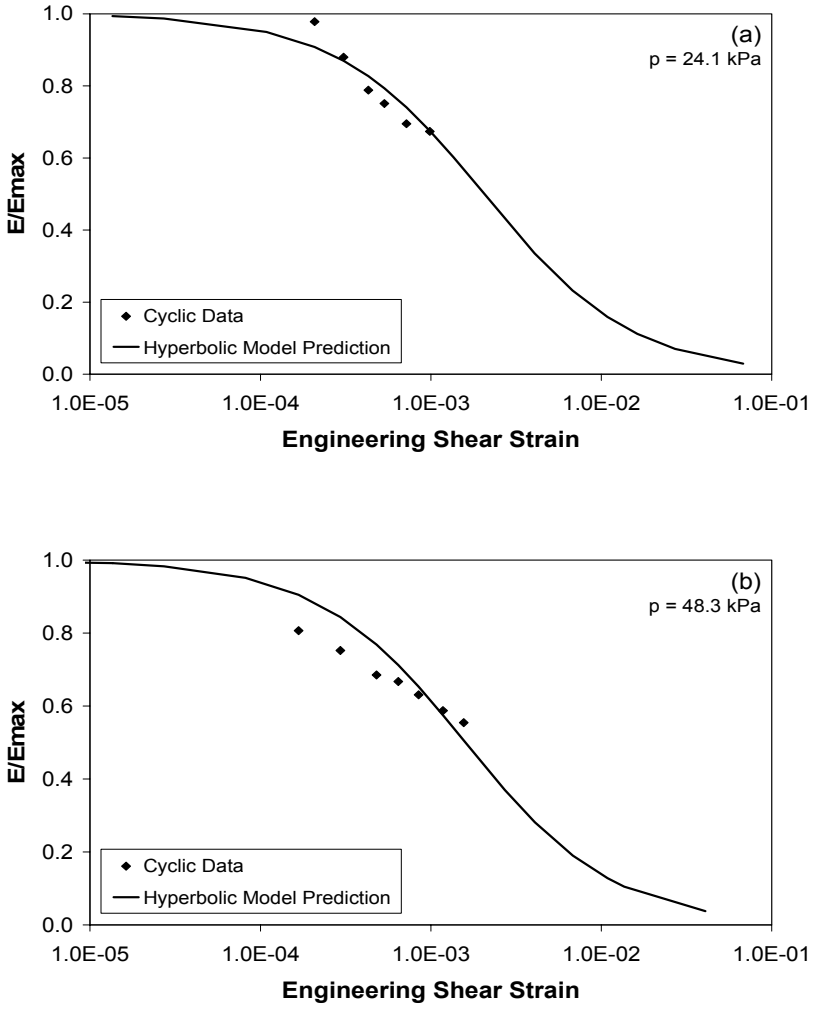

Figure 4.13: Hyperbolic Predictions of Cyclic Triaxial Results

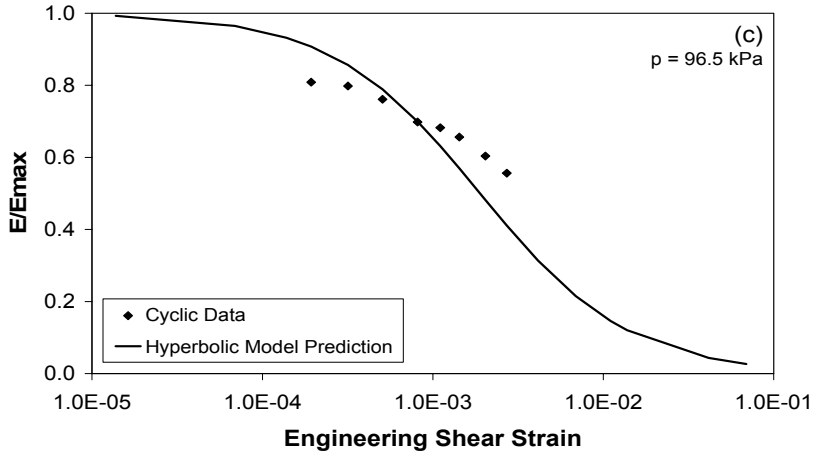

Figure 4.13 Continued: Hyperbolic Predictions of Cyclic Triaxial Results

The hyperbolic model predictions match the experimental data closely. The majority of the cyclic triaxial data points are within 5% of the predicted values for that strain level. Some of the points at the limits of each sequence differ from the predicted values by up to 15%. However, many of the points at the smallest strain were calculated near the resolution limit of the displacement measurements. In addition, α values for the points with the smallest strains were relatively large compared to the other points as indicated by Table 4.3.

The hyperbolic model appears to predict a slightly steeper E/E_{MAX} slope than the data would suggest over the strain region being tested. The cause for this is unknown. However, if the curves suggested by the cyclic triaxial data trends were extended they would not reach an E/E_{MAX} value of 1.0 at a strain level of 0.001%. As stated in section 2.2.3, most researchers agree that sandy soils are within the linear region of the stress-strain curve below this strain threshold. Based on these observations the hyperbolic model appears to provide a good fit for the experimental data.

Chapter 5
Summary and Conclusions

This study involved a comparative resilient modulus and bender element testing of 36 triaxial specimens. Six granular soils representative of base and subgrade materials found in Minnesota were used. These specimens were prepared at three different moisture contents per soil and compacted to their standard Proctor optimum dry density. Each specimen was subjected to resilient modulus testing as specified by Mn/DOT modified LTPP P46. The loading sequences of this test were halted periodically to perform small strain bender element testing, which can establish relative maximum modulus values by measuring wave speeds. Following the test protocol, the specimens were loaded until failure to determine their shear strength. The objective of this testing was to measure the resilient modulus values of reference soil samples while establishing a relationship between the resilient modulus and the maximum modulus of these soils. A number of conclusions were reached during this investigation.

1) The hyperbolic model is able to accurately model the strain-dependent modulus reduction of a soil using only the small-strain modulus, friction angle, and cohesion as input parameters. As a result, the maximum modulus values calculated from the wave speeds measured by small strain testing instruments can be converted into resilient modulus values knowing only the cohesion and friction angle of the soil. The cohesion and friction angle of the soil can be established during shear strength testing. Therefore, pavement inspectors can use this relation to relate the results of the small-strain testing instruments used in the field to the laboratory-measured resilient modulus values used in pavement design.

2) The modulus and strength of soils tested increased as their moisture contents decreased. This trend was visible in the results from the resilient modulus, bender element, and triaxial strength testing. This is a reasonable result that is consistent with the large amount of energy used to compact the specimens with smaller moisture contents.

3) The three LVDTs used as a part of the triaxial testing setup often measured displacement values that were in poor agreement with each other. Possible causes for this include uneven specimen deformation, an uneven specimen surface, or a poor bond between the LVDT apparatus and the specimens' membranes. A quantity called an α-value was used to model the degree to which the displacement measures were inconsistent for each loading sequence of each test. Loading sequences performed with relatively low deviator stresses had larger α-values than the other tests.

4) The best estimate of the gravimetric moisture content from the dielectric permittivity values in this study is

$$\omega = 1.18k - 3.47$$

However, this relation often produces moisture content differences of 0.03 to 4.63 percent from the oven dried values, and is unproven for soils other than the six used in this study.

References

[1] Hoffmann, O. *Verification and Enhancements of Portable Deflectometer Devices* (Minneapolis, MN.: University of Minnesota, 2003).

[2] Federal Highway Administration Pavement Performance Division, *Resilient Modulus of Unbound Granular Base/Subbase Materials and Subgrade Soils*, *Long Term Pavement Performance, Protocol 46* (Federal Highway Administration Pavement Performance Division, 1996).

[3] National Cooperative Highway Research Program, *Recommended Standard Method for Routine Resilient Modulus Testing of Unbound Granular Base/Subbase Materials and Subgrade Soils, Protocol 1-28A* (National Cooperative Highway Research Program, 2002).

[4] Atkinson, J.H. and Sallfors, G. (1991). Exerimental determination of stress-strain-time characteristics in laboratory and in situ tests. *Proceedings of the International Conference on Soil Mechanics and Foundation Engineering*, V3: 915-956.

[5] Lai, C. G. and Rix, G. J. (2002). Solution of the Rayleigh Eigenproblem in Viscoelastic Materials. *Bulletin of the Seismological Society of America*, V92(6): 2297- 2309.

[6] Tatsuoka, F., Teachavorasinskun, S., Dong, J., Kohata, Y., and Sato T. (1994). Importance of measuring local strains in cyclic triaxial tests on granular materials. *ASTM Special Technical Publication*, No. 1213: 288-302.

[7] Cuccovillo, T. and Coop, M.R. (1997). The measurement of local axial strains in triaxial tests using LVDTs. *Geotechnique,* V47(1): 167-171.

[8] Jovicic, V. and Coop, M.R. (1997). Stiffness of coarse-grained soils at small strains. *Geotechnique,* V47(3): 545-561.

[9] Iwasaki, T., Tatsuoka, F., and Takagi, Y. (1978). Shear moduli of sands under cyclic torsional shear loading. *Soils and Foundations*, V18(1): 39-56.

[10] Bolton, M.D. and Wilson, J.M.R. (1989). Experimental and theoretical comparison between static and dynamic torsional soil tests. *Geotechnique*, V39(4): 585-599.

[11] Jovicic, V. and Coop, M.R. (1998). The measurement of stiffness anisotropy in clays with bender element tests in the triaxial apparatus. *Geotechnical Testing Journal,* V21(1): 3-10.

[12] Jovicic, V. and Coop, M.R. (1996). Objective criteria for determining G_{max} from bender element tests. *Geotechnique,* V46(2): 357-362.

[13] Schmertmann, J. H. (1991). The mechanical aging of soils. The twenty-fifth Karl Terzaghi lecture. *Journal of Geotechnical Engineering, ASCE*, V105(9): 1288-1330.

[14] Santamarina, J.C. and Fratta, D. (1998). Introduction to Discrete Signals and Inverse Problems in Civil Engineering. *ASCE Press*, Reston, VA: 63-71.

[15] Ishibashi, I. (1992). Discussion to "Effect of soil plasticity on cyclic response". *Journal of Geotechnical Engineering*, V118(5): 830-832.

[16] Sanches-Salinero, I., Roesset, J. M.and Stokoe, K. H. . *Analytical studies of body wave propagation and attenuation* (Austin, TX.: University of Texas, Report GR 86-15, 1986).

[17] Viggiani, G. and Atkinson, J.H. (1995). Interpretation of bender element tests. *Geotechnique,* V45(1): 149-154.

Appendix A

Soil Sample Data

Mn/DOT performed gradations and prepared compaction curves for the soil samples used in this study. These curves were used to determine the target values of moisture content and dry density of the test specimens; this process was outlined in section 2.1.1. The gradation data is contained in Table A.1 and Figure A.1. The compaction plots are included as figures A.1 through A.6

Table A.1: Soil Gradation Data

Sieve Mesh	Sample					
	A	D	F	H	J	N
(mm)						
63	100	100	100	100	100	100
50	94	100	100	100	100	100
37.5	90	100	100	100	100	100
31.5	87	98	100	100	100	100
25	81	97	100	100	100	100
19	77	95	100	100	100	100
16	73	94	100	100	100	100
12.5	69	93	100	100	100	98
9.5	65	90	99	100	100	96
4.75	55	84	98	100	100	86
2.36	48	76	98	100	100	76
2	47	74	98	100	100	73
1.18	41	65	98	99	100	64
0.6	30	44	96	98	93	48
0.425	24	31	92	97	83	38
0.3	16	18	78	91	64	26
0.15	7	6	29	53	21	12
0.075	3.6	4.3	10.3	21.4	2	7.4

Figure A.1: Gradations for Samples

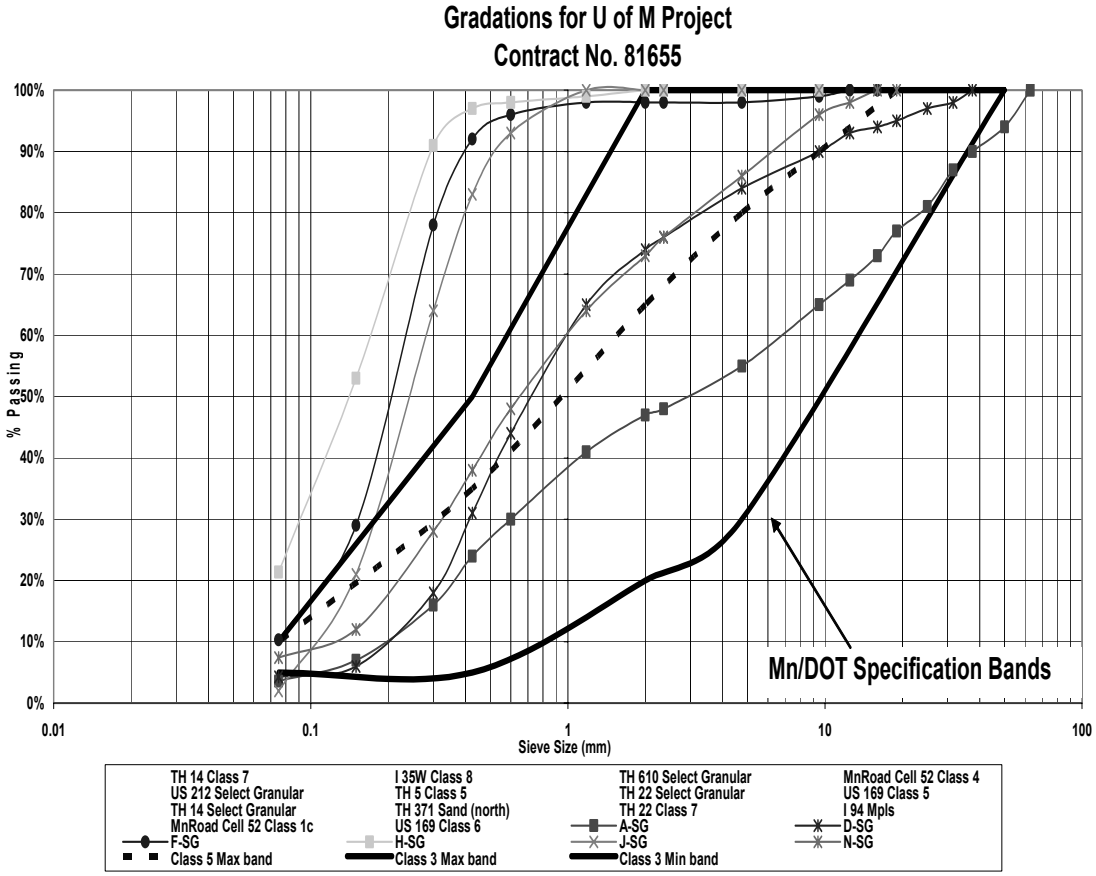

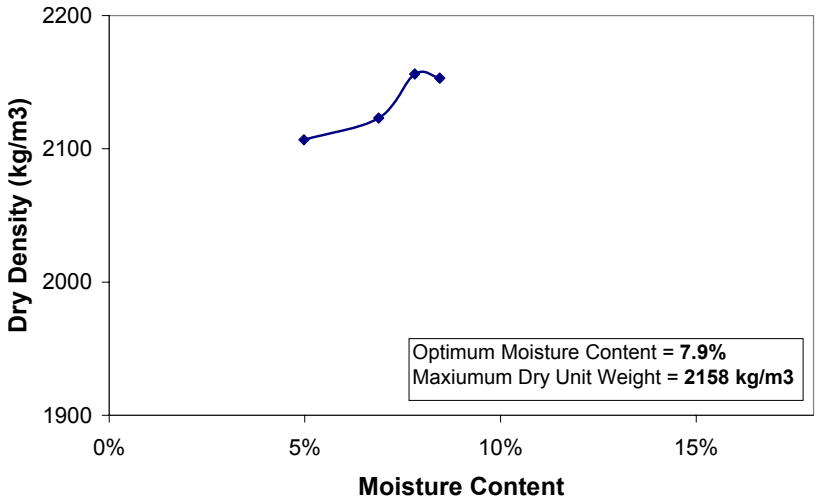

Figure A.2: Standard Proctor Compaction Curve for Sample A

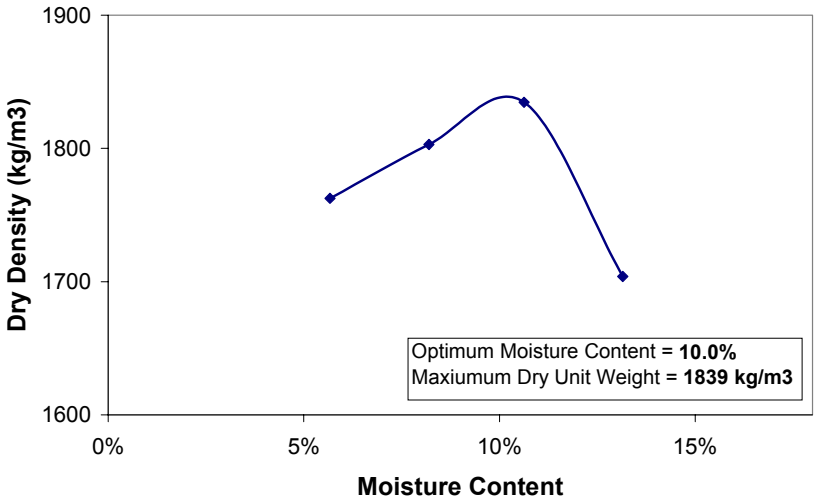

Figure A.3: Standard Proctor Compaction Curve for Sample D

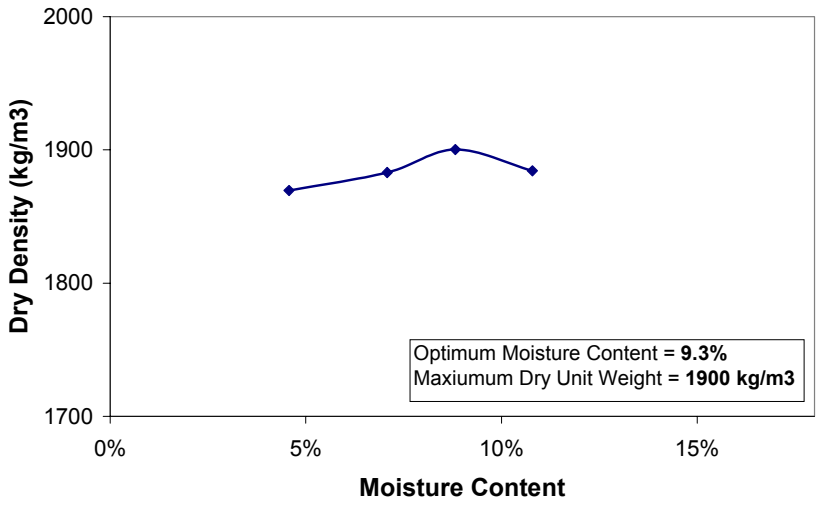

Figure A.4: Standard Proctor Compaction Curve for Sample F

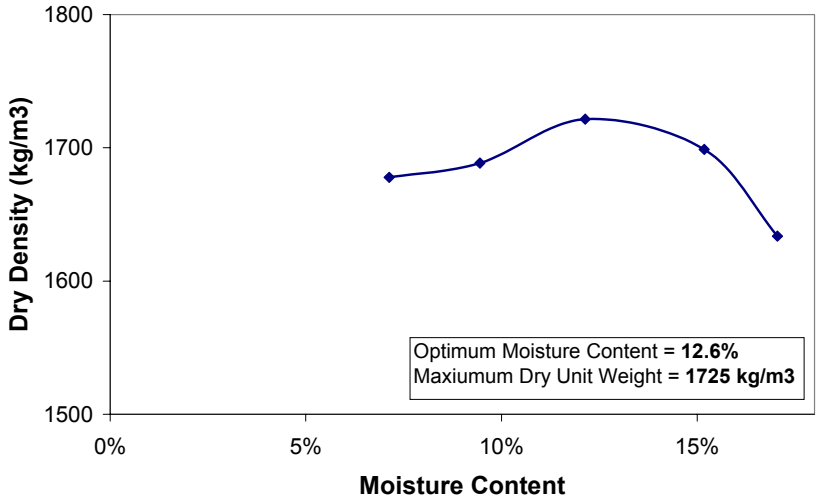

Figure A.5: Standard Proctor Compaction Curve for Sample H

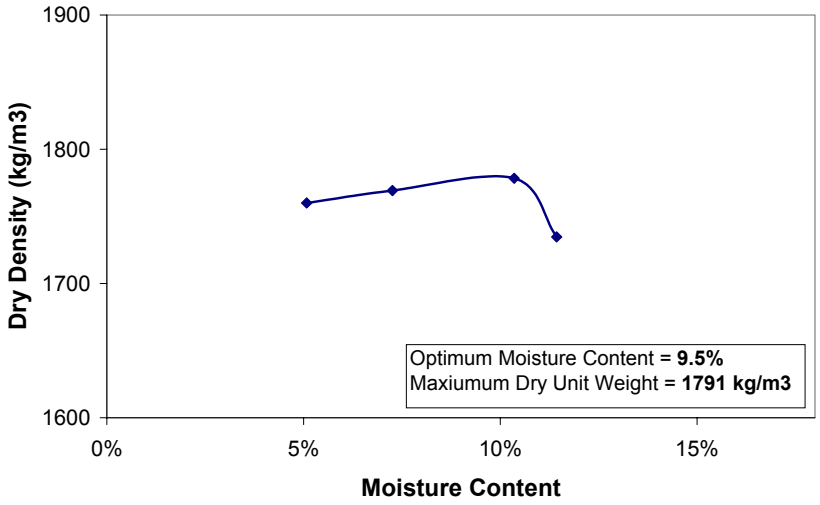

Figure A.6: Standard Proctor Compaction Curve for Sample J

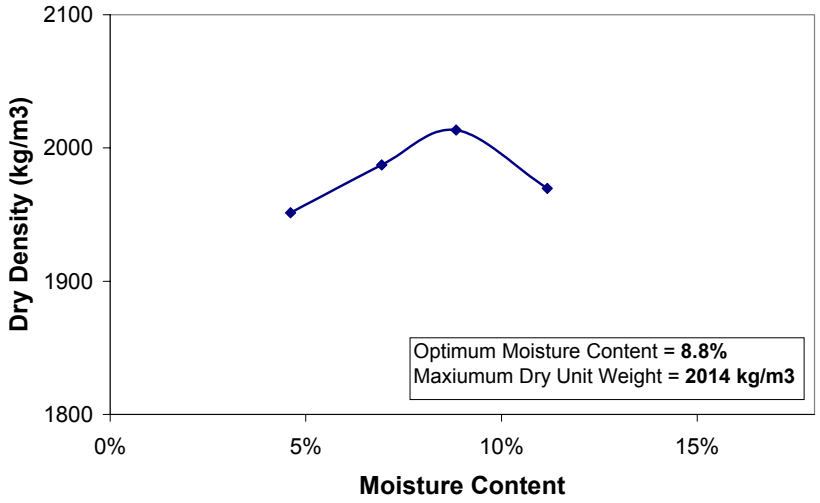

Figure A.7: Standard Proctor Compaction Curve for Sample N

Appendix B

System Calibration

The 22.2 kN (5 kip) load cell and 13 mm (0.5 in.) LVDTs were calibrated prior to testing to ensure their accuracy. The load cell was calibrated using a 22.2 kN (5 kip) proving ring. The LVDTs were calibrated using a Vernier scale. In addition, the phase angle of the system's load and displacement response was calculated and the instrument calibration was compared to the resilient modulus system at Mn/DOT using proving rings. These results of the phase angle calculation and system comparison are included in this appendix.

Appendix B.1 Phase Angle

The phase angle of the load frame was calculated using method proposed within the LTPP P46 Laboratory Startup and Quality Control Procedure. This method involves using Microsoft Excel's LINEST command to calculate the relative phases of associated load and LVDT data. This data can then be used to calculate the time delay and the phase angle of the system.

The load and displacement data for use in this method was generated by performing the LTPP P46 loading sequence on an aluminum proving ring in place of a soil sample. The phase angles between the load cell and each of the individual LVDTs are summarized in Table B.1.

Table B.1: Phase Angles for Test System

	Delay	Phase Angle
	(s)	(Degrees)
LVDT 1	2.40E-04	-0.432
LVDT 2	1.13E-04	-0.204
LVDT 3	5.77E-05	-0.104
Average	**1.37E-04**	**-0.247**

Appendix B.2 Calibration Against Mn/DOT System

The load cell and LVDTs used in this study were compared to the load cell and LVDTs used by Mn/DOT's Materials Office. To do this, a 8.9 kN (2,000 lbf) proving ring that was used to calibrate Mn/DOT's system was brought to the University of Minnesota and placed underneath the load frame used in this research. A spare platen was placed on top of the proving ring so that a ball bearing could be used to transfer the load from the shaft to the proving ring; the load shaft would have been unable to connect cleanly with the proving ring without taking this precaution. The two LVDT collars used on triaxial specimens were placed within grooves set into the proving ring and held in place with an O-ring . The proving ring was then loaded manually over its full range. The data recorded during this comparison is displayed in Table B.2.

Table B.2. Load and Displacement Measurements for University's Load Frame

Load			Displacement		
Triaxial Load Cell	**Proving Ring Calculated**	**Percentage Discrepancy**	**Average LVDT Reading**	**Proving Ring Dial Reading**	**Percentage Discrepancy**
(lb)	(lb)		(in)	(in)	
10	0.0	-	0.0000	0.0000	-
100	89.1	12.2%	0.0049	0.0047	3.5%
200	189.8	5.4%	0.0104	0.0101	2.6%
300	285.6	5.1%	0.0156	0.0154	1.3%
400	389.3	2.7%	0.0213	0.0209	1.8%
500	488.8	2.3%	0.0267	0.0262	1.9%
600	590.7	1.6%	0.0323	0.0317	1.8%
700	693.2	1.0%	0.0379	0.0371	2.1%
800	795.7	0.5%	0.0435	0.0426	2.0%
900	896.4	0.4%	0.0490	0.0479	2.2%
1000	997.7	0.2%	0.0545	0.0535	1.9%
1100	1099.0	0.1%	0.0600	0.0588	2.1%
1200	1200.9	-0.1%	0.0656	0.0644	1.9%
1300	1304.6	-0.4%	0.0713	0.0700	1.8%
1400	1404.7	-0.3%	0.0767	0.0754	1.8%
1500	1506.0	-0.4%	0.0823	0.0809	1.7%
1400	1403.5	-0.2%	0.0767	0.0753	1.8%
1300	1305.8	-0.4%	0.0713	0.0700	1.9%
1200	1202.7	-0.2%	0.0657	0.0645	1.9%
1100	1103.2	-0.3%	0.0603	0.0591	2.0%
1000	999.5	0.0%	0.0546	0.0535	2.1%
900	899.4	0.1%	0.0491	0.0481	2.1%
800	793.3	0.8%	0.0433	0.0425	2.0%
700	696.2	0.5%	0.0380	0.0372	2.2%
600	591.9	1.4%	0.0323	0.0316	2.3%
500	494.3	1.2%	0.0270	0.0264	2.3%
400	390.5	2.4%	0.0213	0.0208	2.6%
300	290.5	3.3%	0.0159	0.0155	2.4%
200	189.8	5.4%	0.0104	0.0102	1.6%
100	88.5	13.0%	0.0048	0.0048	0.7%
10	-0.6	-	0.0000	-0.0001	-

The University of Minnesota's load frame produced results in good agreement with Mn/DOT's proving ring. The load readings were within 1% of the proving ring's value for the majority of its range; the less accurate readings at low load levels were the result of seating. The average LVDT displacement readings were consistently about 2% larger than the displacements measured by the dial gage of the proving ring.

One of the University of Minnesota's 8.9 kN (2 kip) proving rings was loaded inside of Mn/DOT load frame, however, due to an incompatible LVDT attachment system the displacement of the proving ring could not be recorded. The load data recorded during this test is displayed in Table B.3.

Table B.3. Load Measurements for Mn/DOT's Load Frame

Load		
Triaxial Load Cell	**Proving Ring Calculated**	**Percentage Discrepancy**
(lb)	(lb)	
9.0	14.7	-
244.9	239.7	2.2%
491.5	488.1	0.7%
736.4	729.8	0.9%
982.9	981.2	0.2%
886.3	893.1	-0.8%
788.0	796.3	-1.0%
689.7	700.4	-1.5%
589.8	600.6	-1.8%
491.5	497.9	-1.3%
393.2	403.0	-2.4%
294.9	304.2	-3.1%
244.9	252.4	-3.0%
195.0	206.4	-5.5%
95.1	102.7	-7.4%
6.5	18.6	-65.3%

The maximum load tested within the Mn/DOT load frame was lower than the maximum load tested within the load frame used for this research due to concerns about the stability of the proving ring within the system. However, the existing data indicates that both systems have similar contact problems at small loads and similar success measuring loads above 2.22 kN (500 lbf). The one noticeable difference between the systems was that the Mn/DOT system overestimated the load on the return section of the test while the load frame used during this research underestimated it by a similar amount. However, the load values measured during resilient modulus testing were taken at peaks and during rest periods between pulses; the data recorded by both systems should be comparable at these times.

The resilient modulus test is dynamic, therefore, an extra test was performed to determine whether both load frames would determine the same resilient modulus for the same material. This comparison would be impossible to carry out on a soil specimen without damaging the soil, therefore, the resilient modulus test regimen was carried out on a proving ring. The modulus calculated from a test of a proving ring would have little physical meaning, however, it would serve to compare systems. After performing a resilient modulus test procedure on a proving ring using both load frames the calculated M_R values were within 5% of each other.

It is reasonable to assume, based upon the data presented in this section, that the University of Minnesota's load frame would produce results comparable to the results from Mn/DOT's load frame.

Appendix C

Resilient Modulus Data Calculation Program

The following MATLAB 5.3 program was written to convert the data files produced during resilient modulus testing into a matrix containing load, displacement, stress, strain, and modulus data. The 15 data files produced during the resilient modulus testing are named Cycle1, Cycle2, etc. The program is run once for each of these cycles & the data from each is automatically placed into a spreadsheet within the MATLAB folder. The calculations take place using English units.

```
**************************************************************************
% Load Cycle number 'i'

clear;
load Data.txt;
N = Data;
load Cyclei;
M = Cyclei;
O = i;

% Confining Pressure of Cycle 'i' = 'j'

N(((((O-1)*5)+1):(((O-1)*5)+5)), 1) = j;

% Location of first load peak = 'k'

y = k;

% Set location to begin local maxima search

y = y - 100;

% Reset variables

count = 1;
W = 0;
X = 0;
Y = 0;
Z = 0;

% Search for load/displacement peaks
```

```
for z = 0:1:99
   A = M((y+201*z):(y+201*z+201),1);
   B = M((y+201*z):(y+201*z+201),3);
   C = M((y+201*z):(y+201*z+201),4);
   D = M((y+201*z):(y+201*z+201),5);
   M(count,7) = min(A);
   M(count,8) = min(B);
   M(count,9) = min(C);
   M(count,10) = min (D);

% Sum baseline load and displacement values after pulses

   for p = 0:1:200
      if M((y+201*z+p),1)==min(A)
         for k = 49:1:190
            W = W + M((y+201*z+p+k),1);
            X = X + M((y+201*z+p+k),3);
            Y = Y + M((y+201*z+p+k),4);
            Z = Z + M((y+201*z+p+k),5);
         end
      break
      end
   end

% Calculate average of summed load and displacement values

   W = W / 142;
   X = X / 142;
   Y = Y / 142;
   Z = Z / 142;

% Place baseline load/displacement values into working matrix

   M(count,12) = W;
   M(count,13) = X;
   M(count,14) = Y;
   M(count,15) = Z;

% Calculate change between peak and baseline values

   M(count,17) = (M(count,7) - W);
   M(count,18) = (M(count,8) - X);
   M(count,19) = (M(count,9) - Y);
   M(count,20) = (M(count,10) - Z);

% Reset variables

   W = 0;
   X = 0;
   Y = 0;
   Z = 0;
   count = count + 1;
   A = 0;
end
```

```
% Calculate average of the three displacement values

for m = 1:1:100
   M(m, 22) = (M(m, 18) + M(m, 19) + M(m, 20)) / 3;
end

Modulus = 0;

% Place data from final five cycles into final matrix

for l = 96:1:100
   N(l-95+((O-1)*5), 2) = (-1 * M(l,17));
   N(l-95+((O-1)*5), 3) = (-1 * M(l,18));
   N(l-95+((O-1)*5), 4) = (-1 * M(l,19));
   N(l-95+((O-1)*5), 5) = (-1 * M(l,20));
   N(l-95+((O-1)*5), 8) = (-1 * (M(l,22)/6));

% Calculate Young's modulus values

   M((l-95), 24) = M(l,17) / 9 / pi / M(l,22) * 6;
end

% Calculate deviator stress, bulk stress, and place values in final
     matrix

for q = 1:1:5
   N((((O-1)*5)+q), 6) = (N((((O-1)*5)+q), 2) / 3 / 3 / pi);
   N((((O-1)*5)+q), 7) = ((N((((O-1)*5)+q), 2) / 3 / 3 / pi) + (3 *...
     ...(N((((O-1)*5)+q), 1)))) / 3;
   N((((O-1)*5)+q), 9) = M(q,24);
end

% Export and format final matrix

Data = N
fid = fopen('Data.txt','w');
fprintf(fid,'%e %e %e %e %e %e %e %e %e\n',Data');
fclose(fid);

% Calculate average Young's modulus value for cycle

Modulus = (M(1,24) + M(2,24) + M(3,24) + M(4,24) + M(5,24)) / 5 / 1000


**********************************************************************
```

Appendix D

Data

Two of the most interesting ways to plot the resilient modulus and bender element data from this study are on plots using the Young's modulus versus confining pressure. This appendix contains these plots for each sample at every moisture content tested. The data from both repeats are included on the plot; the trendlines are created using the average of the data from both. Section D.1 contains the comparisons between the resilient modulus and E_{MAX}; section D.2 contains the comparisons between the resilient modulus and confining pressure.

D.1 Resilient Modulus and E_{MAX} Versus Confining Pressure

One of the primary goals of this research was to formulate a correlation between the resilient modulus and E_{MAX}. Figures D.1 through D.6 display data from both of these variables plotted against the confining pressure.

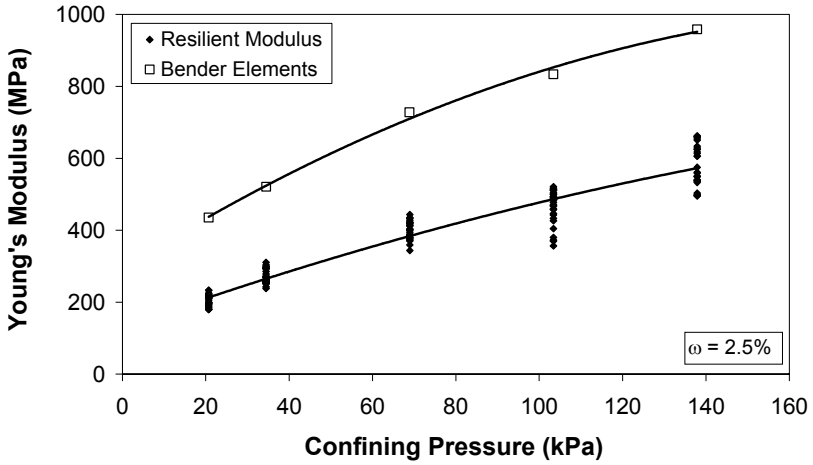

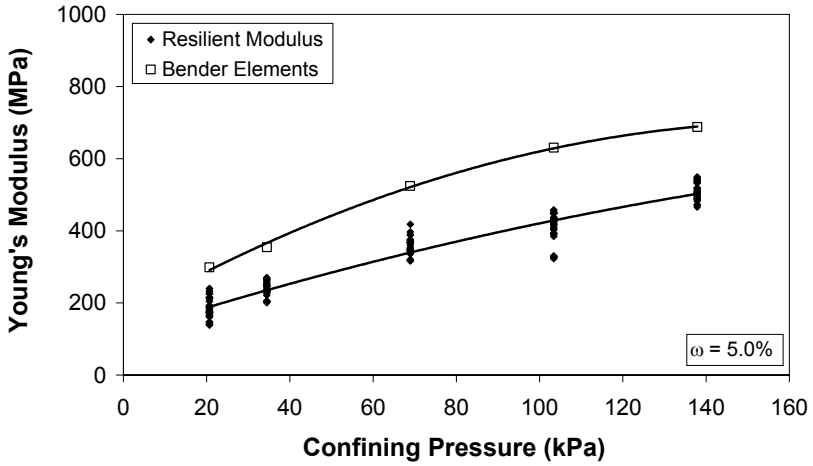

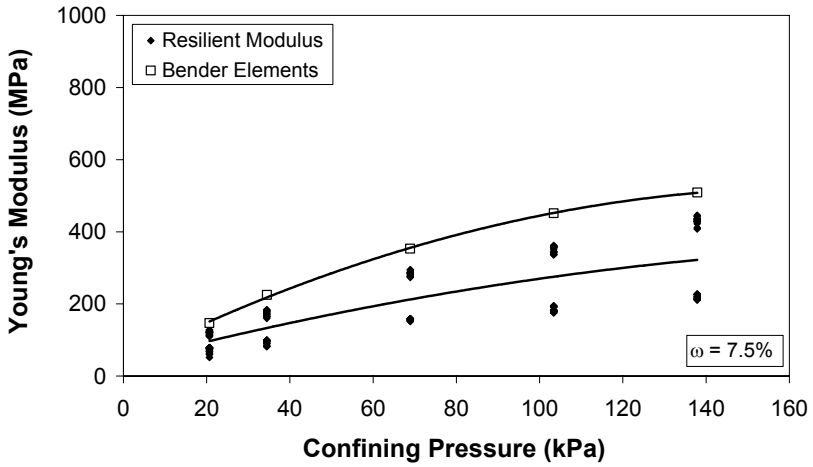

Figure D.1: Young Modulus Data from Sample A

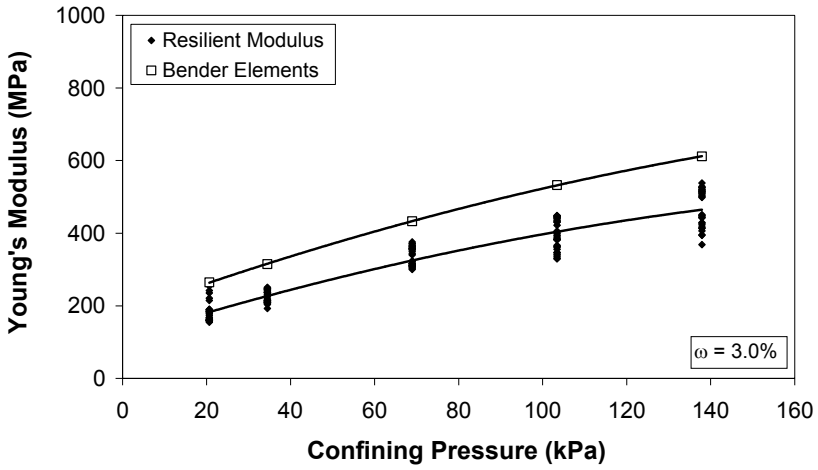

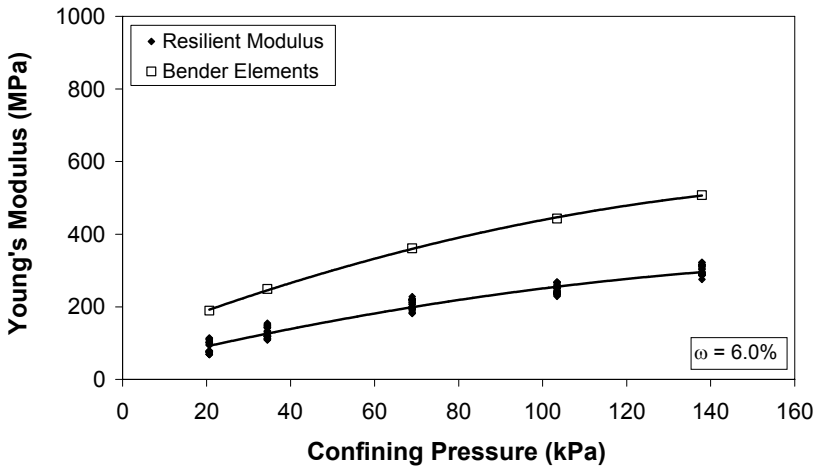

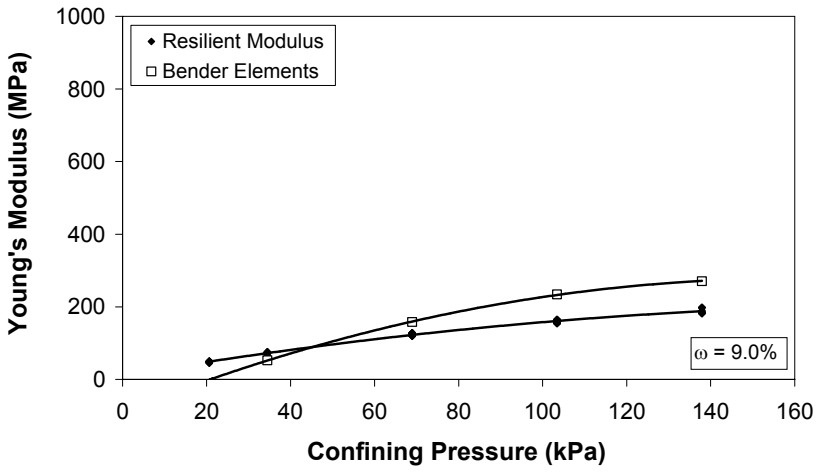

Figure D.2: Young Modulus Data from Sample D

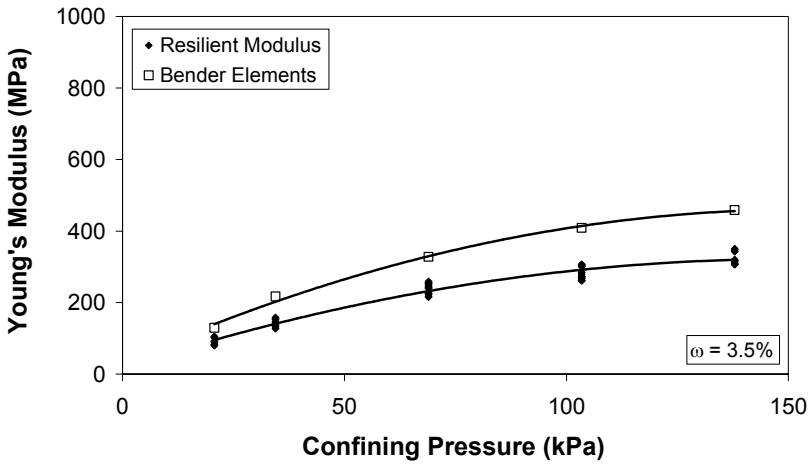

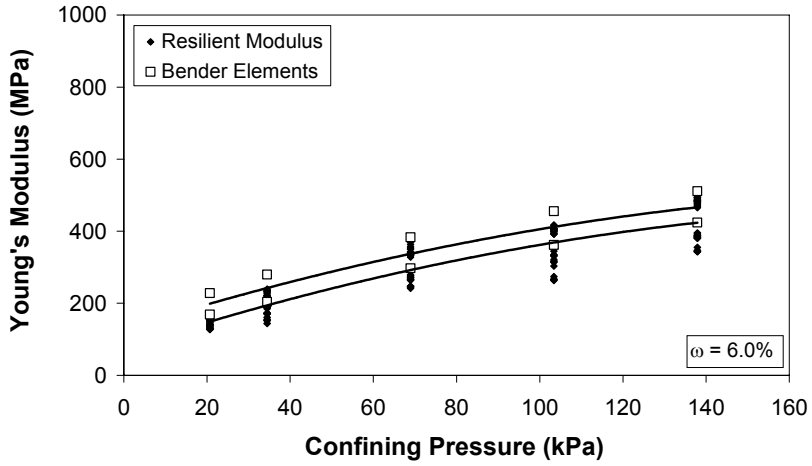

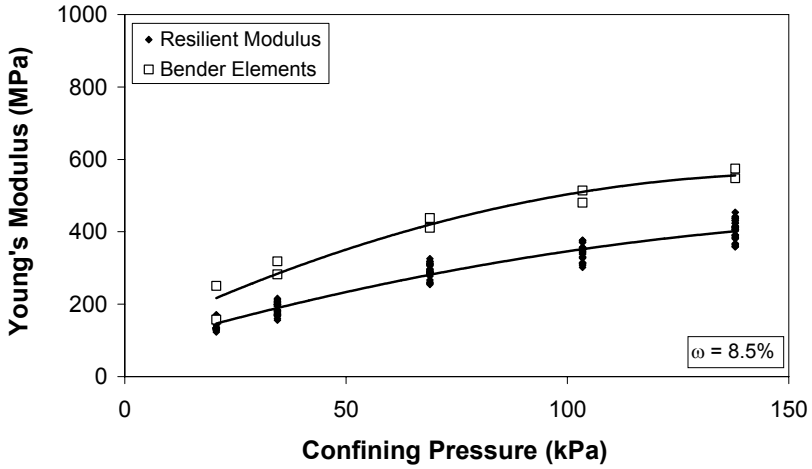

Figure D.3: Young Modulus Data from Sample F

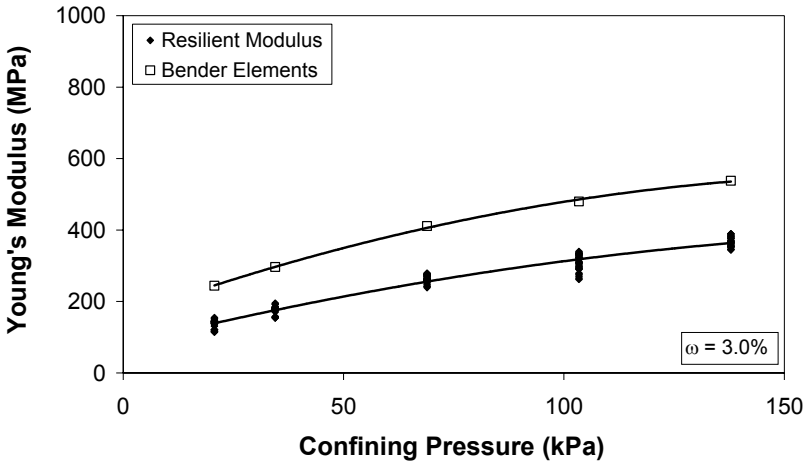

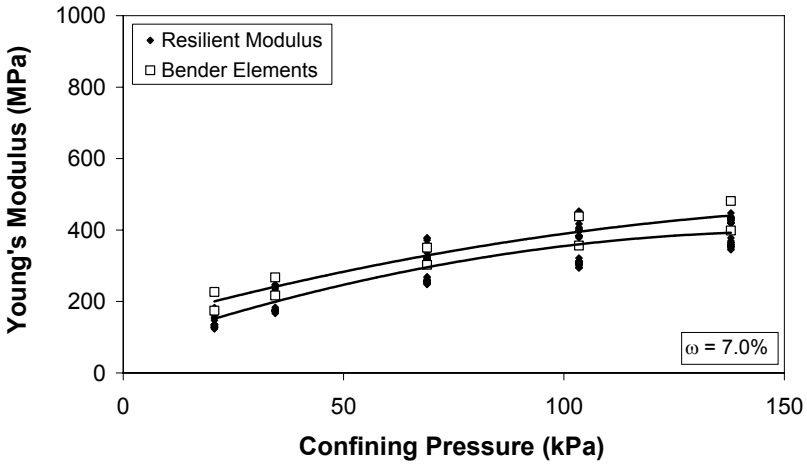

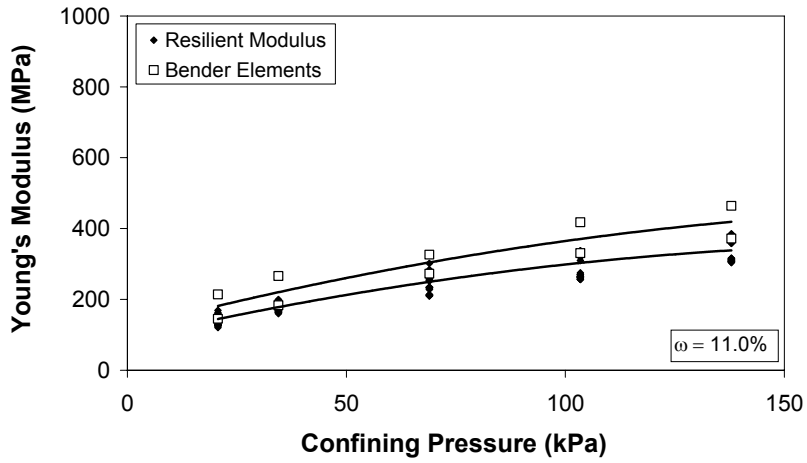

Figure D.4: Young Modulus Data from Sample H

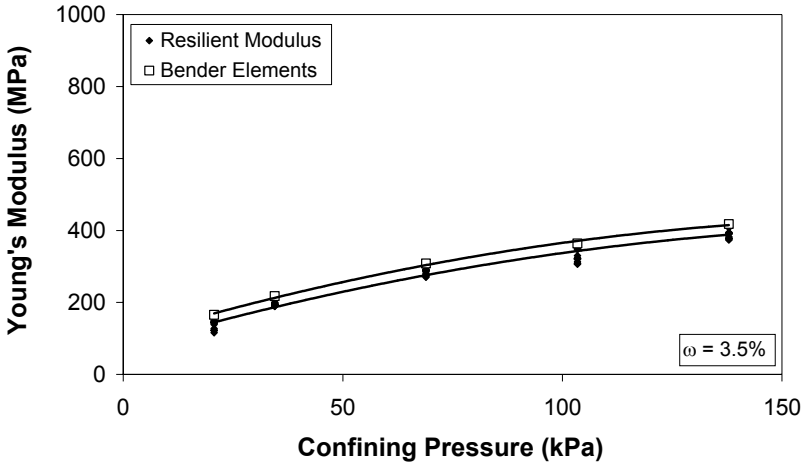

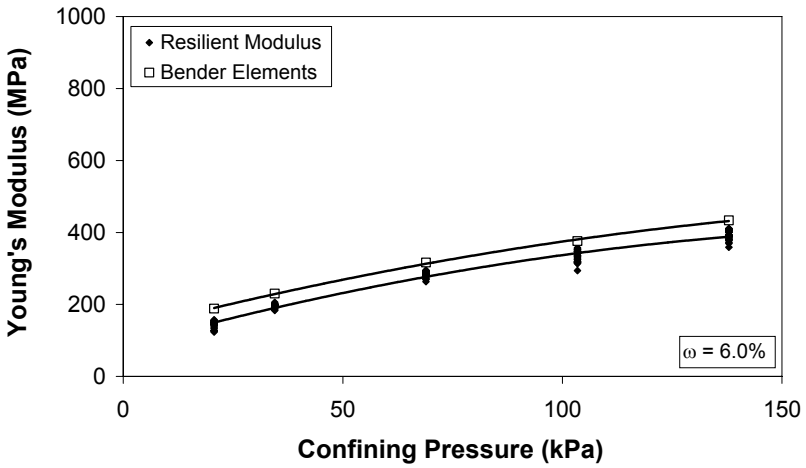

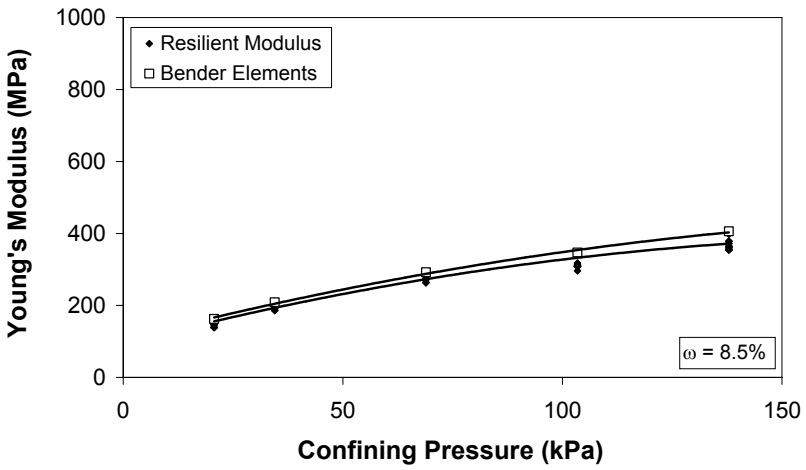

Figure D.5: Young Modulus Data from Sample J

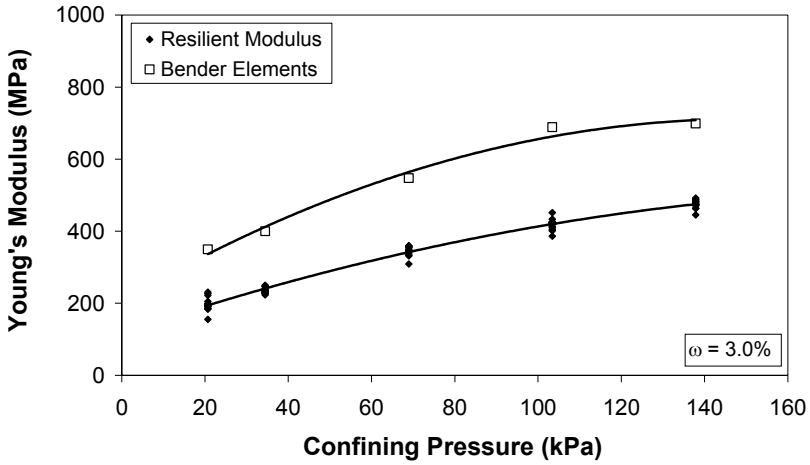

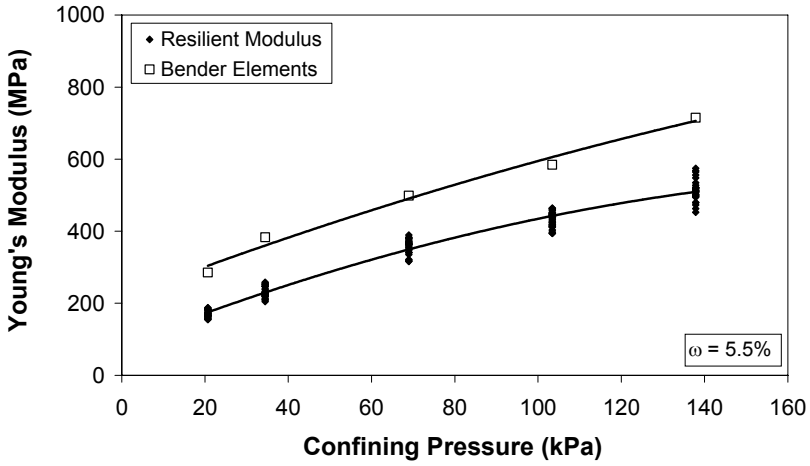

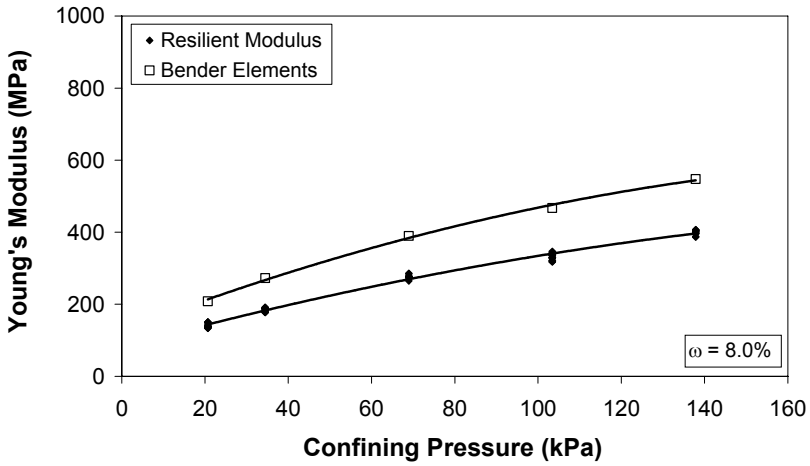

Figure D.6: Young Modulus Data from Sample N

D.2 Resilient Modulus Versus Confining Pressure

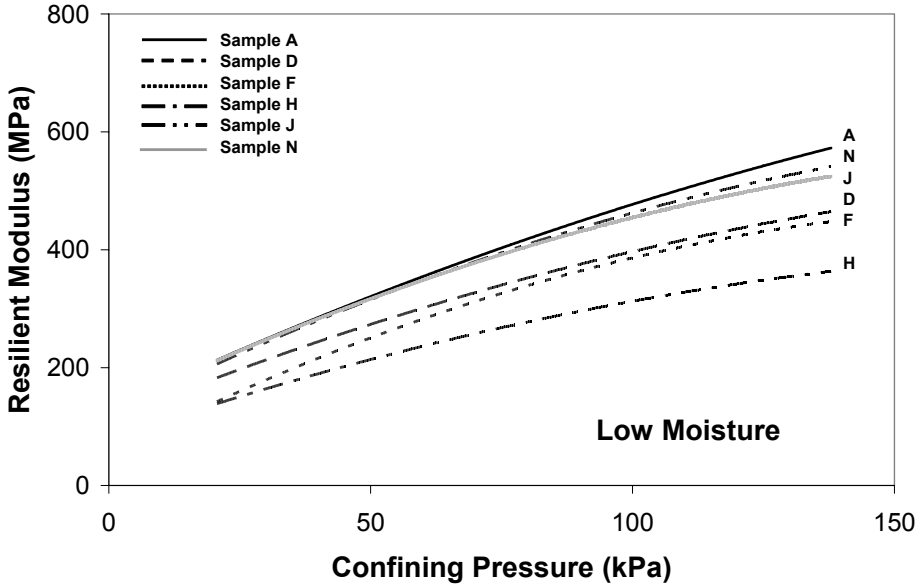

(a) Low Moisture Content (2.5%-3.5%)

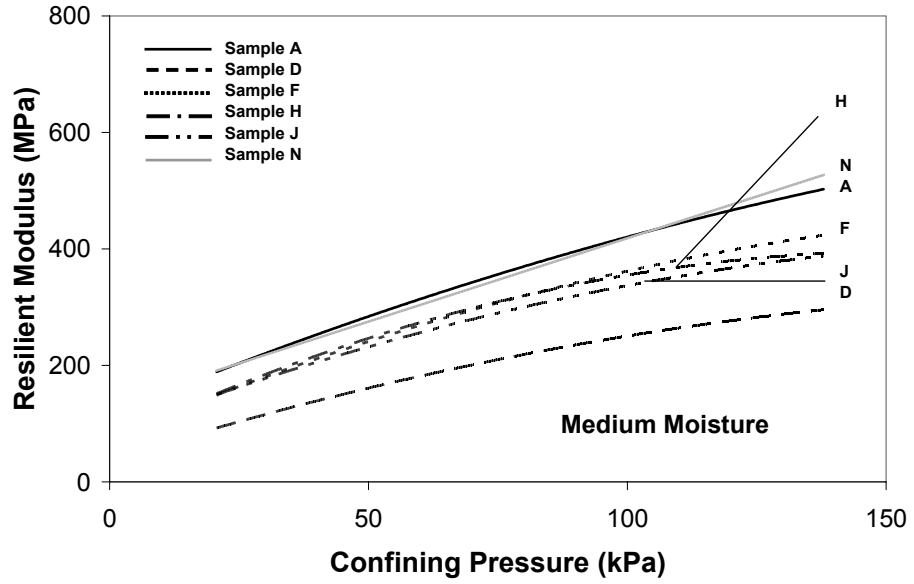

(b) Medium Moisture Content (5%-7%)

Figure D.7: Resilient Modulus Versus Confining Pressure Data

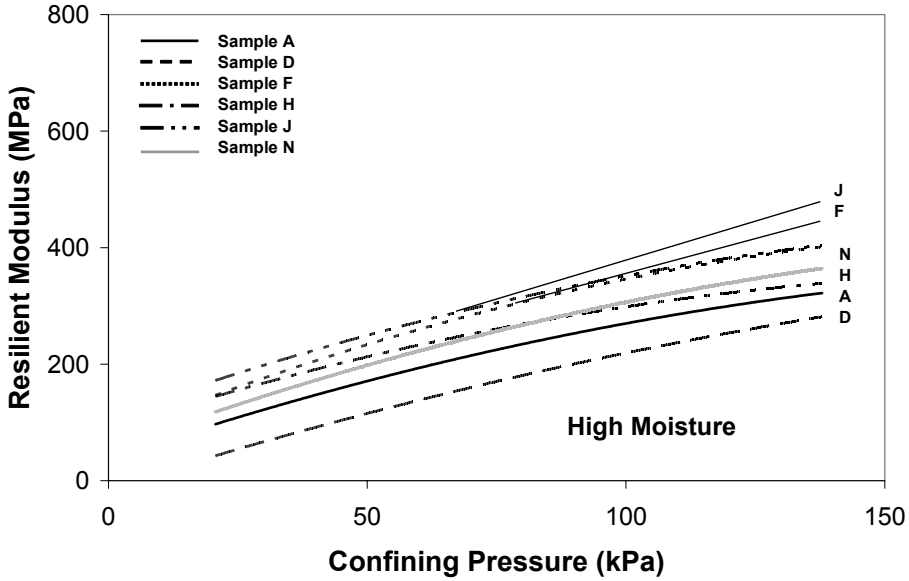

(c) High Moisture Content (7.5%-11%)

Figure D.7 Continued: Resilient Modulus Versus Confining Pressure Data

D.3 Resilient Modulus Versus Mean Stress

The mean stress is another quantity that was calculated during this study. Figures D.8 to D.13 plot the resilient modulus against the mean stress against the confining for each sample and moisture content.

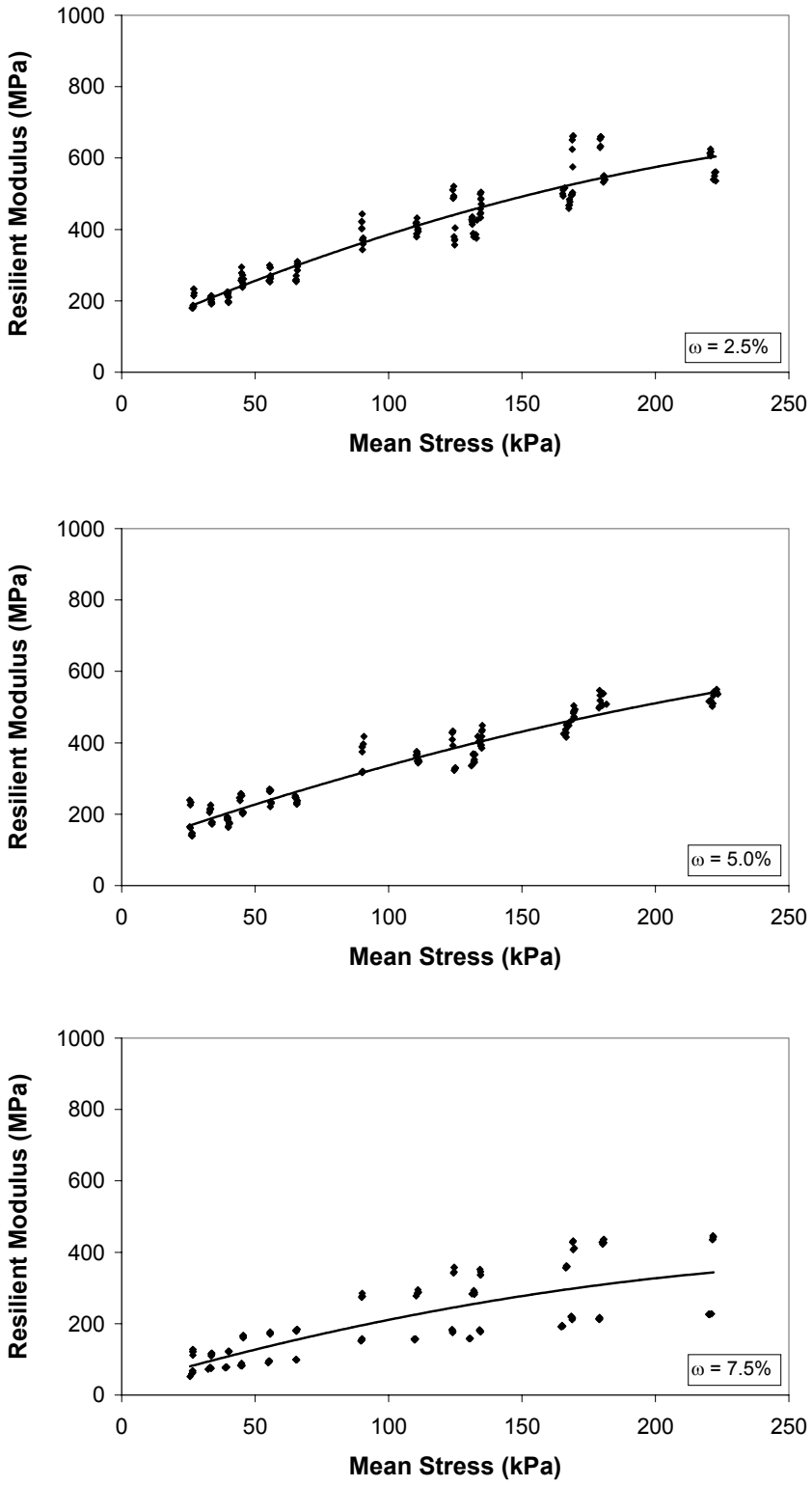

Figure D.8: Resilient Modulus and Mean Stress Data from Sample A

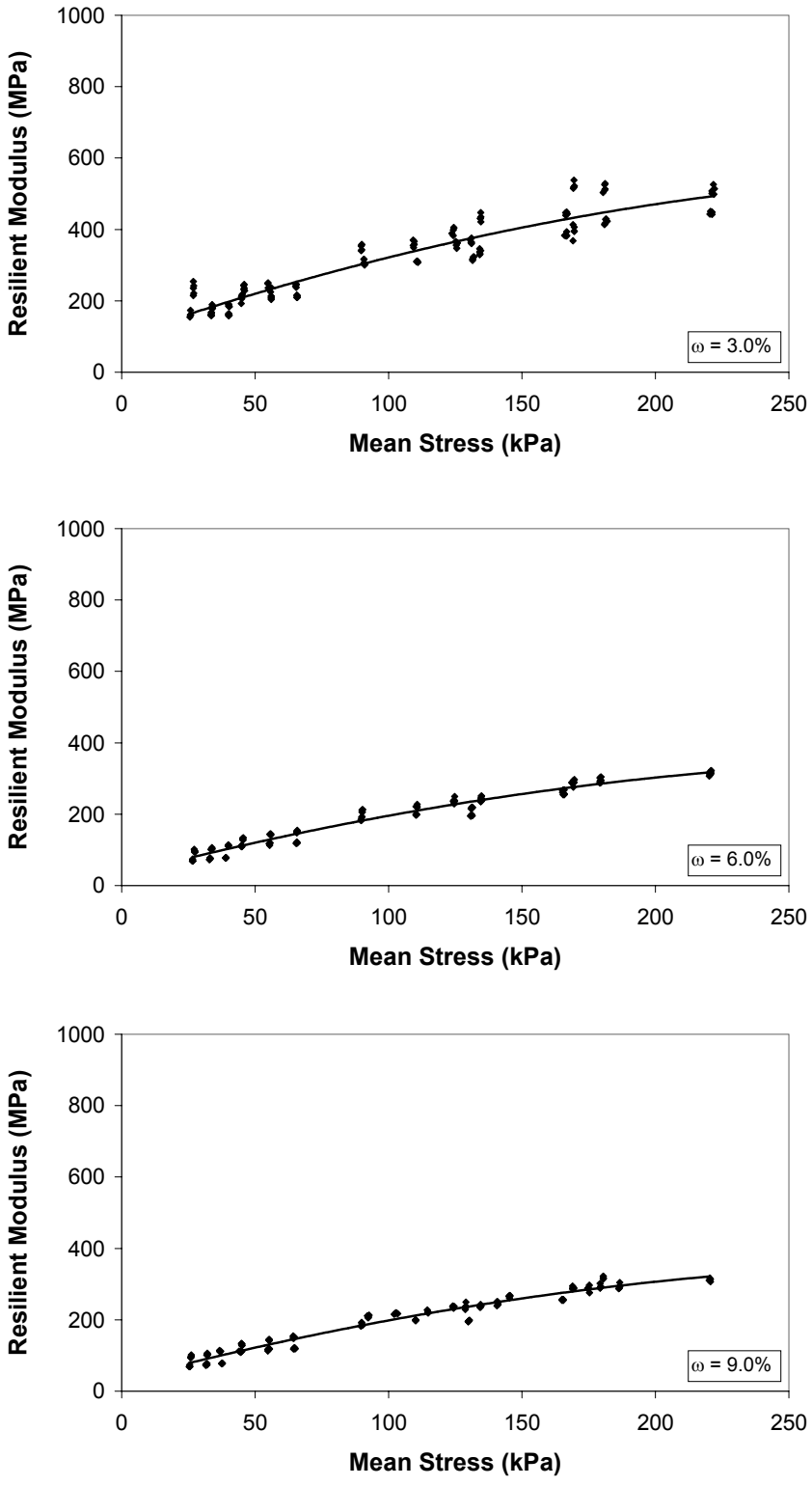

Figure D.9: Resilient Modulus and Mean Stress Data from Sample D

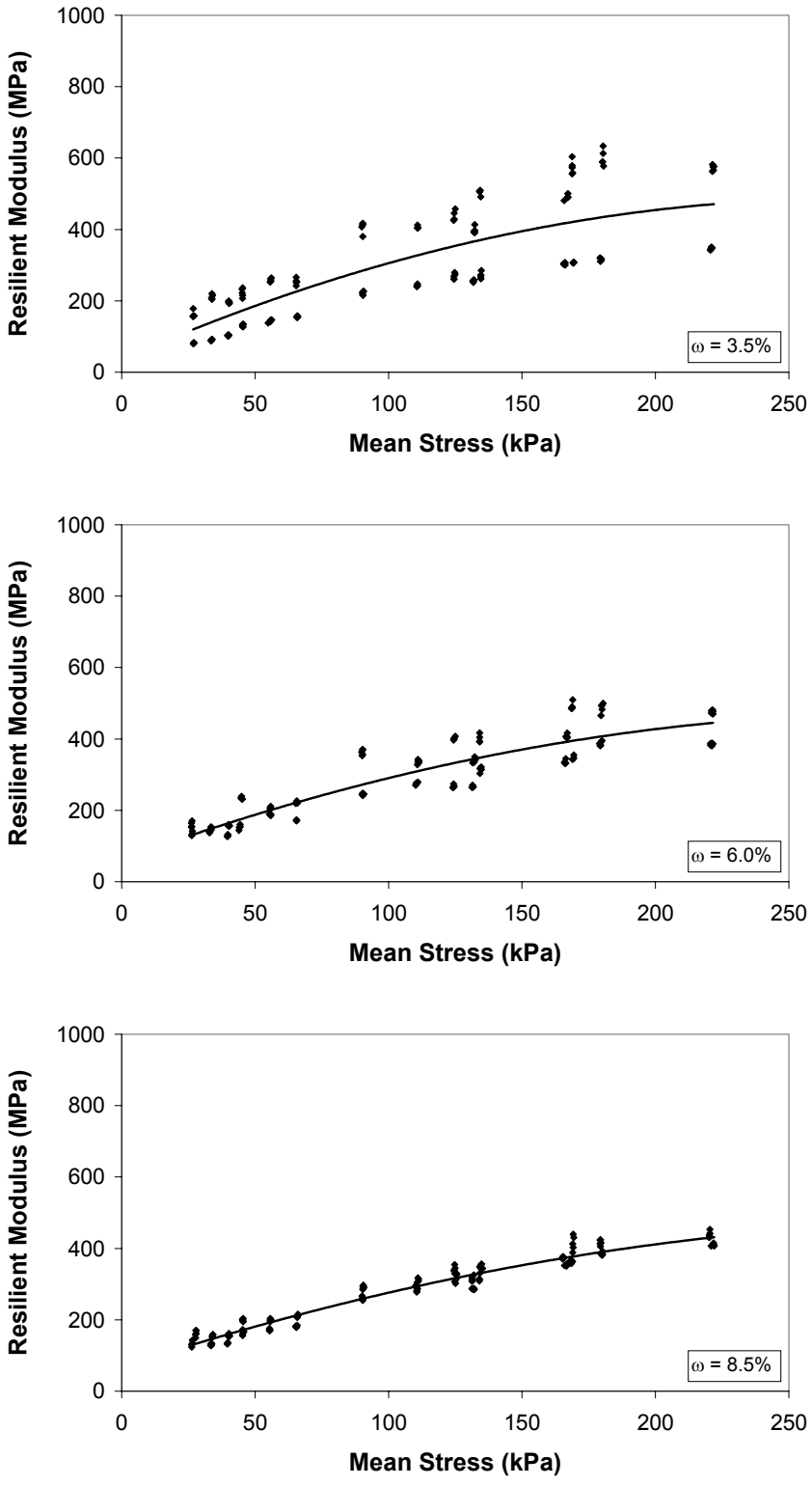

Figure D.10: Resilient Modulus and Mean Stress Data from Sample F

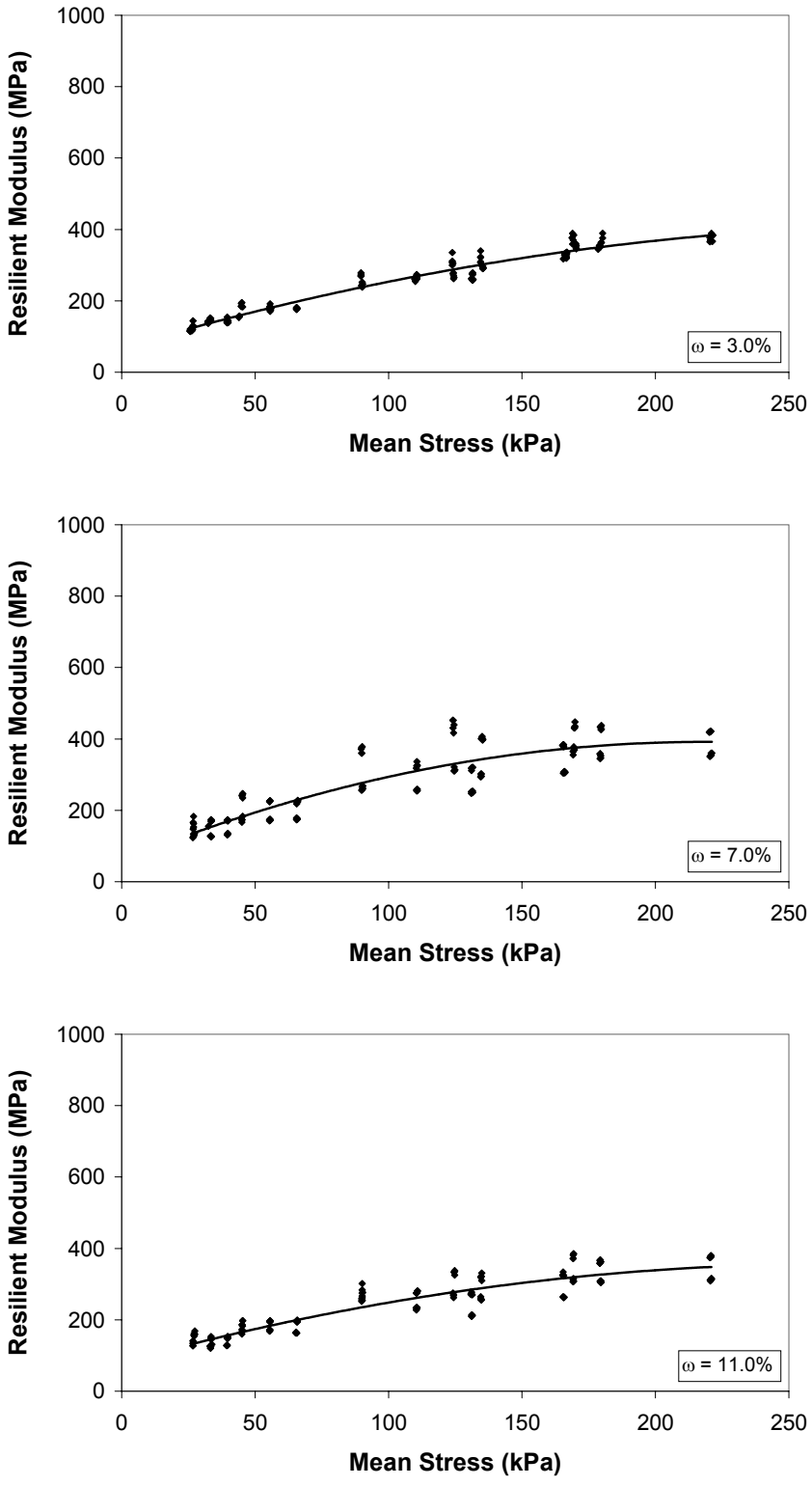

Figure D.11: Resilient Modulus and Mean Stress Data from Sample H

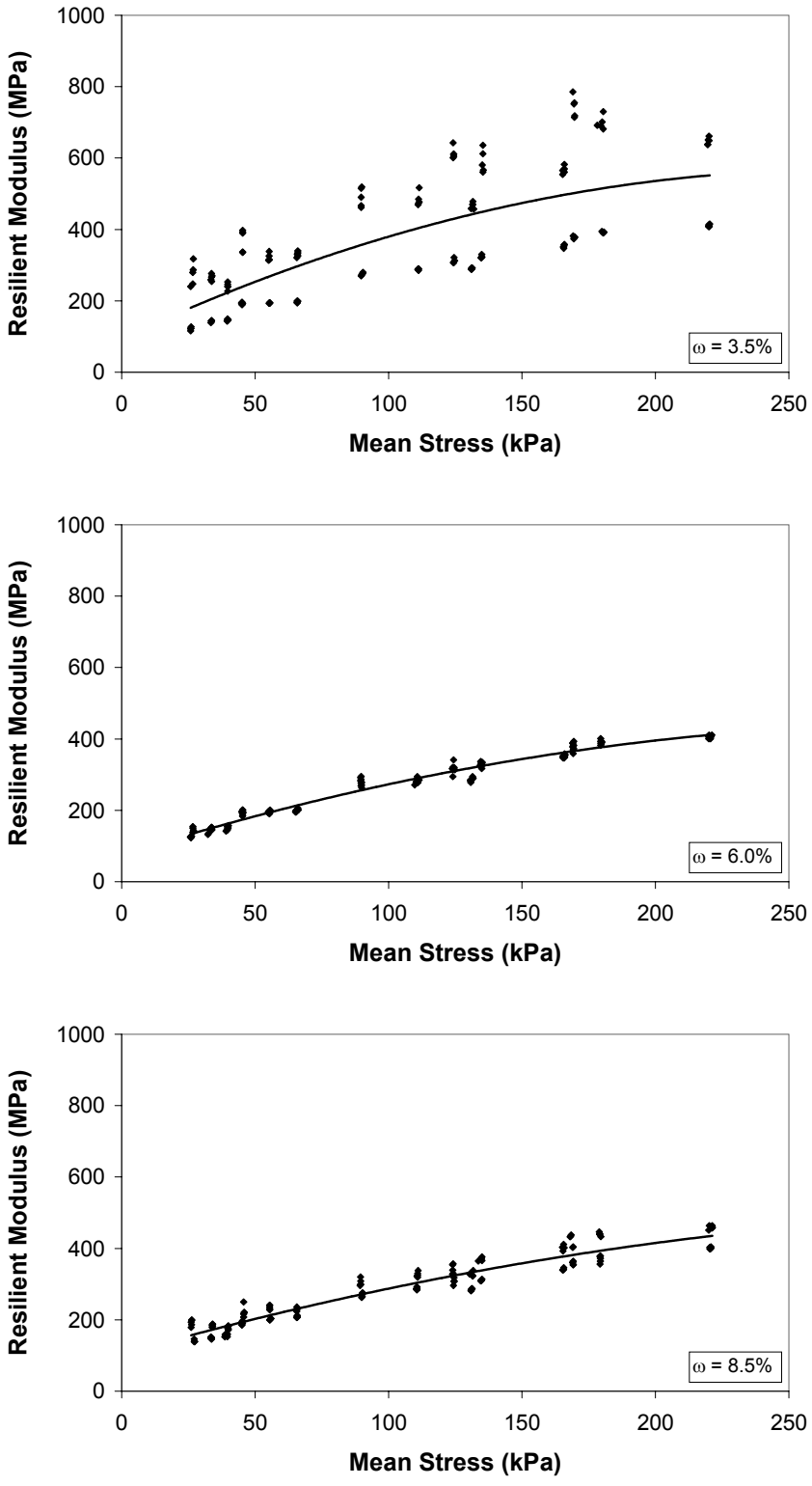

Figure D.12: Resilient Modulus and Mean Stress Data from Sample J

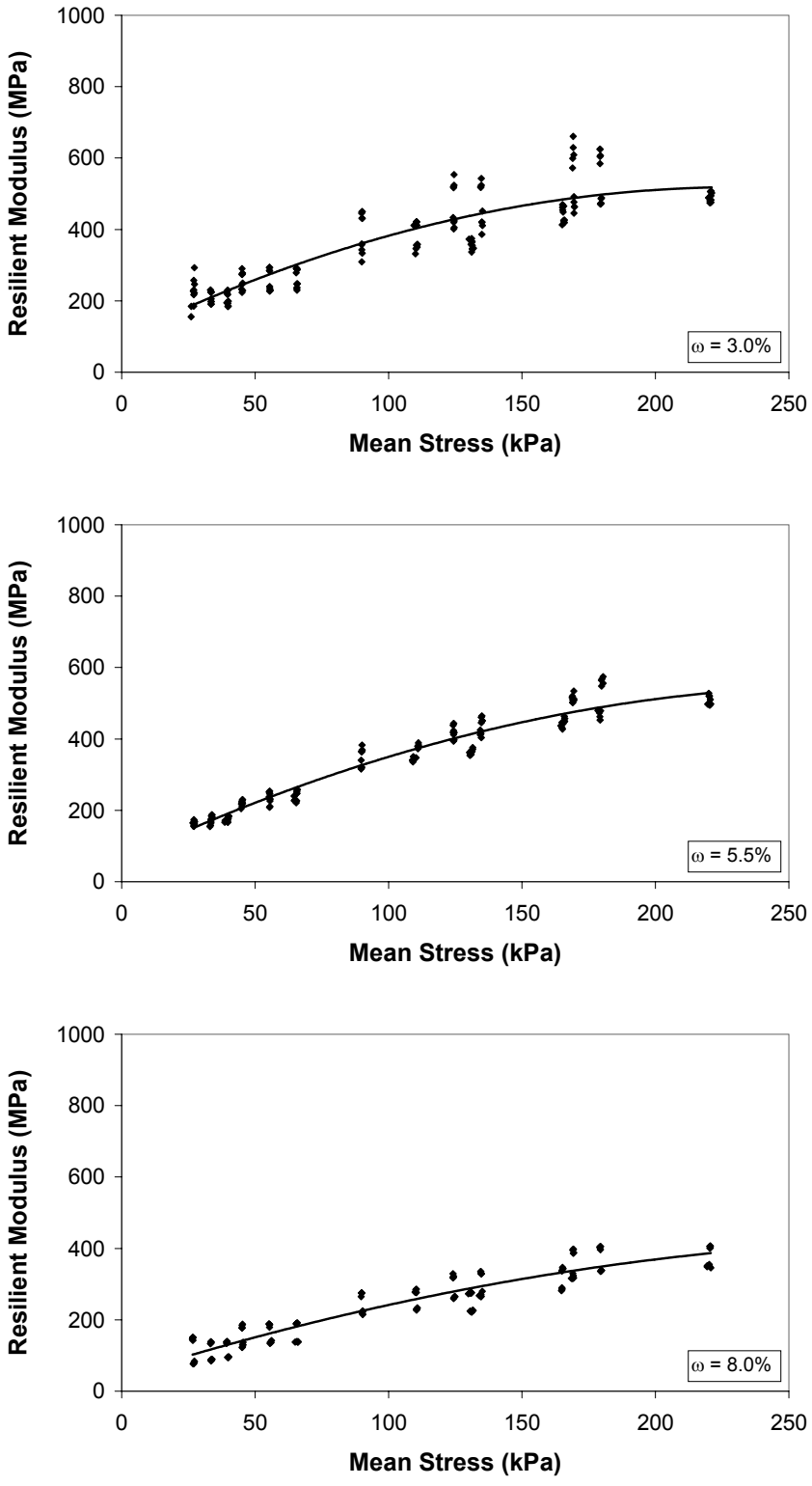

Figure D.13: Resilient Modulus and Mean Stress Data from Sample N

Appendix E

M_R Protocol Comparison

AASHTO's LTPP P46 was used to direct the resilient modulus testing performed during this study. However, a new resilient modulus test protocol entitled NCHRP 1-28A was released in 2002 with revised procedure as stated in section 2.1. One resilient modulus test was carried out using the standard equipment for this study within the new protocol to establish that the individual M_R values recorded during the tests are similar. This appendix contains an itemized test procedure as well as the results of the protocol comparison.

E.1 Itemized Test Procedure (LTPP P46)

1. Pour one 50 lb bag of the sample to be tested (there are three bags per sample) into a large container. Mix until homogeneous.

2. Determine the amount of soil and water to be mixed for the sample using the equations provided in Attachment A of LTPP P46.

3. Mix the correct amount of water and soil until the moisture content of the sample is relatively homogeneous. Take a moisture content sample from several locations within the sample; place this sample within an oven at approximately 125 degrees Fahrenheit.

4. Seal the remainder of the sample in an airtight container and allow it to temper overnight.

5. Before compaction remove the dry moisture content sample, calculate the moisture content of the sample, and adjust if necessary. Take three moisture content samples from the soil.

6. Inspect the base unit, mold, and top and bottom platens for damage and cleanliness. Place the porous stone on top of the platen and bender element if not already in place.

7. Attach a membrane to the lower bender element platen using two O-rings in the appropriate grooves. A third O-ring may be placed between the grooves if the vacuum mold does not seal properly without it.

8. Place the vacuum mold on top of the platen and tighten the ring supports; the upper ring support should be placed over the excess rubber membrane to hold it in place.

9. Apply a 10 in.-Hg vacuum to the mold. Check to make certain that the vacuum is acting uniformly on the membrane.

10. Weigh the split mold assembly with ring supports in place. Record the weight on the data sheet.

11. Calculate the amount of soil needed for a 2-inch lift using the equations provided in Attachment B of LTPP P46.

12. Measure the soil for the lift into a clean metal pan. Place a small amount of fine (Ottawa) sand around the lower bender element to protect it.

13. Pour the soil into the vacuum mold. Use a trowel to give the soil a relatively flat surface.

14. Lower a plastic spacer and the compaction plate into the vacuum mold. Make certain that they sit evenly on the sample.

15. Compact each lift using a 3000 beats-per-minute rotary hammer (spec AASHTOT-307). Make certain that the top of the specimen remains level and that only a small amount of soil escapes around the edges of the compaction plate. The length of compaction varies between soil types.

16. Use threaded rods to pull the plate and spacer from the vacuum mold.

17. Record the height and weight of the specimen and check to see that the correct dry density was achieved.

18. Repeat steps #12-17 five times.

19. Perform three Percometer measurements across the diameter of the specimen using mode 4. Record both the conductivity and dielectric values.

20. Place a wire mesh over the top of the specimen to protect the upper bender element. Cover this mesh with approximately ¼ in. of fine (Ottawa) sand and compact using a short burst from the rotary hammer.

21. Place the upper platen and porous stone on top of the specimen. Make certain that there is enough fine sand around the bender element to ensure a good contact.

22. Remove the split mold and use one O-ring to hold the membrane to the upper platen. The soils used in this study will hold together due to apparent cohesion.

23. Pull a second membrane over the exterior of the first. After reaching the bottom, slide all but one O-ring from the surface of the first membrane over the surface of the second. Place four O-rings in the platens' grooves to seal the membrane.

24. Carefully place the specimen in the center of the triaxial cell. Clean all surfaces to ensure that the cell and specimen are airtight.

25. Attach the air hoses to the platens.

26. Slide the LVDT holder into place over the membrane. Make certain that there is a good contact between the LVDT holder and the membrane. In addition, check that the LVDTs are resting evenly on top of their pedestals and that none of the lead wires in the cell are impeding their movement. Attach the LVDT holder with two elastic bands.

27. Check to make certain that the LVDTs have a sufficient stroke range. (For example, set them to 80% of their negative range.)

28. Remove the spacers from the LVDT holder.

29. Connect the interior load cell lead wire, the three LVDT lead wires, and both of the bender element lead wires to their respective LEMO connectors.

30. Place a steel ball bearing on top of the upper platen and the plexiglass chamber around the outside of the specimen. Make certain that none of the wires are pinched.

31. Place the cell inside of the load frame.

32. Place the top cap and load cell on top of the cell and screw the load shafts together. Press the top cap down into the plexiglass chamber. The location of the cell may have to be shifted slightly to prevent lateral pressure on the shaft. Attach the top cap with three bolts.

33. Lock the chamber by screwing down the circular plates on top of the top cap.

34. Attach all of the external wiring to the back of the cell and the two air hoses to the front of the cell.

35. Look over the entire system to make certain that everything is connected properly.

36. Pressurize the cell by opening the valve on the air supply. Listen for leaks in the system.

37. Pressurize the cell to 15 psi.

38. Open the TestWare program (on the MTS computer) named "M_R Test – Final External". Also open the LabView program (on the Dell personal computer) named "M_R Data Acquisition".

39. Define the data channels in LabView and make certain that it records data at a rate of 200 points per second.

40. Use the MTS pod to lower the load cell down onto the top of the specimen. Make certain that the system is in load control and turn off the pod. Run M_R Data Acquisition followed by M_R Test - Final External.

41. After the conditioning cycle is finished, use the pod to lift the load cell off from the top platen. Open the GDS bender element program.

42. Enter the specimen height, a sampling time of 5 ms, a period of 0.5 ms, and an amplitude of 14V.

43. Run and stack a sufficient number of P and S-wave tests to obtain a clear signal (often 50 or more). Save the signals and exit the program.

44. Change the confining pressure to 3 psi and wait for the system to reach equilibrium. Lower the load cell onto the upper platen.

45. Open the M_R Data Acquisition screen. Run the data collection; name the 30 cycles N3 3-3 9-22, A5 20-40 10-31, etc where the letter is the sample, the first number is the moisture content, the middle numbers are the confining pressure and maximum axial stress, and the last numbers are the date. As soon as the data collection is running resume the M_R test.

46. Shut off the data collection when each cycle is completed. Perform bender element tests and change the confining pressure as needed. The peak loads/confining pressures are defined in Table 2 of LTPP P46.

47. After the protocol is finished the TestWare program will automatically run a shear strength routine. The specimen will be loaded in stroke control; terminate the program when the specimen fails. Record the data using the same LabVIEW program.

48. After the test is completed remove the specimen from the chamber and put away all components. Take soil samples from the top and bottom of the failed specimen.

E.2 Resilient Modulus Value Comparison

It is necessary to compare the results from LTPP P46 to the results of the new resilient modulus protocol, NCHRP 1-28A, in order to verify that results obtained using both methods are comparable. To do this a resilient modulus test was performed using sample N at an 8% moisture content. Sample N was used because its gradation is closest to the average of the six samples. In addition, sample N is much more homogeneous then some of the other samples.

Figure E.1 shows the results of this comparison. The trendline calculated for the resilient modulus values from NCHRP 1-28A falls slightly below the trendline calculated for the resilient modulus values from LTPP P46. However, the discrepancy falls within the standard range of moduli variation observed in these tests. In fact, the data points from the NCHRP 1-28A test plot almost directly over the data points from one of the two tests performed using LTPP P46.

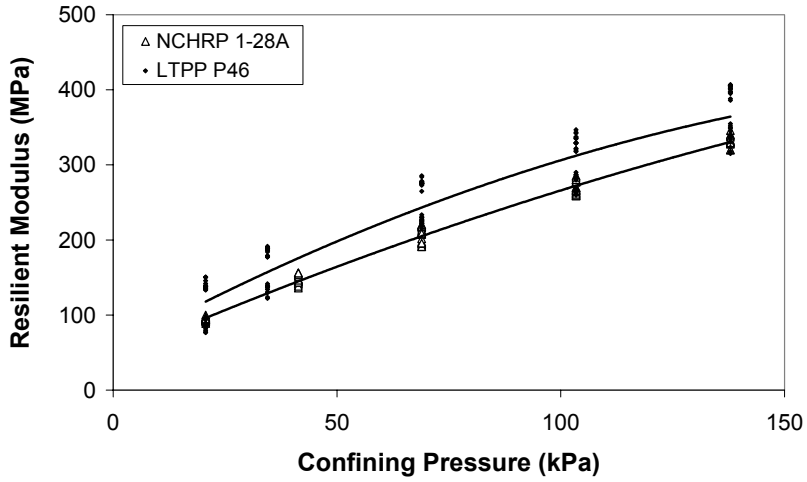

Figure E.1: Resilient Modulus Values from both Protocols

The resilient modulus values from NCHRP 1-28A were also plotted against E_{MAX} values from the bender elements. This data is shown in Figure E.2.

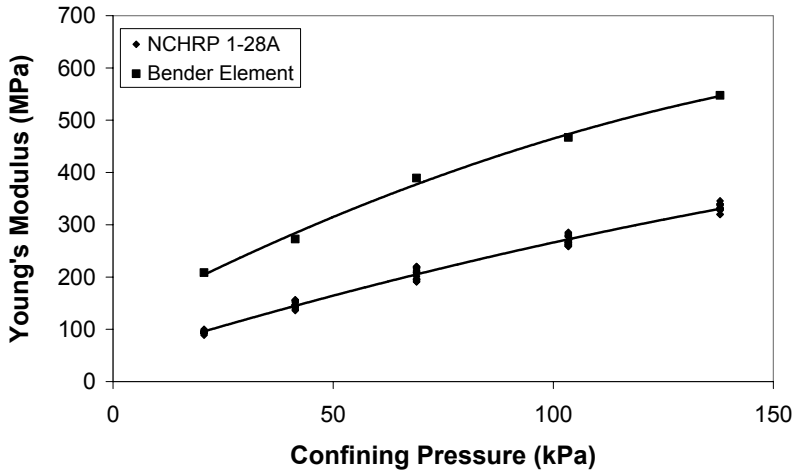

Figure E.2: NCHRP 1-28A and Bender Element Moduli

The M_R values recorded during the NCHRP 1-28A protocol fall significantly below E_{MAX}, but their relation is not unreasonable. Based upon the results of this analysis it is reasonable to assume that resilient modulus values calculated using the NCHRP 1-28A protocol are comparable to the values from LTPP P46.